

290
2001



Proceedings of I. Javakhishvili Tbilisi State University

ივ. ჯავახიშვილის სახელობის თბილისის
სახელმწიფო უნივერსიტეტის შრომები

345

ISSN 1512-1461

PHYSICS
ფიზიკა

36-37





Proceedings of I. Javakhishvili Tbilisi State University

ივ. ჯავახიშვილის სახელობის თბილისის
სახელმწიფო უნივერსიტეტის შრომები

345

97

PHYSICS

ფიზიკა

36-37

TBILISI UNIVERSITY PRESS



თბილისის უნივერსიტეტის გამომცემლობა

Tbilisi 2001 თბილისი

ББК 22.3

УДК 53

ფ 505

Editorial board

N. Amaglobeli, A. Gerasimov, Z. Kachlishvili, N. Kekelidze,
A. Khelashvili, Z. Khvedelidze, T. Kopaleishvili (editor),
L. Kurdadze, R. Kvatadze, J. Mebonia, G. Mrevlishvili, T. Sanadze,
A. Ugulava (secretary).

სარედაქციო კოლეგია

ნ. ამაღლობელი, ა. გერასიმოვი, ნ. კეკელიძე,
თ. კოპალეიშვილი (რედაქტორი), ჯ. მებონია,
გ. მრევლიშვილი, თ. სანაძე, ა. უგულავა (მდივანი),
ლ. ქაჩლიშვილი, რ. ქვათაძე, ღ. ქურდაძე, ზ. ხვედელიძე,
ა. ხელაშვილი.

© Tbilisi University Press, 2001

© თბილისის უნივერსიტეტის გამომცემლობა, 2001

1604010000

ფ 608(06) - 02

ON THE OPTIMAL CONFIGURATION OF THE GEOMAGNETIC TAIL



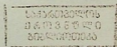
N. Toloraya

Accepted for publication January, 2001

ABSTRACT. This paper is devoted to the problem of Kelvin-Helmholtz instability which takes place on the Earth's surface magnetosphere and its magneto-tailed layers system.

22313

The tail of magnetosphere represents the system of varied plasma flows having a slightly deformed cylindrical configuration. The boundaries between the layers are represented by the surfaces of tangential discontinuity on the cross of which MHD parameters of plasma considerably change. The tail of magnetosphere is formed by force lines of the Earth's magnetic field, pushed to the night side of it by the solar wind at high speed and stretched at $1000 R_E$ distance (R_E is radius of the Earth) and as a result it becomes impossible to distinguish them from the force line of interplanetary magnetic field. It is obvious that at different sides of equatorial section of the tail, force lines of magnetic field should have contrary direction and therefore in its central part there should exist an area where the tension of magnetic field equals 0. This kind of area has been truly discovered by means of satellites [1,2]. It was called neutral layer. It starts at the distance of $10 R_E$ from the Earth, where its thickness is $1 R_E$ and reduces to $0,1 R_E$ at the distance of $20 R_E$. The neutral layer is surrounded by plasma layer where the tension of magnetic field is $H \approx 10\gamma = 10^{-5} H$ of value and maximal thickness equals $6 R_E$. The cover of plasma layer is surrounded by relatively thin layer called magnetopause. Its thickness equals 100-200 km. Then comes transitional layer between the interplanetary magnetic field and the magnetosphere. Fig.1 represents a cross-section of the magnetosphere and we can see that in the whole it is of cylindrical configuration and is



slightly extended to northern and southern direction [2]. The neutral layer is an exception and it can be considered as a plane plasma jet.

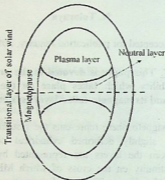


Fig.1. Cross-section of the tail of magnetosphere

Such a considerable difference in shape of neutral layer from other layers of magnetosphere tail should have some explanation.

In [4] it was shown that the influence of surface shape on the stability of plasma jet is determined by $\beta = \sqrt{\frac{\rho_2}{\rho_1}} \frac{H_2}{H_1}$ parameter, where

ρ_1, H_1 and ρ_2, H_2 are density of plasma and tension of magnetic field, respectively. In inner and external areas of the jet, in particular if $\beta > 1$ – plane jet is more stable than cylindrical, and if $\beta < 1$ – vice versa, cylindrical jet is more stable than the plane one. This paper considers the quantitative side of this problem.

The critical speed of plasma stream, at exceeding of which there appears instability, is represented as follows:

$$a_c = \left\{ \frac{[vG(\delta) + 1] [b_2^2 + b_1^2 vG(\delta)]}{vG(\delta)} \right\}^{1/2} \quad (1)$$

Here are used the following non-dimensional values:

$$v = \frac{\rho_1}{\rho_2}; \quad b_1 = \frac{V_{A1}}{c}; \quad b_2 = \frac{V_{A2}}{c}; \quad a_c = \frac{V_c}{c}; \quad \delta = \frac{kd}{2};$$

where $V_{Ai} = \frac{H_i}{\sqrt{4\pi\pi_i}}$, ($i = 1, 2$) are Alfvén's speed in the inner and

outer areas of the jet, respectively, $k = \frac{2\pi}{\lambda}$ is the wave number of disturbances, d is either thickness or diameter of the stream and c any volume owing speed dimension. The dependence of critical speed on the configuration of the jet is determined by $G(\delta)$ function giving the following way:

$$G(\delta) = \begin{cases} th(\delta) & \text{plane jet} \\ \frac{I_0(\delta)K_1(\delta)}{I_1(\delta)K_0(\delta)} & \text{cylindrical jet} \end{cases} \quad (2)$$

I_0 , I_1 , K_0 and K_1 are Bessel's modified functions. Fig. 2 shows dependence of function $G(\delta)$ on δ . We can see, that in case of plane jet, it monotonously increases from 0 to 1, while for cylindrical one it decreases from ∞ to 1. We also see that for short-wave disturbances ($\lambda \ll d$) when $\delta \gg 1$, $G(\delta) \approx 1$ for both configurations and it means that the configuration does not make influence on the stability of jet towards short-wave disturbances. This is obvious as when length of disturbance wave is much less than diameter we can consider that for these

disturbances the curvatures of the jet surface is $\frac{1}{r} = \frac{2}{d} = 0$ and it can be considered as flat.

Thus, the influence of the shape of stream surface on its stability is significant only regarding long-wave disturbances when $\delta \ll 1$ and the values of critical speeds for flat $G(\delta) \ll 1$ and cylindrical ($G(\delta) \gg 1$) streams respectively can be written down as follows:

$$a_c = \frac{b_2}{\sqrt{\nu G(\delta)}}, \quad \text{plane jet} \quad (3)$$

$$a_c = b_1 \sqrt{\nu G(\delta)} \quad \text{cylindrical jet} \quad (4)$$

From (3) and (4) we can see that when $\lambda \gg d$ the critical speed of the flow can be whatever big and this means that when there is no disturbance ($\lambda \rightarrow \infty$) the flow is absolutely stable. Besides, according to the same formulas stabilization of the plane jet is mainly determined by the tension of magnetic field outside the stream and for cylindrical - inside the jet.

The analysis of formula (1) has made it obvious that value a_c^2 has extreme point $G(\delta) = \beta = \frac{b_1}{\nu b_2}$ and it represents minimum point, in which

$$\left(a_c^2 \right)_{\min} = (b_1 + b_2)^2. \quad (5)$$

For plane jet $G(\delta) \leq 1$ and therefore, if $\beta > 1$ the square root of critical speed of the jet does not have the extreme point and when $G(\delta)$ increases from 0 to 1 it monotonously decreases from ∞ to minimal value $G(\delta) = 1$ in the point which equals

$$\left(a_c^2\right)_{min} = (b_1 + b_2)^2 + vb^2 \left(1 - \frac{b_2}{vb_1}\right)^2. \quad (6)$$

Analogously, when $\beta < 1$, the square root of critical speed of the cylindrical jet does not have extreme point and at increase of $G(\delta)$ from 1 to ∞ it monotonously grows from value (6) to ∞ . The aforementioned is illustrated in Fig.3, where the dependence of a_c^2 on $G(\delta)$ for flat and cylindrical streams for two values of β parameter, when $\beta = 0.5$ and $\beta = 2$.

Fig.4 shows the same dependence for $\beta = 1$. In this case critical speeds of both streams change monotonously.

The case of neutral layer represents the extreme interest to us when $b_1 = 0$ and $\beta = \infty$ respectively. Fig.5 features exactly this case for the following values of parameters: $b_1 = 0$; $b_2 = 1$; $v = 10$. We see that according to formula (6) the minimal value of critical speed of calculated plane jet equals

$$\left(a_{cr}\right)_{min} = b_2 \left(1 + \frac{1}{v}\right)^{1/2} = 1.05, \quad (7)$$

and for cylindrical jet, according to formula (5) we have

$$\left(a_{cr}\right)_{min} = b_2 = 1. \quad (8)$$

We can see that when the tension of magnetic field inside the stream equals 0, plane jet is $\left(1 + \frac{1}{v}\right)^{1/2}$ initially more stable than cylindrical and when $v \rightarrow 0$ this value can be whatever high.

In conditions of quiet magnetosphere the values of MHD parameters of neutral and plasma layers [5]:

$$H_1 = 0; \quad \rho_1 = n_1 \cdot m_p = 4 \cdot 1.66 \cdot 10^{-24} \approx 0.65 \text{ g/cm}^3;$$

$$H_2 = 10\gamma; \quad \rho_2 = n_2 \cdot m_p = 0.4 \cdot 1.66 \cdot 10^{-24} \approx 0.66 \text{ g/cm}^3$$

where m_p is proton mass, determining elasticity of magnetosphere plasma. According to these data $V_{A2} = 350 \text{ km/s}$ and in formula (7) after transition to the initial values, for the minimal value of critical speed of plasma flow in neutral layer we will have

$$(V_c)_{min} = V_{A2} \left(1 + \frac{\rho_2}{\rho_1} \right)^{1/2} = 370 \text{ km/s} \quad (9)$$

According to the experimental data [5], in the neutral layer plasma flows towards the Earth with speed $V_1 \approx -50 \text{ km/s}$ and in plasma layer in opposite direction with speed $V_2 \approx 300 \text{ km/s}$ and therefore for the relative speed we will have $V = V_2 - V_1 \approx 350 \text{ km/s}$.

As we see, this value is less than the minimal value of the critical speed and it means, that in the conditions of the quiet magnetosphere the neutral layer is stable relative to the disturbance of any wave length.

If the neutral layer were of cylindrical configuration, according to (8) we would get $(V_c)_{min} = V_{A2} = 350 \text{ km/s}$. So, the minimal value of the critical speed would equal the relative speed of the flow and the flow would be at the boundary of instability.

It is obvious that the numerical calculations represented here cannot provide the precise picture, but they reflect qualitative as well as quantitative features of stability of the neutral layer of the tail of magnetosphere.

Acknowledgment. I would like to thank Dr. A. Gvelesiani for statement of the problem and constant attention to the work.

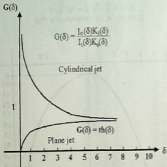


Fig. 2. Dependence of function $G(\delta)$ and δ on the plane and cylindrical configuration

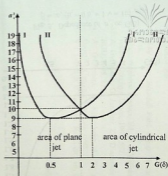


Fig. 3. Dependence of α_1^2 on $G(\delta)$:
 I curve: $\beta=0.5$, ($b_1 = 2$ $b_2 = 1$ $\nu = 1$)
 II curve: $\beta=2$, ($b_1 = 1$ $b_2 = 2$ $\nu = 1$)

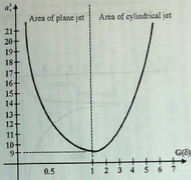


Fig. 4. Dependence of α_1^2 on $G(\delta)$:
 $\beta=1, (b_1 = 1, b_2 = 2, \nu = 2)$

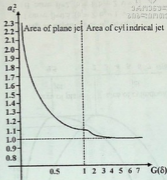


Fig. 5. Dependence of α_1^2 on $G(\delta)$
 $\beta = \infty, (b_1 = 0, b_2 = 1, \nu = 10)$



REFERENCES

1. N.W. Hess. Blaisdell Publ. Comp., Toronto - London. 1968, 548.
2. Magnetospheric Physics, Ed. D. J, Williams and G. D. Mead. Americ. Geophys. Union, 1969, 592.
3. A. Gvelesiani, G. Jandieri, Zh. Diasamidze. Tbilisi - Batumi: BGU, 1998, 278.
4. A. Gvelesiani, V. Kirtskhalia, I. Zhvania, N. Toloraya. Georgian Geophys. Soc., **3B**, 1998, 113.
5. S. I. Blame at al. Geophys. Res. Lett., **10**, 1983, 912.

Tbilisi State University

6. თოლორაია

ბეომაგნიტური კულის კონფიგურაციის
ოპტიმალურობა

დასკენა

სტატიაში განხილულია კვლეინ-ჰელმჰოლციის არამდგრადობის განხორციელების პირობები დედამიწის მაგნიტოსფეროს ზედაპირისათვის და მისი მაგნიტური კულის მრავალფენოვანი სისტემისათვის.

ON FORMATION MECHANISMS OF SINGLE-PULSE AND SECONDARY ECHOES IN SYSTEMS WITH A LARGE INHOMOGENEOUS BROADENING OF NMR LINES

T. Gegechkori, G. Mamniashvili

Accepted for publication October, 2001

ABSTRACT. In the frames of Mims transformation matrix method the equations for nuclear magnetization are obtained describing the dynamics of nuclear spin-systems with a strong Larmor and Rabi inhomogeneous broadenings of NMR line in conditions of their unequilibrium earlier obtained by the method of statistical tensors.

The single-pulse echo (SPE) is a resonance response of the inhomogeneously broadened nuclear spin-system to the application of a solitary radiofrequency (RF) pulse arising at a time moment τ approximately equal to the pulse duration after its termination. Though SPE was discovered by Bloom in 1955 for protons in water placed in an inhomogeneous magnetic field, the mechanism of SPE formation has not been yet so clear-out as for the classical Hahn two-pulse echo (TPE) and it continues to attract researchers' attention [1].

SPE formation mechanisms could be conditionally subdivided into two classes: the first one is so-called edge-type mechanisms where RF pulse edges act like RF pulses in the TPE method, such as the distortion mechanism [1], and mechanism connected with the consideration of spectral densities of sufficiently step RF pulse edges [2], and the second class is mechanisms of internal nature due to particular type nonlinearities in the dynamics of spin-systems, for example, connected with a strong dynamic frequency shift of NMR frequency, or with a nonlinear dynamics of nuclear spins due to the simultaneous presence of large Larmor and Rabi inhomogeneous broadenings of NMR line [1].

In this work we consider in some more details so-called multipulse mechanism of SPE formation, presented in [1], for systems with the both types of frequency inhomogeneities of NMR lines. An important example of such systems is presented by lithium ferrite. Earlier in [3]

we have investigated properties of the SPE formation in this magnetics. It has been established that its properties are sharply different from SPE properties in hexagonal cobalt, where it is formed by the distortion mechanism. Therefore, the conclusion was made on a possible effectivity of the intrinsic mechanism of SPE formation in lithium ferrite. But its concrete mechanism has not been finally established

In [1] it was shown that multipulse mechanism of SPE formation was effective in some multidomain ferromagnets like Fe and FeV. From this point of view further theoretical and experimental investigations of SPE multipulse mechanism formation are of practical interest.

In [1] using the formalism of statistical tensors the theoretical investigation of SPE and its secondary echo signals formation mechanism was made in the presence of large Larmor and Rabi inhomogeneous broadenings of NMR line when repetition period of RF pulses of T obeys the inequality $T_3 \ll T_2 < T < T_1$, where T_1 , T_2 , T_3 are characteristic NMR relaxation parameters and therefore a spin-system was in the unequilibrium state before the application of exciting RF pulse, and thereby only a longitudinal component of the nuclear magnetization was important before RF pulse. It was shown that a dephasing of nuclear spin-system was accumulated during n -time pulse excitations and restored within a time interval elapsing from the trailing edge of the last "counting" $[(n + 1)$ -th] pulse in the multipulse train. This resulted in the SPE formation and also its secondary signals at time moments which were multiples of the RF pulse duration after the termination of the "counting" RF pulse.

The aim of this work is to obtain the equations describing the nuclear spin-system dynamics in the investigated case, in the frames of usual classical approach by solving Bloch equations or by the equivalent Mim's transformation matrix method [4]. We will use the last one as the most visual from the experimental point of view.

Let us consider a case when a local static field H_n is directed along Z axis, and a RF field is along X axis of RSC [4]. The H_{eff} modulus in RSC could be expressed by:

$$H_{\text{eff}} = \frac{1}{\gamma} \sqrt{\Delta\omega_j^2 + \omega_1^2} = \frac{\omega_1}{\gamma_n} \sqrt{a^2 + x^2}$$

Here $x = \Delta\omega_j / \omega_1$, where $\Delta\omega_j = \omega_j - \omega_0$ isochromate frequency; $a = \eta / \bar{\eta}$ (or $a = \omega_1 / \omega_1$), where η is the RF field gain factor and $\bar{\eta}$ its mean value; $\omega = \bar{\eta} \omega_1^{APPL}$ is a mean value of RF amplitude in frequency units; $\omega_1 = \eta \omega_1^{APPL}$ is Rabi frequency of applied RF field. Besides this, correspondingly to [1], let us introduce following designations for a mean value of a pulse area $y = \bar{\omega}_1 \Delta t$, where Δt is a RF pulse duration and $b = \bar{\omega} \tau$ is a characteristic of a time interval following a pulsed excitation and it is measured from the trailing edge of RF pulse; ω_0 designates for a center of the resonance line, and ω_j is a frequency of j -th isochromate, correspondingly. The transformation matrix describing a rotation of the magnetization vector $\bar{m} = (\bar{m}_x, \bar{m}_y, \bar{m}_z)$ around H_{eff} is [4]:

$$(R) = \begin{bmatrix} S_\phi^2 + C_\phi^2 C_\theta & -C_\phi S_\theta & S_\phi C_\phi (1 - C_\theta) \\ C_\phi S_\theta & C_\theta & -S_\phi S_\theta \\ S_\phi C_\phi (1 - C_\theta) & S_\phi S_\theta & C_\phi^2 + S_\phi^2 C_\theta \end{bmatrix}, \quad (2)$$

where C_ϕ, S_ϕ, C_θ and S_θ stand for $\cos \phi, \sin \phi, \cos \theta$ and $\sin \theta$, and

$\Psi = \text{tg}^{-1} \left(\frac{\omega_1}{\Delta\omega_j} \right)$ is the angle between the effective field H_{eff} and Z

axis; θ is the angle, by which the magnetization turns about the effective field H_{eff} during the pulse time Δt :

$$\theta = \gamma_n H_{\text{eff}} t,$$

where H_{eff} is given by (1).

Let us consider firstly the case of single-pulse excitation. Let

$X_j = m_{xj}/m$; $Y_j = m_{yj}/m$; $Z_j = m_{zj}/m$ and $\bar{\mu} = (X_j; Y_j; Z_j)$, where m is an equilibrium nuclear magnetization and at the equilibrium $\bar{\mu}_{eq} = (0; 0; 1)$.

If before the excitation by RF pulse a nuclear spin-system was at equilibrium conditions, and therefore $\bar{\mu}_{eq} = (0; 0; 1)$, then a result of RF pulse action would be presented by $\bar{\mu} = (R)\bar{\mu}_{eq}$.

After termination of RF pulse isochromates precess freely around Z axis that is described by the matrix:

$$R_\varphi = \begin{pmatrix} C_\varphi & -S_\varphi & 0 \\ S_\varphi & C_\varphi & 0 \\ 0 & 0 & 1 \end{pmatrix},$$

where $\varphi = \Delta\omega_j\tau$ is the deflection angle of isochromate around Z axis, and τ is a time clapsing from the trailing edge of a pulse. Therefore, finally we have:

$$\bar{\mu}_1 = (R_\Phi)(R)\bar{\mu}_{eq} = \begin{pmatrix} C_\varphi S_\Phi C_\Phi (1 - C_\Theta) + S_\varphi S_\Phi S_\Theta \\ S_\varphi S_\Phi C_\Phi (1 - C_\Theta) - C_\varphi S_\Phi S_\Theta \\ C_\Phi^2 + S_\Phi^2 C_\Theta \end{pmatrix},$$

or in the accepted designations:

$$\frac{m_x}{m} = \cos bx \frac{ax}{a^2 + x^2} \left(1 - \cos y \sqrt{a^2 + x^2} \right) +$$

$$+ \sin bx \frac{a}{\sqrt{a^2 + x^2}} \sin y \sqrt{a^2 + x^2}$$

$$\frac{m_y}{m} = \sin bx \frac{ax}{a^2 + x^2} \left(1 - \cos y \sqrt{a^2 + x^2} \right) -$$

$$-\cos bx \frac{a}{\sqrt{a^2 + x^2}} \sin y \sqrt{a^2 + x^2}$$

$$\frac{m_z}{m} = 1 - \frac{a^2}{a^2 + x^2} \left(1 - \cos y \sqrt{a^2 + x^2} \right)$$

These expressions coincide with the corresponding ones obtained in [1] for the case of single-pulse excitation, and similar expressions in [5], obtained by solving the system of Bloch equations for inhomogeneously broadened Hahn systems.

Now let us find the effect of n-time RF excitation in the frames of model [1] allowing for (1) when before RF pulse only the longitudinal component of nuclear magnetization remains. It is not difficult to prove by successive matrix multiplication that expressions for nuclear magnetization before the final "counting" (n + 1)-th pulse are:

$$\bar{\mu}_n = (C_\phi^2 + S_\phi^2 C_0)^n \bar{\mu}_{eq},$$

where $\bar{\mu}_{eq} = (0; 0; 1)$.

Then the result of excitation by the "counting" pulse and the following free precession of magnetization is described by expressions:

$$\bar{\mu}_{n+1} = (R_\phi)(R)\bar{\mu}_n = (C_\phi^2 + S_\phi^2 C_0)^n \begin{pmatrix} C_\phi S_\phi C_\phi (1 - C_\phi) + S_\phi S_\phi S_\theta \\ S_\phi S_\phi C_\phi (1 - C_\phi) - C_\phi S_\phi S_\theta \\ C_\phi^2 + S_\phi^2 C_0 \end{pmatrix},$$

which is similar to the one for single-pulse excitation but allowing for a new initial condition.

From the previous expression in the accepted designations follows:

$$\frac{m_x}{m} = \left(1 - \frac{a^2}{a^2 + x^2} \left[1 - \cos y \sqrt{a^2 + x^2} \right] \right)^n \times$$

$$\times \left[\cos bx \frac{ax}{a^2 + x^2} \left(1 - \cos y \sqrt{a^2 + x^2} \right) + \right.$$

$$\left. + \sin bx \frac{a}{\sqrt{a^2 + x^2}} \sin y \sqrt{a^2 + x^2} \right]$$

$$\frac{m_y}{m} = \left(1 - \frac{a^2}{a^2 + x^2} \left[1 - \cos y \sqrt{a^2 + x^2} \right] \right)^n \times$$

$$\times \left[\sin bx \frac{ax}{a^2 + x^2} \left(1 - \cos y \sqrt{a^2 + x^2} \right) + \right.$$

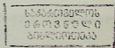
$$\left. + \cos bx \frac{a}{\sqrt{a^2 + x^2}} \sin y \sqrt{a^2 + x^2} \right]$$

22313

These expressions coincide with those obtained in [1] using the formalism of statistical tensors. The expressions for SPE and its secondary echo signal amplitudes using similar expressions for nuclear magnetization vectors were already obtained in [1]. It is easy to prove that above considered approach could be immediately applied to the case of periodical two-pulse excitation, that is of interest for the description of secondary two-pulse echo signals in the investigated systems.

Acknowledgement

This work was partly supported by International Science and Technology Centre, Project G-389.





REFERENCES

1. L.N. Shakhmuratova, D.K. Fowler, D.H. Chaplin. Phys. Rev. A, **55**, 1997, 2955.
2. B.P. Smoliakov, E.P. Khaimovich. Zh. Eksp. Teor. Fiz. **76**, 1979, 1303.
3. A.M. Akhalkatsi, G.I. Mamniashvili. Fiz. Met. Metalloved. **81**, 1996, 79.
4. W.B. Mims, K. Nassau, J.D. McGee. Phys. Rev. **123**, 1961, 2059.
5. V.P. Chekmarev, M.I. Kurkin, S.I. Goloshapov. Zh. Eksp. Teor. Fiz. **76**, 1979, 1675.

**Georgian Academy of Sciences
Institute of Physics**

ტ. გუგუჯკორი, გ. შამნიაშვილი

**ერთიმგულსიანი ექოს და მეორადი ექოების
ფორმირების მექანიზმები ბმრ ხაზების
არაერთგვაროვანი გაგანიერების მქონე სისტემებში**

დასკვნა

მიმსის გარდაქმნის მატრიცების მეთოდის ფარგლებში მიღებულია დიდი ბმრ ხაზის ლარმორისა და რაბის არაერთგვაროვანი გაგანიერების არაწონასწორულ პირობებში ბირთვული დამაგნიტების განტოლებები, რომლებიც აღწერენ ბირთვულ სპინ-სისტემების დინამიკას.

MODIFIED KNO-SCALING FOR THE MULTIPLICITY DISTRIBUTION OF CHARGED SECONDARY π^- -MESONS CREATED IN THE COLLISIONS OF RELATIVISTIC NUCLEI

T. Jalagania, G. Kuratashvili, Yu. Tevzadze, G. Vanishvili

Accepted for publication March, 2001

ABSTRACT. This paper is devoted to the study of multiplicity distribution of π^- -mesons created in $A_i A_t$ -nuclei-nuclei interactions in the energy range of $(2 \div 200)$ AGeV/c. The corresponding analysis has been carried out in the framework of MKNO - modified KNO -scaling. It has been shown that $A_i A_t$ -nuclei-nuclei, pp -nucleon-nucleon and e^+e^- -collision are well defined by means of the so-called soft scaling.

INTRODUCTION

Based on Feynman scaling hypothesis and on particular physical reasons, Koba, Nielsen and Olesen [1] have formulated the assertion about independence of the shape of multiplicity distribution as a function of primary energy - KNO-scaling [2], which is expressed by the relation:

$$\langle n \rangle P_n = \Psi\left(\frac{n}{\langle n \rangle}\right) = \Psi(z), \quad (1)$$

where P_n is the probability of creation of n secondary particles, $\langle n \rangle$ - the average multiplicity of secondary particles, and $z = n/\langle n \rangle$; $\Psi(z)$ - independent from the energy function, normalized according to following conditions

$$\int_0^{\infty} \Psi(z) dz = 1 \quad \text{and} \quad \int_0^{\infty} z^2 \Psi(z) dz = 1 \quad (2)$$

From formulae (1) and (2) directly follows the known relation:

$$\frac{D}{\langle n \rangle} = \sqrt{\int_0^{\infty} (z^2 - 1) \Psi(z) dz} = \text{const}, \quad (3)$$

where

$$D = \sqrt{\langle n^2 \rangle - \langle n \rangle^2}, \quad (4)$$

D^2 is dispersion of π^- -meson multiplicity distribution.

The analogous expressions are valid also for the other absolute momentum, i.e.:

$$\langle n \rangle \sim \langle n^N \rangle^{1/N} \sim D_N \quad (5)$$

KNO-scaling (1) represents the special case of relatively soft statement, according to which the distribution function becomes independent from energy only if it may be expressed as the function of ratios of relative deflections from the average [3], i.e.:

$$DP_n = \Psi_1\left(\frac{n - \langle n \rangle}{D}\right), \quad (6)$$

which one is transformed to scaling (1) in case of fulfillment of conditions expressed by the relation (3). The scaling (6) may be expressed in the following form:

$$(\langle n \rangle - \alpha) P_n = \Psi_2\left(\frac{n - \alpha}{\langle n \rangle - \alpha}\right), \quad (7)$$

where the parameter α depends on energy [4].

The normalization conditions in this case look like:

$$\frac{\int_0^{\infty} \Psi_2(z) dz}{\alpha - \langle n \rangle} = 1 \qquad \frac{\int_0^{\infty} z \Psi_2(z) dz}{\alpha - \langle n \rangle} = 1 \quad (8)$$

And the correlation analogous to the formula (3) looks like:

$$\frac{D}{\langle n \rangle - \alpha} = \sqrt{\frac{\int_{\alpha - \langle n \rangle}^{\infty} (z^2 - 1) \Psi_2(z) dz}{\alpha}} = B \quad (9)$$

Taking into account the independence from energy of integrals (8) it is possible to make the conclusion that the integral in formula (9) is also approximately constant and is independent from energy, i.e.:

$$\frac{D}{\langle n \rangle - \alpha} = B = \text{const} . \quad (10)$$

Further, if we assume that at high energies α does not depend on energy, then the relation (10) written for the total multiplicity of the secondary charged particles undergoes the transition to the well-known law of Wroblewski (for pp, π^-p , K^+p - interactions the parameter $\alpha = 1$) [3].

As seen from its explicit form, the expression (7) depends on energy-dependent two parameters $\langle n \rangle$ and α in their turn. The Negative Binomial Distribution (NBD or the so-called Pascal distribution) is close to it in this sense and sometimes is used for the analysis of secondary particles and also depends on two parameters $\langle n \rangle$ and k . The parameter k determines the form of the distribution [5,6]. The parameter k is related to the dispersion D^2 by the formula [5].

$$D^2 = \langle n \rangle^2 \left(\frac{1}{\langle n \rangle} + \frac{1}{k} \right), \quad (11)$$

which is expanded in a series on the extent of $k / \langle n \rangle$ at high energies (large $\langle n \rangle$) and undergoes transition to the following approximate expression:

$$D \equiv \frac{1}{\sqrt{k}} \left(\langle n \rangle + \frac{k}{2} \right)$$

The parameter k certainly depends on energy but in accordance with the growth of energy and of the masses of incident nucleus ($AiAt$)- decreases and comes to 1 (this is observed during the experiment [7]).

Therefore in an extreme case at $k = 1$ the relation (12) takes the form:

$$D = (\langle n \rangle + 0.5). \quad (13)$$

And the corresponding relation between the probability P_n and the scaling function Ψ is defined by the following expression:

$$(\langle n \rangle + 0.5)P_n = \Psi \left(\frac{n + 0.5}{\langle n \rangle + 0.5} \right). \quad (14)$$

It must be noted that relations (13) and (14) were obtained also on the basis of other considerations [8].

It is necessary to make the following remarks to the formulae (11÷14): although NBD sometimes is used for the analysis of multiplicity distribution of all charged secondary particles, but in fact it represents the distribution of n Bose particles among k cells [5].

Therefore, strictly speaking, the expressions (13) and (14) are correct only for the analysis of multiplicity distribution of secondary charged bosons. According to the above-mentioned statement in present article we are limited by consideration of only negatively charged particles, which are confined by π^- -mesons, since the admixture of the negatively strange particles does not exceed 1 % in the experiment [9].

It must be noted that such a choice allows us to solve the methodical problems of isolation of truly created particles, since π^- -mesons, in the $AiAt$ -collisions just are of this type.

The experimental data were obtained by means of two-meter propane bubble chamber (PBC-500) of the laboratory of the High Energies of JINR (Dubna). The chamber was irradiated with beam of relativistic nuclei (p, d, He, C, F, Mg) in the momentum range of $(2 \div 10)$ AGeV/c [9]. As the target in the detector was the tantalum -Ta (the heavy target) and Carbon -C (the light target), i.e. it was possible to study interactions of both heavy and light targets. Our results were compared with the corresponding data at different energies (including OCu interactions at 60 and 200 AGeV/c). (A. Bamberger et al., Phys. Let., B205 (1988) 583).

The dependence of the dispersion on the average multiplicity $D(<n>)$ for the negative charged secondary π^- -mesons, created from (p, d, He, C)(C, Ta) interactions at momentum 2.3 AGeV/c (8 dots) is given in Fig.1a. The same dependence for π^- -mesons, created from (p, d, He, C)(C, Ta) and (F, Mg)C -interactions at momentum 4.2 AGeV/c is given in Fig.1b. Here in the same place are shown the data from Fig.1a and also from (d, He)Ta - interactions at momentum of 5.1 AGeV/c [10, 11,12] and six (6) points from He (C, Pb) and C (Ne, S, Cu, Zr) at momentum of 4.5 AGeV/c [13]. All 26 dots. As seen from Fig.1a (data at 2.3 AGeV/c) the dependence $D(<n>)$ is linear and enough sloping (steep) (angle of inclination $\sim 45^\circ$). Approximation by linear function:

$$D = a + b <n> = b (\alpha + <n>) \quad (15)$$

(where $\alpha = a/b$) gives: $a = 0.22 \pm 0.02$; $b = 0.92 \pm 0.04$; $\alpha = 0.24 \pm 0.03$.

In Fig.1b there are given all the data together (26 dots) but approximation is given only for 22 dots; those dots are excluded, which evidently are slipped out from linear dependence - PC and PTa at 2.3 AGeV/c and CTa at 2.3 and 4.2 AGeV/c. The approximation of $D(<n>)$ dependence by the function (15) gives us the following results:

$$a = 0.35 \pm 0.02; b = 0.63 \pm 0.03; \alpha = 0.53 \pm 0.04 \quad (16)$$

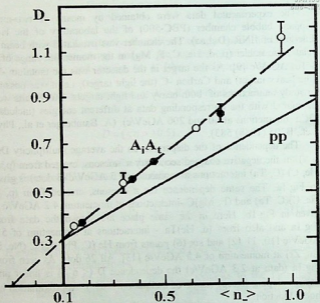


Fig.1a. The dependence of π -mesons dispersion on the average multiplicity of π -mesons created in (p, d, He, C) (C,Ta) interactions at momentum per nucleon 2.3 AGeV/c. Designations: • - (p, d, He, C) C - interactions on the carbon; o - (p, d, He, C) Ta - interactions on the tantalum

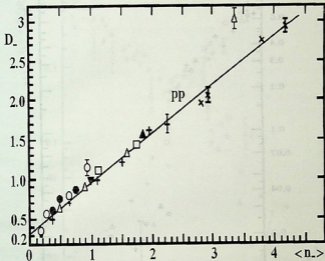


Fig.1b. The $D(\langle n \rangle)$ -dependence for π^- -mesons distribution created in (p, d, He, C)(C, Ta) -interactions at momentum per nucleon 2.3 and 4.2 AGeV/c. The (d, He)Ta -interactions at momentum per nucleon 5.1 AGeV/c. The (F, Mg)C -interactions at momentum per nucleon 4.2 AGeV/c. Designations: \bullet - (p, d, He, C) C; \circ - (p, d, He, C)Ta at 2.3 AGeV/c. $+$ - (p, d, He, C) C; ∇ - (F, Mg)C 4.2 AGeV/c; Δ - (p, d, He, C)Ta at 4.2 AGeV/c. \blacktriangledown - dTa, \blacktriangle -HeTa at 5.1 AGeV/c. \square - He(C, Pb). \times - C(Ne, Si, Cu, Zr) at 4.5 AGeV/c [13].

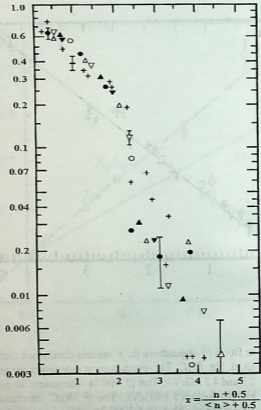


Fig.2. The distribution of π^- -mesons, created in $A_1 A_2$ -nuclei-nuclei collisions have been drawn in variables of MKNO-scaling [8] (formula 14) $\psi(z) = (\langle n \rangle + 0.5)P_n$, $z = (n + 0.5)/(\langle n \rangle + 0.5)$; o - P (C, Ta), \blacktriangledown - d (C, Ta), \blacktriangle - HeC, ∇ - HeTa, Δ - CC, \bullet - CTa at 2.3 AGeV/c, + - CTa at 4.2 AGeV/c.

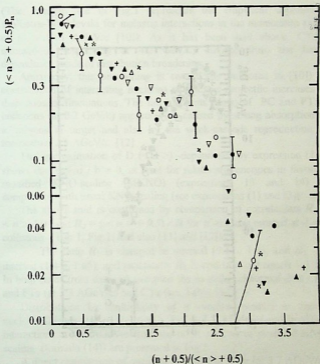


Fig.3. Immediate comparison of our data. * - PC, x - dC; ▲ - CC, ▼ - CTa (at 4.2 AGeV/c), △ - CC, + - CTa (at 2.3 AGeV/c) with data [8] ● - OCu (at 3.7 AGeV/c), □ - OCu (at 60 AGeV/c) and ○ - OCu (at 200 AGeV/c)

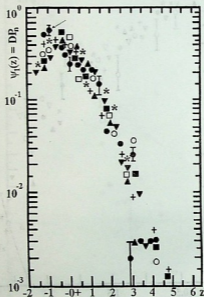


Fig.4. The π -meson distribution, created in A, A_1 -nuclei-nuclei collisions according to the so-called soft scaling (look at expression (6), with the objective of comparison have been given data of \blacktriangledown - pp ($\sqrt{S} = 19.65$ GeV) [14] and of \blacktriangle - e^+e^- -interactions ($\sqrt{S} = 91$ GeV) [8]. * - MgC, o - dTa, \square - HeC, \blacksquare - HeTa, + - CC, \bullet - CTa (at 4.2 GeV/c)



(The straight line in Fig.1 represents the empirical dependence Malhotra-Wroblevski for inelastic interactions in the momentum range of $(4 \div 400)$ AGeV/c [10]). As it has been said above, CTa - interactions (especially at 4.2 GeV/c) deviate from the linear dependence aside of distribution broadening.

Apparently, this broadening is caused (as indicated in [10]) as contribution of interacting nucleons of nucleus-projectile increases in dispersion of fluctuations. The fall of points (dots) of PC and PTa - collisions (at 2.3 GeV/c) apparently is caused by strong absorption of π^- -mesons in target and also by the weak-cascade reproduction at momentum 2.3 AGeV/c [12].

The approximation of $D (< n >)$ -dependence by expression (15), shows that $\alpha = a / b \neq 0$, at least for relativistic energies in favor of modified KNO-scaling (MKNO) (expressions 13 and 14) in comparison with usual KNO-scaling (see expressions (1) and (3)).

The above said is confirmed by comparison of correlations $R_1 = < n > / D$ and $R_2 = (< n > + 0.5) / D$ for π^- -mesons created at AA₁ - collisions (Tab.1, Fig.1; and also [11] and [12]).

The ratio R_1 is changed in interval $(0.6 \div 1.4)$, and R_2 - in interval $(1.4 \div 1.65)$, and practically R_2 is constant and equals ~ 1.50 . In both cases from data are excepted the so-called abnormal dots - PC and PTa (at 2.3 AGeV/c) and CTa (see Table 1).

Distributions by multiplicity of π^- -mesons, created in nuclei-nuclei collisions ((p, d, He, C)(C, Ta) at 2.3 AGeV/c) and in CTa - interactions at 4.2 AGeV/c from the point of view of modified KNO-scaling (formula (14)) are presented in Fig.2.

A direct comparison of our data with that of OCu (at 3.7 AGeV/c), OCu at 60 AGeV/c and OCu at 200 AGeV/c is presented in Fig.3.

It is clear from Figs.2 and 3 that experimental points are located at the same curve for different pairs and energies of colliding nuclei.

On the other hand curves in Figs.2 and 3, essentially differ from the curves of similar distributions for e^+e^- -lepton-lepton and of pp - hadrons-hadrons interactions, obtained in frames of MKNO -scaling (formula (14)) [8].

Table 1.

Expressions $R_1 = \langle n \rangle / D$ and $R_2 = (\langle n \rangle + 0.5) / D$ for π^- -mesons created in $A_1 A_2$ -nuclei-nuclei collisions at momentum per nucleon of 2.3; 4.2; 5.1 GeV/c

Table 1a.

$A_1 A_1$ -collisions at momentum per nucleon of 2.3 GeV/c

	PC	DC	HeC	CC	PTa	DTa	HeTa	CTa
R_1	0.42±0.03	0.64±0.06	0.72±0.06	0.86±0.06	0.40±0.03	0.63±0.06	0.78±0.06	0.82±0.08
R_2	1.80±0.06	1.54±0.10	1.50±0.10	1.45±0.08	1.83±0.06	1.55±0.13	1.42±0.07	1.25±0.10

Table 1b.

$A_1 A_1$ -collisions at momentum per nucleon of 4.2 GeV/c

	PC	dC	HeC	CC	FC	MgC	PTa	dTa	HeTa	CTa
R_1	0.61± ±0.04	0.87± ±0.06	1.09± ±0.07	1.13± ±0.08	1.25± ±0.10	1.36± ±0.12	0.73± ±0.04	0.82± ±0.08	1.20± ±0.10	1.12± ±0.09
R_2	1.54± ±0.10	1.58± ±0.10	1.60± ±0.11	1.51± ±0.11	1.57± ±0.14	1.65± ±0.18	1.53± ±0.08	1.53± ±0.11	1.58± ±0.14	1.28± ±0.11

Table 1c.

 $A_i A_t$ - collisions at momentum per nucleon of 5.1 GeV/c

	dTa	HeTa
R_1	1.13±0.07	1.24±0.08
R_2	1.62±0.11	1.58±0.12

The multiplicity distributions for π^- -mesons according to the weak (soft) scaling (see expression (6)) created at $A_i A_t$ nuclei-nuclei (at 4.2 AGeV/c), e^+e^- (at $\sqrt{S}=91$ GeV) and pp (at $\sqrt{S}=19.65$ GeV) collisions are given in Fig.4 [8, 14].

It is evident that all dots are on same curve, with the exception of CTa -collisions. (Again CTa !) is denoted by the arrows.

Thus, it is possible to make conclusion, that only in the frame of soft KNO-scaling (expression (6)) dots corresponding to the multiplicity in $A_i A_t$ -nuclei-nuclei, pp-nucleon-nucleon and e^+e^- -collision (at substantially different energies) fall to single universal curve.

However, if we were limited only by $A_i A_t$ - nuclei-nuclei collisions, it would be evident that at the energies considered in MKNO variables becomes apparent more clearly gauge-invariant behavior of the multiplicity distribution of the secondary π^- -mesons, than in the framework of usual KNO -scaling (Figs.2 and 3).

This statement is supported by the fact that the parameter α in expression (15) substantially differs from zero.

It should be noted that when speaking about the scaling behavior of multiplicity distribution, we mean the independence of shape of distribution both from the energy of particles and from the mass number of projectile-hadrons and targets.

REFERENCES

1. R. Feinman. Phys. Rev. Lett. **23**, 1969, 1415.
2. Z. Koba et al. Nucl. Phys. **B40**, 1972, 317.
3. O. Czizewski, K. Rybicki, Nucl. Phys. **B47**, 1972, 633.



4. M. Blazek. Z. Phys. C32, 1986, 309.
5. A. Giovanini. Nuovo Cimento. A15, 1973, 543.
6. W. Knox. Phys. Rev. D10, 1974, 65.
7. G. Alner et al. Phys Lett. B167, 1986, 476.
L. Akhobadze et al. Proc. TSU, 337 (35), 2001, 152.
8. A. I. Golokhvastov. KNO-scaling. Preprint JINR, R2-98-181, Dubna, 1998.
9. E. Abdrakhmanov et al. JINR, R1-10779, Dubna, 1977; Sov. J. Nucl. Physics, 27, 1978, 1020.
10. N. Angelov et al. JINR, R1-12281, Dubna, 1979; Sov. J. Nucl. Physics, 30, 1979, 1590.
11. G. Agakishiev et al. Soobshch. JINR, 1-83-22, 1983.
12. N. S. Grigalashvili et al. Sov. J. Nucl. Phys., 48, 1988, 476.
13. M. Anikina et al., JINR, R1-10590, Dubna, 1976; Nucl. Physics. 27, 1976, 724; Aknisenko et al. Nucl. Phys. A348, 1980, 518.
14. E. R. Muradian. Preprint Dubna, JINR, R2-676, 1972 and references in it.

Tbilisi State University

თ. ჯალაღანია, გ. კურატაშვილი, ი. თევზაძე,
გ. ვანიშვილი

რელატიური ბირთვების ურთიერთქმედებაში
დაბადებული დამუხტული მეორადი π^- -მეზონების
მრავლობითობის განაწილების ანალიზი
მოდულირებული KNO-სკეილინგის უარბლებაში

დასკვნა

ნაშრომი მიძღვნილია $(2 \div 200)$ AGeV/c ენერგიის ინტერვალში ბირთვ-ბირთულ ურთიერთქმედებაში დაბადებული π^- -მეზონების მრავლობითობის განაწილების შესწავლისადმი. ანალიზი ჩატარებულია MKNO - მოდიფიცირებული KNO - სკეილინგის ჩარჩოებში. ნაჩვენებია, რომ ბირთვული

- (A₁, A₂), პროტონ-პროტონული - (pp) და ლეპტონ-
ლეპტონური (ელექტრონულ-პოზიტრონული) - (e⁺e⁻)
ურთიერთქმედებებისას საუკეთესოდ მუშაობს ე.წ. რბილი
სკეილინგი.

DOUBLE IONIZATION OF HELIUM-LIKE IONS IN THE METASTABLE STATES BY FAST ELECTRON



P. Defrance^{*}, T. Kereselidze, I. Noselidze, M. Tsulukidze

Accepted for publication April, 2001

ABSTRACT. An asymptotic formula for the total cross section of electron impact double ionization of helium like ions in 2^1S and 2^3S metastable states at high incident energies is derived. The first two coefficients of this formula are found within the framework of the first Born approximation. The model of noninteracting electrons is employed for the description of the ejected electrons.

Double ionization in the various processes occurring at electron-atom and electron-ion collisions is the subject of growing interest. The main attention of both theorists and experimentalists is focused on the electron impact double ionization (DI) of the simplest targets - helium atom and helium-like ions. In these two-electron atomic systems ejection of electrons is realized only through the direct ionization and no intermediate transitions to autoionizing states are involved. The investigation of mentioned processes has particular interest for studying electron-electron correlation both in the bound and continuum states.

Nowadays a great number of theoretical and experimental works, which deal with differential cross sections of DI of helium-like ions, is available [1-8], whereas there are only a few attempts in literature concerning the total cross section [9-12]. Especially theoretical calculations of the total cross sections (TCS) remain scarce [13-15].

In the recent experiments ionization processes are usually measured by means of the crossing beam technique [16]. The electron beam intersects the ion (atom) beam resulting in single and double ionization in the crossing area. The beam of helium atoms and helium-like ions always contains metastable states. In some cases the metastable component content reaches 30% [17]. Due to the long lifetime metastable components easily survive the flight times of the

ions (atoms) from the source to the region of the collision. Consequently, the metastable species participate in ionization processes as well. The good evidence for this is the fact that the TCS of helium-like ions differs from zero even if the incident energy is less than the ground state DI potential [18].

Thus, it is clear that the knowledge of the double ionization TCS of metastable states is highly desired in order to interpret experimental results correctly.

In this paper, we study the double ionization of the two-electron atomic systems He, Li⁺, Be²⁺, B³⁺ by high energy electron impact. Using the first Born approximation we have investigated the asymptotic behaviour of the TCS and calculated the leading term in the asymptotic expansion. The second term of the mentioned expansion has been determined by fitting the asymptotic formula to the TCS obtained earlier numerically [19].

In the present study, we consider the incident electron with energies high enough to employ the first Born approximation: $Z/k_i \ll 1$, where k_i is the wavevector of the incident electron and Z is the charge of target nucleus. So, in the framework of this approximation we can present the initial wave function of the colliding system as a product of a plane wave and a wave function $\Phi_i^{(\pm)}(\vec{r}_1, \vec{r}_2)$ describing the two bound electrons in the singlet or triplet metastable states in helium-like ion

$$\Psi_i^{(\pm)}(\vec{r}, \vec{r}_1, \vec{r}_2) = \frac{e^{i\vec{k}_i \cdot \vec{r}}}{(2\pi)^{3/2}} \Phi_i^{(\pm)}(\vec{r}_1, \vec{r}_2). \quad (1)$$

Here $\vec{r}, \vec{r}_1, \vec{r}_2$ are the position vectors of the incident and the bound electrons, respectively. For $\Phi_i^{(\pm)}(\vec{r}_1, \vec{r}_2)$ we have chosen the Hylleraas-type wave function with radial correlation only

$$\Psi_i^{(\pm)}(\vec{r}_1, \vec{r}_2) = C_i^{(\pm)} \left[\varphi_\alpha(\vec{r}_1) \varphi_\beta(\vec{r}_2) \pm \varphi_\alpha(\vec{r}_2) \varphi_\beta(\vec{r}_1) \right], \quad (2)$$

where

$$\varphi_{\alpha}(\vec{r}) = e^{-\alpha r}, \quad \varphi_{\beta}(\vec{r}) = e^{-\beta r} (1 - \beta r)$$

In (2) and (3) α and β are the variation parameters and $C_i^{(\pm)}$ is a normalization constant. They are calculated in [20].

Supposing that the fast incident electron after the collision remains still sufficiently energetic we describe the scattered electron by a plane wave. As to the two ejected electrons we completely neglect their repulsion and describe them by the double-continuum wave function orthogonalized with respect to the initial state wave function $\Phi_i^{(\pm)}(\vec{r}_1, \vec{r}_2)$:

$$\Psi_f^{(\pm)} = \frac{e^{i\vec{k}_f \vec{r}}}{(2\pi)^{3/2}} \left[\Phi_f^{(\pm)}(\vec{r}_1, \vec{r}_2) - S^{(\pm)} \Phi_i^{(\pm)}(\vec{r}_1, \vec{r}_2) \right], \quad (4)$$

where

$$S^{(\pm)} = \int \Phi_f^{(\pm)*} \Phi_i^{(\pm)} d\vec{r}_1 d\vec{r}_2$$

and

$$\Phi_f^{(\pm)} = \frac{1}{\sqrt{2}} \left(f_{\vec{k}_1}(\vec{r}_1) f_{\vec{k}_2}(\vec{r}_2) \pm f_{\vec{k}_1}(\vec{r}_2) f_{\vec{k}_2}(\vec{r}_1) \right). \quad (5)$$

Here $\vec{k}, \vec{k}_1, \vec{k}_2$ are the wavevectors of the scattered and ejected electrons, respectively, and $f_{\vec{k}}(\vec{r})$ denotes the Coulomb-continuum wave function

$$f_{\vec{k}_j}(\vec{r}) =$$

$$= \frac{1}{(2\pi)^{3/2}} e^{\frac{Z\pi}{2k_j}} \Gamma(1 + iZ/k_j) e^{i\vec{k}_j \vec{r}} F(-iZ/k_j, 1, -i(k_j r + \vec{k}_j \vec{r})) \quad (6)$$

$$V_{int} = -\frac{Z}{r} + \frac{1}{|\vec{r} - \vec{r}_1|} + \frac{1}{|\vec{r} - \vec{r}_2|}$$

as a perturbing potential and using the initial and final state wave functions (1) and (4) for the transition matrix element one can get the following expression:

$$T_{fi}^{(\pm)} = \frac{C_i^{(\pm)}}{\sqrt{2\pi^2 q^2}} \left[I_\alpha(\vec{k}_1) J_\beta(k_2) \pm \right. \\ \left. \pm I_\alpha(\vec{k}_2) J_\beta(k_1) + I_\beta(\vec{k}_1) J_\alpha(k_2) \pm I_\beta(\vec{k}_2) J_\alpha(k_1) \right], \quad (7)$$

where $\vec{q} = \vec{k}_i - \vec{k}_f$ is the momentum transfer. The matrix element $I_\mu(\vec{k}_j)$ describes an amplitude of direct ejection of a bound electron by the incident electron and it can be written as

$$I_\mu(\vec{k}_j) = \frac{1}{(2\pi)^{3/2}} e^{\frac{2k_j}{Z}} \Gamma(1 - iZ/k_j) A_\mu(\vec{k}_j), \quad (8)$$

where

$$A_\mu(\vec{k}_j) = \int e^{-i\vec{k}_j \cdot \vec{r}} F(iZ/k_j, l, i(k_j r + \vec{k}_j \cdot \vec{r})) e^{i\vec{q} \cdot \vec{r}} \varphi_\mu(\vec{r}) d\vec{r}. \quad (9)$$

In (7) the second matrix element $J_\nu(k_k)$ describes ionization of the second target electron due to the sudden change in potential. It can be given as

$$J_\nu(k_j) = \frac{1}{(2\pi)^{3/2}} e^{\frac{2k_j}{Z}} \Gamma(1 - iZ/k_j) B_\nu(k_j), \quad (10)$$

where

$$B_v(k_j) = \int e^{-i\vec{k}_j \vec{r}} F(iZ/k_j, 1, i(k_j r + \vec{k}_j \vec{r})) \varphi_v(\vec{r}) d\vec{r}. \quad (11)$$

In the theory of inelastic processes it is well known that at asymptotically high incident energies collisions between electron and target are mainly accompanied with small momentum transfer. Relying on this fact one can expand $e^{i\vec{q}\vec{r}}$ in (9) in a series. Then keeping the first non-vanishing term only we obtain the following expressions for $A_\alpha(\vec{k}_j)$ and $A_\beta(\vec{k}_j)$ (the dipole approximation):

$$A_\alpha(\vec{k}_j) = -16\pi(k_j - iZ) \frac{Z - 2\alpha}{(\alpha^2 + k_j^2)^3} q \cos(\vec{q}\vec{k}_j) e^{-\frac{Z}{k_j} \text{arctg} \frac{2\alpha k_j}{\alpha^2 - k_j^2}}, \quad (12)$$

$$A_\beta(\vec{k}_j) = -16\pi(k_j - iZ) \frac{q \cos(\vec{q}\vec{k}_j)}{(\beta^2 + k_j^2)^4} e^{-\frac{Z}{k_j} \text{arctg} \frac{2\beta k_j}{\beta^2 - k_j^2}} \times \\ \times \left\{ (Z - 2\beta)(\beta^2 + k_j^2) - 2\beta [5\beta(Z - \beta) - (Z^2 - k_j^2)] \right\} \quad (13)$$

The integration in (11) gives for $B_\alpha(k_j)$ and $B_\beta(k_j)$:

$$B_\alpha(k_j) = -8\pi \frac{Z - \alpha}{(\alpha^2 + k_j^2)^2} e^{-\frac{Z}{k_j} \text{arctg} \frac{2\alpha k_j}{\alpha^2 - k_j^2}}, \quad (14)$$

$$B_\beta(k_j) = -8\pi \frac{1}{(\beta^2 + k_j^2)^3} e^{-\frac{Z}{k_j} \text{arctg} \frac{2\beta k_j}{\beta^2 - k_j^2}} \left\{ (Z - \beta)(\beta^2 + k_j^2) + \right.$$

$$+ \beta \left[2Z^2 - k_j^2 + 3\beta(2Z - \beta) \right] \Big\}$$

The fully (eightfold) differential cross section (FDCS) for double ionization of helium-like ion is determined by the square of modulus of $T_{\beta}^{(\pm)}$:

$$\frac{d^8 \sigma^{(\pm)}}{d\Omega_s d\Omega_1 d\Omega_2 d(k_1^2/2) d(k_2^2/2)} = \frac{(2\pi)^4 k_s k_1 k_2}{k_i} |T_{\beta}^{(\pm)}|^2, \quad (16)$$

where $d\Omega$ is the element of the solid angle surrounding the corresponding wavevector.

If substitute expression (7) in (16) and take into consideration (8), (10) and (12)-(15), we get for the FDSC:

$$\begin{aligned} \frac{d^8 \sigma^{(\pm)}}{d\Omega_s d\Omega_1 d\Omega_2 d(k_1^2/2) d(k_2^2/2)} &= \\ &= \frac{Z^2 C_i^{(\pm)^2} N(k_1, k_2) k_s}{2\pi^4 q^4 k_i} \left[M_{\alpha\beta}^{(\pm)} + M_{\beta\alpha}^{(\pm)} + M_{int}^{(\pm)} \right], \quad (17) \end{aligned}$$

where

$$N(k_1, k_2) = \left[\left(1 - e^{-2\pi Z/k_1} \right) \left(1 - e^{-2\pi Z/k_2} \right) \right]^{-1},$$

$$\begin{aligned} M_{\alpha\beta}^{(\pm)} &= |A_{\alpha}(\bar{k}_1)|^2 |B_{\beta}(k_2)|^2 + |A_{\alpha}(\bar{k}_2)|^2 |B_{\beta}(k_1)|^2 \pm \\ &\pm 2 \operatorname{Re} \left[A_{\alpha}(\bar{k}_1) A_{\alpha}^*(\bar{k}_2) \right] B_{\beta}(k_1) B_{\beta}(k_2), \end{aligned}$$

$$M_{\beta\alpha}^{(\pm)} = |A_{\beta}(\bar{k}_1)|^2 |B_{\alpha}(k_2)|^2 + |A_{\beta}(\bar{k}_2)|^2 |B_{\alpha}(k_1)|^2 \pm$$

$$\pm 2 \operatorname{Re} [A_{\beta}(\bar{k}_1) A_{\beta}^*(\bar{k}_2)] B_{\alpha}(k_1) B_{\alpha}(k_2),$$

$$M_{\alpha\beta\beta\alpha} = 2 \operatorname{Re} [A_{\alpha}(\bar{k}_1) A_{\beta}^*(\bar{k}_2)] B_{\alpha}(k_1) B_{\beta}(k_2) +$$

$$+ 2 \operatorname{Re} [A_{\alpha}(\bar{k}_2) A_{\beta}^*(\bar{k}_1)] B_{\alpha}(k_2) B_{\beta}(k_1) \pm$$

$$\pm 2 \operatorname{Re} [A_{\alpha}(\bar{k}_1) A_{\beta}^*(\bar{k}_1)] B_{\alpha}(k_2) B_{\beta}(k_2) \pm$$

$$\pm 2 \operatorname{Re} [A_{\alpha}(\bar{k}_2) A_{\beta}^*(\bar{k}_2)] B_{\alpha}(k_1) B_{\beta}(k_1).$$

Integration of the FDCS over the solid angles of the ejected electrons $d\Omega_1$ and $d\Omega_2$ leads to the fourfold differential cross section of DI:

$$\frac{d^4\sigma}{d\Omega_1 d(k_1^2/2) d(k_2^2/2)} =$$

$$= \frac{4Z^2 C_i^{(\pm)^2} N(k_1, k_2) k_s [W_{\alpha\beta}^{(0)} + W_{\beta\alpha}^{(0)} + W_{\alpha\beta\beta\alpha}^{(0)}]}{\pi^2 q^2 k_i} \quad (18)$$

with

$$W_{\alpha\beta}^{(0)} = \frac{8(Z^2 + k_1^2)(Z - 2\alpha)^2}{3(Z - \alpha)^2(\alpha^2 + k_1^2)^2} [B_{\alpha}(k_1) B_{\beta}(k_2)]^2 +$$

$$+ \frac{8(Z^2 + k_2^2)(Z - 2\alpha)^2}{3(Z - \alpha)^2(\alpha^2 + k_2^2)^2} [B_{\alpha}(k_2) B_{\beta}(k_1)]^2,$$

$$W_{\beta\alpha}^{(0)} = \frac{8(Z^2 + k_1^2)}{3(Z - \beta)^2(\beta^2 + k_1^2)^2} \{ (Z - 2\beta)(\beta^2 + k_1^2) -$$

$$\begin{aligned}
 & -2\beta \left[5\beta(Z - \beta) - (Z^2 - k_1^2) \right] \left\{ \left[B_\beta^{(0)}(k_1) B_\alpha(k_2) \right]^2 + \right. \\
 & \quad \left. + \frac{8}{3} \frac{(Z^2 + k_2^2)}{(Z - \beta)^2 (\beta^2 + k_2^2)^4} \left\{ (Z - 2\beta)(\beta^2 + k_2^2) - \right. \right. \\
 & \quad \left. \left. - 2\beta \left[5\beta(Z - \beta) - (Z^2 - k_2^2) \right] \right\} \left[B_\beta^{(0)}(k_2) B_\alpha(k_1) \right]^2 \right\}.
 \end{aligned}$$

$$\begin{aligned}
 W_{\alpha\beta\alpha}^{(0)} &= \frac{16}{3} \frac{(Z^2 + k_1^2)(Z - 2\alpha)}{(Z - \alpha)(\alpha^2 + k_1^2)(\beta^2 + k_1^2)^2} \left\{ (Z - 2\beta)(\beta^2 + k_1^2) - \right. \\
 & \quad \left. - 2\beta \left[5\beta(Z - \beta) - (Z^2 - k_1^2) \right] \right\} B_\alpha(k_1) B_\beta^{(0)}(k_1) B_\alpha(k_1) B_\beta(k_2) + \\
 & \quad + \frac{16}{3} \frac{(Z^2 + k_2^2)(Z - 2\alpha)}{(Z - \alpha)(\alpha^2 + k_2^2)(\beta^2 + k_2^2)^2} \left\{ (Z - 2\beta)(\beta^2 + k_2^2) - \right. \\
 & \quad \left. - 2\beta \left[5\beta(Z - \beta) - (Z^2 - k_2^2) \right] \right\} B_\alpha(k_2) B_\beta^{(0)}(k_2) B_\alpha(k_1) B_\beta(k_1).
 \end{aligned}$$

In order to investigate the asymptotic behaviour of the cross sections it is convenient to integrate (18) over the momentum transfer q instead of Ω_s . For this we employ the obvious relation

$$q dq = k_1 k_s \sin \theta_s d\theta_s,$$

and write the twofold differential cross section in the following form:

$$\frac{d^2 \sigma^{(\pm)}}{d(k_1^2/2) d(k_2^2/2)} =$$

$$= \frac{4Z^2 C_i^{(\pm)^2} N(k_1, k_2)}{\pi E_i} \left[W_{\alpha\beta}^{(0)} + W_{\beta\alpha}^{(0)} \pm W_{\alpha\beta\beta\alpha}^{(0)} \right] \int \frac{dq}{q}$$

Here E_i is the incident energy.

The integration in (19) should involve those q only which are close to $q_{min} = k_1 - k_s$. The remaining values of momentum transfer do not contribute to the cross section significantly. Taking in view the asymptotic expansion of q_{min}

$$q_{min} = \frac{I^{2+} + k_1^2/2 + k_2^2/2}{\sqrt{2E_i}} \left[1 + \frac{I^{2+} + k_1^2/2 + k_2^2/2}{4E_i} + \dots \right], \quad (20)$$

where I^{2+} denotes the DI potential, one can easily conclude that the first term in the integral in (19) would be logarithmic with respect to E_i , namely it is equal to $\frac{1}{2} \ln E_i$, the next terms would be proportional to E_i^0, E_i^{-1} , etc.

After integration of (19) over the ejection energies we obtain the asymptotic expansion for the total double ionization cross section

$$\sigma_i^{(\pm)}(E_i \gg I^{2+}) = \frac{2\pi}{E_i} \left(a^{(\pm)} \ln E_i + b^{(\pm)} + \frac{c^{(\pm)}}{E_i} + \dots \right), \quad (21)$$

where the first item can be expressed according to the following formula:

$$a^{(\pm)} = \left[\frac{ZC_i^{(\pm)}}{\pi} \right]^2 \int_0^{k_{1max}} \int_0^{k_{2max}} N(k_1, k_2) \times \\ \times \left[W_{\alpha\beta}^{(0)} + W_{\beta\alpha}^{(0)} \pm W_{\alpha\beta\beta\alpha}^{(0)} \right] k_2 dk_2 k_1 dk_1 \quad (22)$$

In connection with the choice of the upper limits of integration in (22) it should be noted the following: the scheme employed here for the description of the scattered and ejected electrons is valid when $k_s > k_1, k_2$; therefore in (22) we restricted the regions of integration over the ejection energies $k_1^2/2$ and $k_2^2/2$ to $(E_i - I^{2+})/2$ and $(E_i - I^{2+})/2 - k_1^2/2$, respectively, because if we had carried out the integration up to $E_i - I^{2+}$ and $E_i - I^{2+} - k_1^2/2$, it would have been $k_s < k_1, k_2$ in the region from $(E_i - I^{2+})/2$ to $E_i - I^{2+}$. We note also that when energy of the incident electron is large enough, the ignored region cannot bring in an appreciable contribution in the TCS because in this region the momentum transfer q is large. So, in (22) we take

$$k_{1max}^2 = E_i - I^{2+} \quad \text{and} \quad k_{2max}^2 = E_i - I^{2+} - k_1^2 \quad (23)$$

The coefficient $a^{(\pm)}$ given by (22) can be testified comparing the results of the asymptotic formula (21) with the TCS calculated numerically in [19]. For this purpose it is useful to present data in the Bethe-plot form, which shows dependence of $E_i \sigma$ on $\ln E_i$. It is clear that in such a plot the coefficient $a^{(\pm)}$ determines the slope of the plotted curve. Figs. 1 and 2 show that if keep only the first two terms in (21) and select the coefficient $b^{(\pm)}$ in an appropriate way, formula (21) quite well reproduces the numerical data from [19] in the asymptotic region.

In Table 1, we present the values of the coefficient $a^{(\pm)}$ calculated for different targets belonging to the isoelectronic sequence of helium. There we give the fitted values for the $b^{(\pm)}$ coefficients also. It should be noted that in asymptotic expansion (21) the logarithmic term is dominant in contrast to the case of ground state DI cross section [15]. For instance, in the asymptotic region $a \ln E_i$ is approximately 3-4 times as large as b , both for the singlet and triplet metastable states of the He atom.

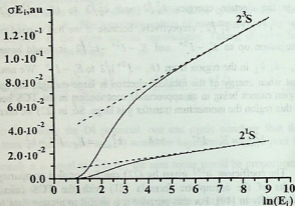


Fig. 1. The total cross sections for electron impact double ionization of the excited He atom in the 2^1S and 2^3S states. The full curves – numerical results obtained in [19], dashed lines – the first two terms in asymptotic formula (21)

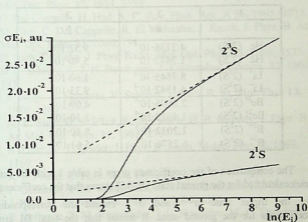


Fig. 2. The total cross sections for electron impact double ionization of the excited Li^+ ion in the 2^1S and 2^3S states. The full curves – numerical results obtained in [19], dashed lines – the first two terms in asymptotic formula (21)

The asymptotic coefficients a and b for different targets from the heliumisoelectronic sequence

1	2	3
	a	b
He (2^1S)	$4.3136 \cdot 10^{-4}$	$9.52 \cdot 10^{-4}$
He (2^3S)	$1.7442 \cdot 10^{-3}$	$5.40 \cdot 10^{-3}$
Li ⁺ (2^1S)	$8.7845 \cdot 10^{-5}$	$1.60 \cdot 10^{-4}$
Li ⁺ (2^3S)	$4.1542 \cdot 10^{-4}$	$9.33 \cdot 10^{-4}$
Be ²⁺ (2^1S)	$2.8995 \cdot 10^{-5}$	$4.09 \cdot 10^{-5}$
Be ²⁺ (2^3S)	$1.4622 \cdot 10^{-4}$	$2.10 \cdot 10^{-4}$
B ³⁺ (2^1S)	$1.2012 \cdot 10^{-5}$	$8.10 \cdot 10^{-6}$
B ³⁺ (2^3S)	$6.2576 \cdot 10^{-5}$	$5.61 \cdot 10^{-5}$

The comparison of the coefficients given in table 1 with the same ones calculated for the ground state DI [15] shows that the coefficients for the triplet state $a^{(-)}$ and $b^{(-)}$ exceed the corresponding coefficients for the ground state. It means that the total DI cross section of helium-like ions from the metastable 2^3S state is larger than the ground state TCS. Taking in view the long life-time of the triplet metastable state (for example, for He $\tau = 7900$ sec [21]) one can conclude that the contribution of the mentioned state in the DI process is significant. Therefore, the consideration of the metastable states seems to be important for the correct interpretation of the experimental data dealing with DI of helium and helium-like ions.

REFERENCES

1. A. Lahmam-Bennani. J. Phys. B: At. Mol. Opt. Phys. **24**, 1991, 2401.
2. A. Duguet, A. Lahmam-Bennani. Z. Phys. **D 23**, 1992, 383.
3. C. Schroter, B. El Marji, A. Lahmam-Bennani, A. Duguet, M. Lecas, L. Spielberger. J. Phys. B: At. Mol. Opt. Phys. **31**, 1998, 131.
4. A. Lahmam-Bennani, I. Taouil, A. Duguet, M. Lecas, L. Avaldi,

- J. Berakdar. *Phys. Rev. A* **59**, 3548, 1999.
4. B. Joulakian, C. Dal Cappello. *Phys. Rev. A* **47**, 1993, 3788.
 5. P. Lamy, C. Dal Cappello, B. Joulakian C. Le Sech. *J. Phys. B: At. Mol. Opt. Phys.* **27**, 1994, 3359.
 6. C. Dal Cappello, H. Had, A. C. Roy. *Phys. Rev. A* **51**, 1995, 3735.
 7. M. Grin, C. Dal Cappello, R. El Mkharter, J. Rasch. *J. Phys. B: At. Mol. Opt. Phys.* **33**, 2000, 131.
 8. B. Nath, C. Sinha. *J. Phys. B: At. Mol. Opt. Phys.* **33**, 2000, 5525.
 9. B. L. Schram, A. J. H. Boerboom, J. Kistemaker. *Physica.* **32**, 1966, 185.
 10. P. Nagy, A. Skutlartz, V. Schmidt. *J. Phys. B: At. Mol. Phys* **13**, 1980, 1249.
 11. M. B. Shah, D. S. Elliot, P. McCallion, H. B. Gilbody. *J. Phys. B: At. Mol. Opt. Phys.* **21**, 1988, 2751.
 12. B. Peart, K. T. Dolder. *J. Phys. B: Atom. Molec. Phys.* **2**, 1969, 1169.
 13. R. I. Tweed. *Z. Phys.* **D23**, 1992, 309.
 14. P. Defrance, T. M. Kereselidze, Z. S. Machavariani, I.L. Noselidze. *J. Phys. B: At. Mol. Opt. Phys.* **33**, 2000, 4323.
 15. P. Defrance, T. M. Kereselidze, I. L. Noselidze, M. P. Tsulukidze. *J. Phys. B: At. Mol. Opt. Phys.* **34**, 2001, 4957.
 16. F. Brouillard, W. Claeys in Book: *Physics of Ion-Ion and Electron - Ion Collisions*. Edited by F. Brouillard and J. W. McGowan (Plenum Press New York and London, 1986).
 17. M. Zamkov, M. Benis, P. Richard, H. Tawara, T. J. M. Zouros XXII-ICPEAC, Int. Conf. on Phot., Electr. and Atomic Collisions July 18-24, 2001, Santa Fe. Abstracts and Contributed Papers. Edited by S. Datz, H. E. Bannister, H. F. Krause, L. H. Saddig, D. Schulte and C.R.Vane 321.
 18. A. Müller, C. Böhme, J. Jacobi, H. Knopp, K. Ariki, S. Schippers XXII-ICPEAC, Int. Conf. on Phot., Electr. and Atomic Collisions, July 18-24, 2001, Santa Fe Abstracts and Contributed Papers. Edited by S. Datz, H.E. Bannister, H F Krause, L.H. Saddig, D. Schulte and C. R. Vane 356.
 19. P. Defrance, T. Kereselidze, I. Noselidze, M. Tsulukidze XXII-ICPEAC, Int. Conf. on Phot., Electr. and Atomic Collisions July 18-24, 2001, Santa Fe. Abstracts and Contributed Papers. Edited by S. Datz, H. E. Bannister, H. F. Krause, L. H. Saddig,



- D. Schulte, C.R.Vane 314.
 20. P. Defrance, T. Kereselidze, I. Noselidze, M. Tsulukidze, Proc. TSU, 337 Physics 35, 2000, 98.
 21. A. A. Radsig, B. M. Smirnov. Parameters of Atoms and Atomic Ions. Handbook. Moscow. 1986 (Russian).

'Universite' Catholique de Louvain, De'partment de Physique,
 Louvain-la-Neuve, Belgium
 Tbilisi State University

პ. დეფრანსი, თ. კერესელიძე, ი. ნოსელიძე, მ. წულუკიძე

მეტასტაბილურ 2^1S და 2^3S მდგომარეობაში მყოფი
 ჰელიუმისმაგვარი იონების სწრაფი ელექტრონებით
 ორჯერადი იონიზაციის

დასკვნა

მიღებულია აღვზნებულ 2^1S და 2^3S მეტასტაბილურ მდგომარეობაში მყოფი ჰელიუმისმაგვარი იონების სწრაფი ელექტრონებით ორჯერადი იონიზაციის სრული განიკვეთების ასიმპტოტიკური ფორმულა. ბორნის პირველ მიახლოებაში გამოთვლილია ამ ფორმულის პირველი ორი კოეფიციენტი. ამოტყორცნილი ელექტრონების ტალღური ფუნქცია აგებულია არაურთიერთქმედ ელექტრონთა მიახლოება.

THE HYDRODYNAMICS EQUATIONS FOR THREE COMPONENT SYSTEM "HELIUM II - POROUS MEDIA" AND ELASTIC COEFFICIENTS



Sh. Kekutia, N. Chkhaidze.

Accepted for publication June, 2001

ABSTRACT. The hydrodynamics equations for helium II - porous media system are deduced. All input coefficients of the theory are determined by physically measured quantities.

1. INTRODUCTION

Flow phenomena in porous media are important to a wide variety of problems and have been studied both theoretically and experimentally for a long time. The study of processes, occurring in porous media, acquires special actuality with the development of low temperature techniques. This topicality becomes more important because of special properties of superfluid helium and peculiarities of porous media. In a series of papers, Biot proposed a simple, semiphenomenological theory of elastic and viscous behavior in porous, macroscopically statistically homogeneous, isotropic, elastic media saturated with a compressible viscous fluid [1]. Because the motion of the solid and fluid parts are followed separately and on equal footing, this theory represents the most general theory possible for two-component porous solid-fluid systems. The theory takes into account the motion of fluid in the interconnected voids of a porous solid. These equations contain a "mass coupling coefficient" which arises from the fact that in a fluid-saturated porous solid the microscopic motion of the porous-fluid is not uniform and in general, is not directed along the macroscopic pressure gradient.

The article aims at extending Biot's theory [1] for the case when the porous media is saturated with helium II. Thus, a three component system is the object of study namely, solid porous media-superfluid helium. Superfluid helium is interesting acoustically because it can support more than one mode, as in ordinary viscous liquid, which gives us the possibility to learn the porous media in details. The task

of the article represents the derivation of hydrodynamics equations for consolidated porous media filled with superfluid He^4 and the determination of all input elastic coefficients of the theory by physically measured quantities without any additional adjustable parameters.

2. RELATIONS BETWEEN STRESS TENSOR AND STRAIN TENSOR

Let us introduce a rectangular system of coordinates and examine the unit cube containing a great number of pores. Under mechanical equilibrium of this picked out volume in the internal part of the system, resultant forces acting on this volume from other parts are equal to zero. Under the deformation the system is getting out from equilibrium state in which it had initially been. In this case forces seeking to return the system to the state of equilibrium appear and these internal forces are called stresses. Also all points of the unit element displace under deformation and by u_x, u_y, u_z we denote the components of the displacement vector of the solid part. Here, this vector is defined here as the displacement of the skeletal frame considered to be uniform and averaged over the element. Similarly, we define displacement vector \vec{U} determining a flow of liquid part of the cube. The normal and tangential stresses of the porous solid-superfluid liquid system can be determined as

$$\begin{pmatrix} \sigma_x + s' + s'' & \tau_z & \tau_y \\ \tau_z & \sigma_y + s' + s'' & \tau_x \\ \tau_y & \tau_x & \sigma_z + s' + s'' \end{pmatrix}, \quad (1)$$

where $\sigma_x, \sigma_y, \sigma_z$ and τ_x, τ_y, τ_z are normal and tangential forces acting on the solid parts of each face of the cube with the following orientation, s' and s'' - forces acting on the liquid part of each face of the cube corresponding to superfluid and normal components of superfluid liquid. Scalars s' and s'' are expressed in the following form

$$s' = -\Phi p^s, s'' = -\Phi p^n.$$

Here $p^s = \rho^s \mu$, $p^s + p^n = p$ [2], where μ is chemical potential, p - liquid pressure and Φ - porosity. Thus, we have taken into consideration the circumstance that existence of pressure gradient is not enough for acceleration of superfluid and normal components of superfluid liquid unlike usual fluid.

Now, following Biot, the strain tensor of solid takes the form

$$\begin{pmatrix} e_x & \frac{1}{2}\gamma_z & \frac{1}{2}\gamma_y \\ \frac{1}{2}\gamma_z & e_y & \frac{1}{2}\gamma_x \\ \frac{1}{2}\gamma_y & \frac{1}{2}\gamma_x & e_z \end{pmatrix}, \quad (3)$$

where

$$e_x = \frac{\partial u_x}{\partial x}, \quad e_y = \frac{\partial u_y}{\partial y}, \quad e_z = \frac{\partial u_z}{\partial z},$$

$$\gamma_x = \frac{\partial u_y}{\partial z} + \frac{\partial u_z}{\partial y}, \quad \gamma_y = \frac{\partial u_x}{\partial z} + \frac{\partial u_z}{\partial x}, \quad \gamma_z = \frac{\partial u_x}{\partial y} + \frac{\partial u_y}{\partial x}.$$

Due to two possible types of motion in He II, \bar{U} breaks down into the sum of two parts

$$\bar{U} = \frac{\rho^s}{\rho} \bar{U}^s + \frac{\rho^n}{\rho} \bar{U}^n, \quad (4)$$

corresponding to displacement of superfluid and normal components. Thus the strain in fluid is defined by the dilatation

$$\epsilon = \frac{\rho^s}{\rho} \nabla \bar{U}^s + \frac{\rho^n}{\rho} \nabla \bar{U}^n.$$

Let us establish relations between the components of stress tensor and strain tensor that have been defined above. We shall digress from dissipative forces and admit that the examined system is in equilibrium state. In this case any deformation is deviation from the state with minimum potential energy. Therefore, in the first approach, potential energy is a positive certain quadratic form

$$2E_p = \sigma_x e_x + \sigma_y e_y + \sigma_z e_z + \tau_x \gamma_x + \tau_y \gamma_y + \tau_z \gamma_z + s' \epsilon^s + s'' \epsilon^n \quad (6)$$

here eight components of stress tensor $\sigma_x, \sigma_y, \sigma_z, \tau_x, \tau_y, \tau_z, s', s''$ are linear combinations of eight components of strain tensor $e_x, e_y, e_z,$

$\gamma_x, \gamma_y, \gamma_z, \epsilon^s, \epsilon^n$. Linear relations between 8 strains and 8 independent stresses (Hook's law) are defined by elastic modulus of 64 components. Vica versa, strain as a function of stress is expressed with the help of 8 relations, also containing 64 coefficients, which are called elastic constants. As potential energy is a real quantity, these coefficients are to be symmetric. Thus, for the most common case with least symmetry only 36 independent elasticity moduli are left. Further simplification will be initiated on the basis of studying the statistically isotropic system. For example, let's examine the relation

$$\begin{aligned} \sigma_x = & a_{11} e_x + a_{12} e_y + a_{13} e_z + a_{14} \gamma_x + \\ & + a_{15} \gamma_y + a_{16} \gamma_z + a_{17} \epsilon^s + a_{18} \epsilon^n. \end{aligned} \quad (7)$$

From the statistically isotropy of the system which is being studied it follows that all directions are equal in it, therefore, $a_{12} = a_{13}$, and it expresses the fact that equal deformation of solid body in y and z directions cause equal stresses in x -direction. Also $a_{14} = a_{15} = a_{16} =$

$= 0$, i.e. stresses in x -direction should not cause shears. According to analogous speculations $a_{11} = a_{22} = a_{33}$, $a_{44} = a_{55} = a_{66}$.

Thus, relations between stress and strain on this stage have the form

$$\sigma_x = (a_{11} - a_{12})e_x + a_{12}e + a_{17}\epsilon^s + a_{18}\epsilon^n,$$

$$\sigma_y = (a_{11} - a_{12})e_y + a_{12}e + a_{17}\epsilon^s + a_{18}\epsilon^n,$$

$$\sigma_z = (a_{11} - a_{12})e_z + a_{12}e + a_{17}\epsilon^s + a_{18}\epsilon^n,$$

$$\tau_x = a_{44}\gamma_x, \tau_y = a_{44}\gamma_y, \tau_z = a_{44}\gamma_z, \quad (8)$$

$$s' = a_{17}e + a_{77}\epsilon^s + a_{78}\epsilon^n,$$

$$s'' = a_{18}e + a_{78}\epsilon^s + a_{88}\epsilon^n,$$


where $e = e_x + e_y + e_z$ characterizes the total volume dilatation as a result of strain and it is invariant. Composition of the rest invariant from $\sigma_x, \sigma_y, \sigma_z, \tau_x, \tau_y, \tau_z$ establishes connection between $(a_{11} - a_{22})$ and a_{44} . Really we can write

$$\sigma_x^2 + \sigma_y^2 + \sigma_z^2 + 2(\tau_x^2 + \tau_y^2 + \tau_z^2) = inv \quad (9)$$

and

$$e_x^2 + e_y^2 + e_z^2 + 2\left[\left(\frac{1}{2}\gamma_x\right)^2 + \left(\frac{1}{2}\gamma_y\right)^2 + \left(\frac{1}{2}\gamma_z\right)^2\right] = inv. \quad (10)$$

Using (8) we obtain



$$\sigma_x^2 + \sigma_y^2 + \sigma_z^2 = (a_{11} - a_{12})^2 (e_x^2 + e_y^2 + e_z^2) + 2(a_{11} - a_{12})(e_x + e_y + e_z)B + 3B, \quad (11)$$

where

$$B = a_{12}e + a_{17}\varepsilon^s + a_{18}\varepsilon^n = inv$$

$$\text{and} \quad 2(\tau_x^2 + \tau_y^2 + \tau_z^2) = 2a_{44}^2(\gamma_x^2 + \gamma_y^2 + \gamma_z^2). \quad (12)$$

Taking into account that $e_x + e_y + e_z = inv$

$$(a_{11} - a_{12})^2 (e_x^2 + e_y^2 + e_z^2) + 2a_{44}^2(\gamma_x^2 + \gamma_y^2 + \gamma_z^2) = inv. \quad (13)$$

Considering (10) and (13) we make a conclusion that $a_{11} - a_{12} = 2a_{44}$.

Thus, introducing the notation

$$a_{44} = N, a_{12} = A, a_{17} = Q^s, a_{18} = Q^n, a_{77} = R^s, a_{88} = R^n, a_{78} = R^{sn},$$

we write instead of (8)

$$\sigma_x = 2Ne_x + Ae + Q^s\varepsilon^s + Q^n\varepsilon^n,$$

$$\sigma_y = 2Ne_y + Ae + Q^s\varepsilon^s + Q^n\varepsilon^n,$$

$$\sigma_z = 2Ne_z + Ae + Q^s\varepsilon^s + Q^n\varepsilon^n,$$

$$\tau_x = N\gamma_x, \quad \tau_y = N\gamma_y, \quad \tau_z = N\gamma_z, \quad (14)$$

$$s' = Q^s e + R^s \varepsilon^s + R^{sn} \varepsilon^n,$$

$$s^n = Q^n e + R^n \varepsilon^n + R^{sn} \varepsilon^s.$$

Because of the fact that superfluid and normal part of He II cannot be divided physically and there is no sense to speak about belonging of some atoms to superfluid or normal components, the following relation is to be fulfilled

$$Q^s \varepsilon^s + Q^n \varepsilon^n = Q \varepsilon \quad (15)$$

from this it follows that

$$Q^s = \frac{\rho^s}{\rho} Q, \quad Q^n = \frac{\rho^n}{\rho} Q,$$

$$s^s + s^n = (Q^s + Q^n) \varepsilon + (R^s + R^{sn}) \varepsilon^s + (R^n + R^{sn}) \varepsilon^n = Q \varepsilon + R \varepsilon. \quad (16)$$

Respectively, the strain in the normal and superfluid components of He II is $\varepsilon^s = \text{div} \vec{U}^s$ and $\varepsilon^n = \text{div} \vec{U}^n$. We notice that the strain in the fluid ε is given by

$$\varepsilon = \frac{\rho^s}{\rho} \varepsilon^s + \frac{\rho^n}{\rho} \varepsilon^n. \quad (17)$$

The coefficients A and N correspond to the well-known Lamé coefficients in the theory of elasticity and are positive. The coefficients Q and R are the familiar Biot's coefficients [3]. $R^s (R^n)$ is a measure of strain, which arises in the superfluid (normal) component during unit deformation of superfluid (normal) component without compression the normal (superfluid) component and porous solid. R^{sn} defines the strain, which arises in the normal (superfluid) component during unit deformation of superfluid (normal) component without compression the normal (superfluid) component and porous media.

Now we discuss some experiments which may be used to relate generalized elastic coefficients of the theory to the directly measurable coefficients: the bulk modulus of fluid K_f , the bulk modulus of solid K_s , the bulk modulus of the skeletal frame K_b and N .

The first case corresponds to theunjacketed compressibility, when a sample of the porous solid is immersed in a superfluid liquid to which a pressure p' is applied. Under the action of pressure liquid penetrates the pores completely and the dilations of the porous solid e and liquids ϵ are measured. Unjacketed elastic coefficients of solid and fluid are determined by

$$\frac{1}{K_s} = -\frac{e}{p'}, \quad \frac{1}{K_f} = -\frac{\epsilon}{p'} \quad (18)$$

and from (14) we have

$$\sigma_x = \sigma_y = \sigma_z = -(1 - \Phi)p',$$

$$s' = -\Phi \frac{\rho^s}{\rho} p', \quad (19)$$

$$s'' = -\Phi \frac{\rho^n}{\rho} p'.$$

Also we take into account the following conditions $\epsilon^s = \epsilon^n = \epsilon$. So, relations (19) transform into

$$\frac{2}{3} Ne + Ae + Q\epsilon = -(1 - \Phi)p',$$

$$\frac{\rho^s}{\rho} Q\epsilon + (R^s + R^n)\epsilon = -\Phi \frac{\rho^s}{\rho} p', \quad (20)$$

$$(15) \quad \frac{\rho^n}{\rho} Q \epsilon + (R^n + R^{sn}) \epsilon = -\Phi \frac{\rho^n}{\rho} P'$$

Two latter equations give

$$R^s + R^{sn} = K_f \frac{\rho^s}{\rho} \left(\Phi - \frac{Q}{K_f} \right),$$

$$(16) \quad R^n + R^{sn} = K_f \frac{\rho^n}{\rho} \left(\Phi - \frac{Q}{K_f} \right).$$

In the second situation or in the jacketed compressibility test the porous solid is enclosed in a thin impermeable jacket and then subjected to an external fluid pressure p' . The superfluid liquid inside the jacket should pass through a tube communicated with the superfluid liquid reservoir to insure constant internal fluid pressure, so $\epsilon^s = \epsilon^n = \epsilon$. In this case we determine the bulk modulus of the skeletal frame

$$(17) \quad \frac{1}{K_b} = -\frac{e}{p'}$$

and we have relations

$$\sigma_x = \sigma_y = \sigma_z = -p',$$

$$s' = s'' = 0,$$

or

$$(18) \quad \left(\frac{2}{3} N + A \right) \frac{1}{K_b} - Q \frac{\epsilon}{p'} = 1,$$

$$\frac{\rho^s}{\rho K_b} Q - (R^s + R^{sn}) \frac{\varepsilon}{p'} = 0,$$

$$\frac{\rho^n}{\rho K_b} Q - (R^n + R^{sn}) \frac{\varepsilon}{p'} = 0,$$

from which it follows

$$\rho^n (R^s + R^{sn}) = \rho^s (R^n + R^{sn}). \quad (25)$$

It is not difficult to show from (20), (21) and (24) that

$$Q = \frac{\Phi K_s \left(1 - \Phi - \frac{K_b}{K_s} \right)}{1 - \Phi + \Phi \frac{K_s}{K_f} - \frac{K_b}{K_s}}, \quad (26)$$

$$\frac{2}{3} N + A = K_s \frac{(1 - \Phi) \left(1 - \Phi - \frac{K_b}{K_s} \right) + \Phi \frac{K_s}{K_f}}{1 - \Phi + \Phi \frac{K_s}{K_f} - \frac{K_b}{K_s}}.$$

In the third situation the jacket is communicated with reservoir by the superleak. Therefore only superfluid component pours into reservoir and because

$$\sigma_x = \sigma_y = \sigma_z = -(1 - \Phi) p',$$

$$s' = 0, \quad (27)$$

$$s^* = -\Phi p',$$

$$\left(\frac{2}{3}N + A\right)e + \frac{\rho^s}{\rho} Q \epsilon^s + \frac{\rho^n}{\rho} Q \epsilon^n = -(1 - \Phi)p',$$

$$\frac{\rho^s}{\rho} Q e + R^s \epsilon^s + R^{sn} \epsilon^n = 0, \quad (28)$$

$$\frac{\rho^n}{\rho} Q e + R^n \epsilon^n + R^{sn} \epsilon^s = -\Phi p'.$$

Here, as we have not the relation between ϵ^s and ϵ^n , we should utilize the conservation laws of mass and entropy. Then we have

$$\epsilon^s - \epsilon^n = \frac{Cp'}{\rho^s \sigma^2 T}, \quad (29)$$

where C and σ are the specific heat and entropy per unit mass of He II respectively.

We find the sought expressions

$$R^{sn} = \frac{\rho^s \rho^n}{\rho^2} R - \frac{\Phi (\rho^s)^2 T \sigma^2}{\rho C},$$

$$R^s = \frac{(\rho^s)^2}{\rho^2} R + \frac{\Phi (\rho^s)^2 T \sigma^2}{\rho C}, \quad (30)$$

$$R^n = \frac{(\rho^n)^2}{\rho^2} R + \frac{\Phi (\rho^s)^2 T \sigma^2}{\rho C},$$

where Biot-Willis coefficient R is equal to

$$R = \frac{\Phi^2 K_s}{1 - \Phi + \Phi \frac{K_s}{K_f} - \frac{K_b}{K_s}}$$

At the end we notice that K_f , K_s , K_b and N are directly measurable coefficients.

3. EQUATIONS OF MOTION

To establish relation between stresses and accelerations in the absence of dissipative forces let's use generally acknowledged LaGrange formalism. To make sought equations we find the expression of kinetic energy and determine them according to the given generalized forces. We assume that pores have fewer dimensions as compared with dimensions of the unit cube of the system, which we consider to be an element. Also, we assume that dimensions of the element of the system are less than the wavelength of the wave. This assumption restricts upper possible values of frequencies and gives a possibility to examine a field of microscopic velocities as a function of nine averaged velocities of liquid and solid ignoring liquid viscosity. Naturally, we choose nine averaged displacement components of the solid and the fluid as the generalized coordinates of the system, i.e., respectively $u_x, u_y, u_z, U_x^s, U_y^s, U_z^s, U_x^n, U_y^n, U_z^n$. As a result kinetic energy T of the system per unit volume takes the following form:

$$2T = \rho_{11} \left[\left(\frac{\partial u_x}{\partial t} \right)^2 + \left(\frac{\partial u_y}{\partial t} \right)^2 + \left(\frac{\partial u_z}{\partial t} \right)^2 \right] + 2\rho_{12} \left[\frac{\partial u_x}{\partial t} \frac{\partial U_x^s}{\partial t} + \frac{\partial u_y}{\partial t} \frac{\partial U_y^s}{\partial t} + \frac{\partial u_z}{\partial t} \frac{\partial U_z^s}{\partial t} \right] +$$

$$\begin{aligned}
 & + 2\rho_{12}^n \left[\frac{\partial u_x}{\partial t} \frac{\partial U_x^n}{\partial t} + \frac{\partial u_y}{\partial t} \frac{\partial U_y^n}{\partial t} + \frac{\partial u_z}{\partial t} \frac{\partial U_z^n}{\partial t} \right] + \\
 & + 2\rho_{22}^s \left[\left(\frac{\partial U_x^s}{\partial t} \right)^2 + \left(\frac{\partial U_y^s}{\partial t} \right)^2 + \left(\frac{\partial U_z^s}{\partial t} \right)^2 \right] + \\
 & + 2\rho_{22}^n \left[\left(\frac{\partial U_x^n}{\partial t} \right)^2 + \left(\frac{\partial U_y^n}{\partial t} \right)^2 + \left(\frac{\partial U_z^n}{\partial t} \right)^2 \right].
 \end{aligned} \tag{32}$$

Expression (32) suggests statistical isotropy of the system.

Let us inquire into nature of mass coefficients in expression (32). As kinetic energy is a positive definite quadratic form mass coefficients satisfy the following inequality:

$$\begin{aligned}
 & \rho_{11} > 0, \quad \rho_{22}^s > 0, \quad \rho_{22}^n > 0, \\
 & \begin{vmatrix} \rho_{11} & \rho_{12}^s \\ \rho_{12}^s & \rho_{22}^s \end{vmatrix} > 0, \quad \begin{vmatrix} \rho_{11} & \rho_{12}^n \\ \rho_{12}^n & \rho_{22}^n \end{vmatrix} > 0, \\
 & \begin{vmatrix} \rho_{11} & \rho_{12}^s & \rho_{12}^n \\ \rho_{12}^s & \rho_{22}^s & 0 \\ \rho_{12}^n & 0 & \rho_{22}^n \end{vmatrix} > 0.
 \end{aligned} \tag{33}$$

Let us assume that there is no relative motion between solid and liquid as well as between components of liquid $u_x = U_x^s = U_x^n$ (we examine motion in x -direction without loss of generality). Then proceeding from (32) we have:

$$\rho_{sys} = \rho_{11} + \rho_{22}^s + \rho_{22}^n + 2(\rho_{12}^s + \rho_{12}^n), \quad (34)$$

where ρ_{sys} represents the total mass of the superfluid-solid system per unit volume. If we denote density of a solid with ρ_{sol} , we have:

$$\rho_{sys} = \rho_{sol}(1 - \Phi) + \rho\Phi = \rho_{sol} + \Phi(\rho - \rho_{sol}). \quad (35)$$

With q_x denoting total force acting on a solid part of unit volume and by Q_x^s and Q_x^n , correspondingly total forces acting on superfluid and normal components per unit volume, LaGrange's equations have the following form:

$$\frac{\partial}{\partial t} \left(\frac{\partial T}{\partial \dot{u}_x} \right) = \frac{\partial^2}{\partial t^2} (\rho_{11} u_x + \rho_{12}^s U_x^s + \rho_{12}^n U_x^n) = q_x,$$

$$\frac{\partial}{\partial t} \left(\frac{\partial T}{\partial \dot{U}_x^s} \right) = \frac{\partial^2}{\partial t^2} (\rho_{12}^s u_x + \rho_{22}^s U_x^s) = Q_x^s, \quad (36)$$

$$\frac{\partial}{\partial t} \left(\frac{\partial T}{\partial \dot{U}_x^n} \right) = \frac{\partial^2}{\partial t^2} (\rho_{12}^n u_x + \rho_{22}^n U_x^n) = Q_x^n.$$

Let us write Newton's equation for superfluid and normal components:

$$\Phi \rho^s \frac{\partial^2 U_x^s}{\partial t^2} = Q_x^s, \quad (37)$$

$$\Phi \rho^n \frac{\partial^2 U_x^n}{\partial t^2} = Q_x^n.$$

Comparison of equation (37) with equations (34) and (36) and taking into account conditions $u_x = U_x^s = U_x^n$ gives

$$\Phi \rho^s = \rho_{22}^s + \rho_{12}^s, \quad \Phi \rho^n = \rho_{22}^n + \rho_{12}^n, \quad (38)$$

$$(1 - \Phi) \rho_{sol} = \rho_{11} + \rho_{12}^s + \rho_{12}^n.$$

Coefficients ρ_{12}^s and ρ_{12}^n are mass parameters of "coupling" between a solid and correspondingly, superfluid and normal components of liquid or the term $\rho_{12}^{s(n)}$ describes the inertial (as opposed to viscous) drag that the fluid exerts on the solid as the latter is accelerated relative to the former and vice versa. It is vividly seen if we examine the case when averaged displacement of both components of superfluid liquid are zero: $U_x^s = U_x^n = 0$. Then Equations (36) take the following form:

$$\frac{\partial^2 \rho_{11} u_x}{\partial t^2} = q_x, \quad \frac{\partial^2 \rho_{12}^s u_x}{\partial t^2} = Q_x^s, \quad \frac{\partial^2 \rho_{12}^n u_x}{\partial t^2} = Q_x^n. \quad (39)$$

Equations (39) show that when a solid is accelerated, the force $Q_x^s(Q_x^n)$ acting on superfluid (normal) component of liquid retards it. It is characterized by coefficients ρ_{12}^s, ρ_{12}^n . As Q_x^s and Q_x^n act against acceleration of a solid, then

$$\rho_{12}^s < 0, \quad \rho_{12}^n < 0. \quad (40)$$

The first equation (39) shows that ρ_{11} is total effective density of the solid moving in the Hell. It consists of the solid own density $(1 - \Phi)\rho_{sol}$ and additional mass ρ_a due to the fluid, so

$$\rho_{11} = (1 - \Phi)\rho_{sol} + \rho_a \quad (41)$$

The third relation from Equation (38) gives

$$\rho_a = -\rho_{12}^s - \rho_{12}^n = \rho_a^s + \rho_a^n \quad (42)$$

Finally we have:

$$\begin{aligned} \rho_{11} &= (1 - \Phi)\rho_{sol} + \rho_a^s + \rho_a^n, & \rho_a^s &= -\rho_{12}^s > 0, \\ \rho_{22}^s &= \Phi\rho^s + \rho_a^s, & \rho_a^n &= -\rho_{12}^n > 0, \\ \rho_{22}^n &= \Phi\rho^n + \rho_a^n. \end{aligned} \quad (43)$$

By analogy with [4], for the induced mass tensor per unit volume we introduce the determination

$$\rho_{12}^{s(n)} = -(\alpha_\infty - 1)\Phi\rho^{s(n)}, \quad (44)$$

where $\alpha_\infty \geq 1$ is a purely geometrical quantity independent of solid or fluid densities and it can vary from unit (for straight pores parallel to the motion) to infinity for isolated pores or pores perpendicular to the motion. Coefficients ρ_{11} , ρ_{22}^s , ρ_{22}^n , ρ_{12}^s , ρ_{12}^n that have been determined according to relation (35-43) ensure positive definite quadratic form of kinetic energy (32).

Expressing force components through stress tensor

$$q_x = \frac{\partial \sigma_x}{\partial x} + \frac{\partial \tau_z}{\partial y} + \frac{\partial \tau_y}{\partial z}, \quad Q_x^s = \frac{\partial s'}{\partial x}, \quad Q_x^n = \frac{\partial s''}{\partial x} \quad (45)$$

we obtain the dynamic equations

$$\frac{\partial \sigma_x}{\partial x} + \frac{\partial \tau_z}{\partial y} + \frac{\partial \tau_y}{\partial z} = \frac{\partial^2}{\partial t^2} (\rho_{11}^s u_x + \rho_{12}^s U_x^s + \rho_{12}^n U_x^n),$$

$$\frac{\partial s'}{\partial x} = \frac{\partial^2}{\partial t^2} (\rho_{22}^s U_x^s + \rho_{12}^s u_x), \quad (46)$$

$$\frac{\partial s''}{\partial x} = \frac{\partial^2}{\partial t^2} (\rho_{22}^n U_x^n + \rho_{12}^n u_x).$$

We shall have analogous equations for y, z directions. Equations for elastic waves are received from (45) expressing stress tensor through strain tensor. For three-dimensional case we have:

$$N \nabla^2 \bar{u} + (A + N) \text{grade} + \frac{\rho^s}{\rho} Q \text{grade}^s + \frac{\rho^n}{\rho} Q \text{grade}^n =$$

$$\frac{\partial^2}{\partial t^2} (\rho_{11} \bar{u} + \rho_{12}^s \bar{U}^s + \rho_{12}^n \bar{U}^n),$$

$$\frac{\rho^s}{\rho} Q \text{grade} + R^s \text{grade}^s + R^{sn} \text{grade}^n = \frac{\partial^2}{\partial t^2} (\rho_{12}^s \bar{u} + \rho_{22}^s \bar{U}^s), \quad (47)$$

$$\frac{\rho^n}{\rho} Q \text{grade} + \frac{\rho^n}{\rho} R^n \text{grade}^n + R^{sn} \text{grade}^s = \frac{\partial^2}{\partial t^2} (\rho_{12}^n \bar{u} + \rho_{22}^n \bar{U}^n).$$

In equation (47) we ignored dissipative processes. In our case the slipping of normal component of superfluid liquid with respect to the pores walls is the main mechanism of dissipation. In most cases velocities of macroscopic motion are so low that dissipation is marginal. Such almost reversible processes might be described with the help of dissipate function. It means that the so-called dissipative forces or frictional forces, which are linear functions of velocities, are

to be added to the non-dissipative equations of motion, where only the forces acting on the system have been taken into account. These forces might be presented in the form of derivatives by generalized velocities or by the form of the dissipative function. Then by analogy with Biot [1] about dissipative terms for the equations of solid and normal component motions we have:

$$\frac{\partial^2}{\partial t^2} (\rho_{11} \bar{u} + \rho_{12}^s \bar{U}^s + \rho_{12}^n \bar{U}^n) + bF(\omega) \frac{\partial}{\partial t} (\bar{u} - \bar{U}^n) =$$

$$= N \nabla^2 \bar{u} + (A + N) \text{grade} +$$

$$\frac{\rho^s}{\rho} Q \text{grade}^s + \frac{\rho^n}{\rho} Q \text{grade}^n \quad (48)$$

$$\frac{\partial^2}{\partial t^2} (\rho_{22}^n \bar{U}^n + \rho_{12}^n \bar{u}) - bF(\omega) \frac{\partial}{\partial t} (\bar{u} - \bar{U}^n) =$$

$$= \frac{\rho^n}{\rho} Q \text{grade} + R^n \text{grade}^n + R^{sn} \text{grade}^s.$$

Complex quantity $F(\omega)$ describes the deviation from Poiseuille flow at finite frequencies. The coefficient $b = \eta \Phi^2 / k_0$ is the ratio of total friction force to the average normal fluid velocity, where η is the fluid viscosity and k_0 is the permeability.

Therefore, the hydrodynamics equations for helium II - porous media system are deduced. All input elastic coefficients of the theory are determined by physically measured quantities. The obtained equations can apply for learning propagation of waves in helium II - porous media system in high and low frequency limits.

REFERENCES

1. M. A. Biot, J. Acoust. Soc. Am. 28, 1956, 168; 28, 1956, 179.
2. S. Putterman. Superfluid Hydrodynamics. New York, 1974.
3. M. A. Biot, D.G. Willis. J. Appl. Mech. 24, 1957, 594.
4. J.G. Berryman. Appl. Phys.Lett., 37, 1980, 382m.

Georgian Academy of Sciences
Institute of Cybernetics

შ. კეკელიძე, ნ. ჩხაიძე

სამკომპონენტური სისტემის "ჰელიუმ II - ფოროვანი გარემო" ჰიდროდინამიკის განტოლებები და მათში შემავალი კოეფიციენტები

დასკვნა

ლაგრანჟის ფორმალიზმის გამოყენებით გამოყვანილია სამკომპონენტური სისტემის "ჰელიუმ II - ფოროვანი გარემო" ჰიდროდინამიკის განტოლებები. მხედველობაში მიიღება როგორც სითხის, ასევე ფოროვანი გარემოს მოძრაობა. განტოლებებში შემავალი ფორმალური კოეფიციენტები გამოსახულია კარგად ცნობილი ფიზიკური შინაარსის მქონე გაზომვადი ფიზიკური სიდიდეებით. მიღებული განტოლებები შესაძლებელია გამოვიყენოთ განხილულ სისტემაში ბგერების გავრცელების შესასწავლად მაღალ-სიხშირულ და დაბალსიხშირულ ზღვრებში.

R. Kokhreidze, S. Odenov, J. Sanikidze

Accepted for publication May, 2001

ABSTRACT. In this article percolation processes of the superconducting composite ceramics $(YBa_2Cu_3O_{7.8})_x(Y_2BaCuO_5)_{1-x}$ are investigated. The three-layer structure is fabricated. Between two HTSC regions there is a layer consisting of the composite near the edge of the percolation limit. We have studied I and II Josephson effects in these structures. The current-voltage characteristics of the sample are durable and stable.

The research of percolation processes was fulfilled in the $(YBa_2Cu_3O_{7.8})_x(Y_2BaCuO_5)_{1-x}$ composition. The purpose of this study was to get the information about the limit concentration of superconducting phase in the samples and to clear up the question of connection percolation processes with Josephson contact phenomena.

It is known, that the classical percolation theory does not take into consideration such quantum effects as Josephson effect, quantization of flux, the proximity effect [1-2], etc. As it was shown in the previous research, the percolation in superconductors exists when the superconducting phase concentration is more than critical, which can be explained by classical processes and coincides quantitatively with the percolation theory. This value is equal to nearly 18% for the classical model and is acknowledged by the experiments both for the classical conducting and for the superconducting systems [3, 4]. In the last case there exist quantum effects, which bring some additional peculiarities. As it seems, these processes don't alter noticeably the critical concentration value, because this value, obtained in experiment in the above-mentioned system, practically coincides with the one, predicted by classical model [5].

On the other hand, the quantum properties, though they don't influence visibly on the critical concentration value, lead to a sequence of new effects in such a system. With the change of superconducting phase concentration in the $YBa_2Cu_3O_{7.5}$ system from the maximal to

critical one its diamagnetic contribution decreases, which affects the magnetic susceptibility value in the crossed magnetic fields [6]. This method was chosen to avoid the complications, connected with the sample heating by the strong alternative fields, and also because of the necessity to suppress the weak influence of links during the measurements. The results are shown in Fig.1. (The mass concentration χ_{sm} can be obtained by the volume concentration counting over from the known values of both phases densities). Some discrepancy between the concentration values and the initial superconducting phase quantity can be explained both by the existence of some impurity in the initial phase and by the chemical interaction between the two phases, so the initial superconducting phase is then somewhat reduced. When the phase is reduced by these two factors below the percolation limit, the critical current is decreased to zero, the value of critical concentration of superconducting phase being very near to the one obtained from the classical model [3]. The experimental error of χ_{cv} is determined by the appliance accuracy and is less than 1%.

When the concentration is near to the critical one, the quantity of weak links between superconducting grains is rapidly decreasing, so at first there are two or three weak links (which is analogous to superconducting interferometer) and then only one weak link (Josephson contact). There is a big probability for superconducting current to exceed the critical value in this region, and simultaneously it can be less than critical in the other regions. When the current exceeds the critical value there is a resistive state of the contact (weak link), so it acts as the analogue of Josephson contact.

For fulfillment of these conditions in the most part of samples it is necessary to observe some requirements — concentrations correlation in the initial components mixture, the processing regime, etc. The samples obtained in this way have rather good Josephson qualities, that are the required values of critical currents, rather steep voltage-current characteristics, steps on the characteristics at the external radio-frequency radiation and interference picture for critical current dependence (or contact voltage) on magnetic field.

Usually the samples consist of three layers — two HTSC layers on the outside and composite layer in the middle. There were fulfilled 34 series of sample producing and measuring (16 samples in each),

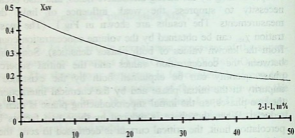


Fig. 1. The dependence of magnetic susceptibility of the composite on the dielectric mass %

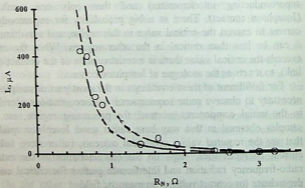


Fig. 2. The critical current dependence on the contact normal resistance

with rather long thermal processing, measuring critical currents and voltage-current characteristics, dependences on magnetic field, etc.

The main purpose of the research was to get satisfactory Josephson contacts, with rather high parameters, such as steepness of voltage-current characteristics, stability, reproducibility of properties, possibility of critical current regulation during the processing, the mechanical firmness, independence of the critical current on the repeated cooling up to liquid nitrogen temperature, the absence of chemical reaction between the two phases. In the result of this research there was worked out technology of Josephson junctions production with high enough technical parameters. The statistical correlation between critical currents and contacts resistivities in the normal state (at room temperature) is presented in Fig.2. The statistical deviation of experimental dots is determined by the difference of critical currents of different sample.

This dependence can be described by the approximate relation $I_c(\mu A) \cong (100 \div 200)R_n^3$. Some of the observed voltage-current characteristics are presented in Fig.3. All of the samples have good stability during the influence of such factors as the temperature change, chemical reactions in the air, water, etc., which allow to con-

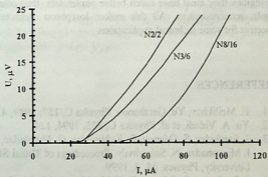


Fig.3. The contact voltage – current dependence for different samples

sider their possible application. An experimental error is determined by the electromagnetic and thermal fluctuations and is of the order 1%.

The obtained Josephson contacts during the ultra-high frequencies radiation have the steps on the voltage-current characteristics at the voltages $U = h\nu/2e$, where ν is frequency, h -Planck's constant, $2e$ -Cooper pair charge, which is specific for Josephson effect. At weak magnetic fields the contacts show interference, that is the critical current and contact voltage dependence on magnetic field of the interference picture type, which is specific for Josephson contacts [7].

The other applications of the percolation effect in the applied superconductivity are connected with the possibility of the strong enhancement of the electrical resistivity of the samples with percolation but still superconducting. Such samples can find an application in different non-linear devices, for example, the direct current transformers, etc.

The application of Josephson contacts can be used in the high-frequency mixers, low-noise amplifiers, spectrometers, and receivers in the infrared and ultra-high frequency regions. Because of the peculiarities of the quantum properties of the Josephson junctions in these regions they must have much better parameters, than others, for example, semiconductors. All this makes Josephson contacts rather perspective for some technical applications.

REFERENCES

1. E. Meilikhov, Yu. Gershanov, *Physika C*, **157**, 1989, 431.
2. Yu. A. Vidadi, et al. *Physika C*, **225**, 1994, 124.
3. J. Sanikidze, S. Odenov, R. Kokhraidze, G. Mumladze, I. Mjavanadze, N. Sabashvily. *Proceedings of Tbilisi State University, Physics*, **34**, 4, 1999.
4. J. Sanikidze, S. Odenov, R. Kokhraidze, O. Modebadze, R. Tatulov, N. Birkaya. *Superconductivity*, **4**, 7, 1991, 1218. (Russian).
5. J. Sanikidze, S. Odenov, R. Kokhraidze. *Proceedings of Institute of Cybernetics*, **1**, 2, 2000, 140.



6. V. I. Chechernikov. Magnetic measurements. Moscow State University, 1989. (Russian).
7. R. Kokhraidze, S. Odenov, J. Sanikidze. Bulletin of the Georgian Academy of Sciences, 159, 2, 1999, 217.

**Georgian Academy of Sciences
Institute of Cybernetics**

რ. კობხრიძე, ს. ოდენოვი, ჯ. სანიკიძე

**პერკოლაციისა და ჯოზეფსონის ეფექტი
მაღალტემპერატურულ ზეპამტარებში**

დასკვნა

შესწავლილია პერკოლაციური პროცესები $(YBa_2Cu_3O_{7-x})_x$ $(Y_2BaCuO_5)_{1-x}$ კომპოზიტურ ნაერთში. შექმნილია სამფენოვანი სტრუქტურები, რომლის შიგა ფენა არის პერკოლაციური გამტარებლობის ზღვარზე მყოფი კომპოზიტი. დამზერილია ჯოზეფსონის I და II ეფექტები ასეთ სტრუქტურებში. მიღებულია მდგრადი მახასიათებლების მქონე ჯოზეფსონის კონტაქტები.

A.Lomidze, Sh.Tsiklauri

Accepted for publication June, 2001

ABSTRACT. This work theoretically investigates four-electron QD in 2D spaces using the method of hyperspherical functions, taking into account Coulomb interaction between particles. Harmonic oscillator has been used as confinement potential.

We have calculated that the binding energy of four-electron system monotonically depends on the global quantum number. The account of the Coulomb interaction considerably changes the disposition of energetic levels.

Considerable attention has been recently paid to the study of the few-body artificial atoms i.e. quantum dots [1]. One- and two-electron dots in the two- (2D) and three- dimensional (3D) spaces [1,2] respectively, have been studied in detail.

The results on three- and more electron quantum dots (experimental as well as theoretical) are described in [3,4]; though by the end of the 20th century considerable results have been obtained on few-body systems taking advantage of using nonmodel approach [5-14], which enables us to avoid the model approach to simplify the task and instead of postulating to receive a wave function by the solution - of the equations in a certain approach. As we know few-electron quantum dot has been studied theoretically using the above mentioned approach in [15]. This paper treats the properties of three quantum dots in the 2D-space considering the interaction of logarithmic potential between the electrons.

Below we shall generalize the hyperspherical function method suggested in [15] to study four-electron quantum dot problem in the 2D-space. At the same time we use the Coulomb interaction between electrons and parabolical type potential - as confinement potential.

Let us consider four identical particles. The appropriate Jacobian coordinates may be represented by the expression:

$$\bar{X}_{ijk} = \frac{1}{2^{1/6}} (\bar{r}_i - \bar{r}_j), \quad \bar{Y}_{ijk} = \frac{1}{2^{2/3}} (\bar{r}_k + \bar{r}_i - (\bar{r}_i + \bar{r}_j)),$$

$$\bar{Z}_{ijk} = \frac{1}{2^{1/6}} (\bar{r}_k - \bar{r}_i), \quad \bar{R} = \frac{1}{2^{2/3}} (\bar{r}_1 + \bar{r}_2 + \bar{r}_3 + \bar{r}_4). \quad (1)$$

We introduce the hyperspherical coordinates by the following relations:

$$|\bar{X}| = \rho \cos \alpha \sin \beta; \quad |\bar{Y}| = \rho \sin \alpha \sin \beta; \quad |\bar{Z}| = \rho \cos \beta,$$

where $\alpha, \beta \in [0, \pi/2]$

Let us expand the four-body wave function in the system of the center mass in a four-body hyperspherical functions:

$$\psi(\rho, \alpha, \beta) = \sum_{KK_3(l)M} \chi_{KL}^{(l)K_3}(\rho) \Phi_{KLM}^{(l)K_3}(\Omega_l), \quad (2)$$

where $(l) = (l_1, l_2, l_3, l_{12})$ are the appropriate orbital moments; K_3, K are three and four body hypermoments, respectively. $\Phi_{KLM}^{(l)K_3}(\Omega_l)$ - in the 2D-space, represents eigenfunctions of square six-dimensional angular moment with eigenvalues $K(K+4)$ and may be represented by the expression:

$$\Phi_{KLM}^{(l)K_3}(\Omega_l) = N_{K_3}^{l_1, l_2} \cos^{l_1} \alpha \sin^{l_2} \alpha P_n^{l_1+l_2+1, l_1+1}(\cos^2 \alpha) \times$$

$$\times N_{K_4}^{l_3, l'} \cos^{l_3} \beta \sin^{l'} \beta P_m^{l_3+r+2, l_3+1}(\cos^2 \beta)$$

$$Y_{l_1 m_1}(\bar{x}) Y_{l_2 m_2}(\bar{y}) Y_{l_3 m_3}(\bar{z}) \quad (3)$$

where

$$N_{K_3}^{l_1, l_2} = \left[\frac{2(l_1+1)(l_1+2)\dots(l_1+n)\Gamma(l_1+l_2+1+n)(l_1+l_2+1+2n)}{\Gamma(l_1+1)\Gamma(l_2+1+n)\Gamma(1+n)} \right]^{1/2}$$

$$N_{K_4}^{l_3, t} = \left(\frac{2(l_3+1)(l_3+2)\dots(l_3+m)\Gamma(l_3+t+2+m)}{\Gamma(l_3+1)\Gamma(t+2+m)} \frac{l_3+t+2+2m}{\Gamma(m+1)} \right)^{1/2}$$

After inserting (2) and (3) in Schrodinger equation in the system of center of mass in the 2D-space we obtained the following set of equations:

$$\left(\frac{\partial^2}{\partial \rho^2} - \frac{(K+2)^2 - 0.25}{\rho^2} - \frac{2^{1/3}m}{\hbar^2} \left(\frac{b}{2^{2/3}} \rho^2 + E \right) \right) \chi_{KL}^{l_1, l_2}(\rho) = \sum_{K', l_1', l_2', M'} W_{KK', LL', MM'}^{(l)(l')}(\rho) \chi_{K'L'}^{l_1', l_2'}(\rho), \quad (4)$$

$$\left[-\frac{\hbar^2}{2^{4/3}m} \left(\frac{\partial^2}{\partial R^2} \right) + R^2 \frac{b}{2^{2/3}} \right] \psi(\vec{R}) = E_R \psi(\vec{R}), \quad (5)$$

where

$$W_{KK', LL', MM'}^{(l)(l')}(\rho) = \frac{2^{4/3}m}{\hbar^2} b + \left[J_{KK', LL', MM'}^{(l)(l')} + \sum_{(\tilde{l})\tilde{K}_3} \langle (\tilde{l})\tilde{K}_3 | (l)K_3 \rangle_{KL}' \langle (\tilde{l})\tilde{K}_3 | (l')K_3' \rangle_{KL} J_{KK', LL', MM'}^{(\tilde{l})\tilde{K}_3(\tilde{l}')\tilde{K}_3'} + \sum_{(\tilde{l})\tilde{K}_3} \langle (\tilde{l})\tilde{K}_3 | (l)K_3 \rangle_{KL}' \langle (\tilde{l})\tilde{K}_3 | (l')K_3' \rangle_{KL} J_{KK', LL', MM'}^{(\tilde{l})\tilde{K}_3(\tilde{l}')\tilde{K}_3'} + \dots \right]$$

$$\begin{aligned}
 J_{KK'LL'MM'}^{(l)K_3(l')K'_3} &= \\
 &= 2^{-n} \sum_{k_1=0}^n \frac{\Gamma(n+l_3+K_3+3)\Gamma(n+l_3+2)}{\Gamma(k_1+1)\Gamma(n+l_3+K_3+3-k_1)\Gamma(n-k_1+1)\Gamma(l_3+k_1+2)} \times \\
 &\times 2^{-n'} \sum_{k_2=0}^{n'} \frac{\Gamma(n'+l'_3+K'_3+3)\Gamma(n'+l'_3+2)}{\Gamma(k_2+1)\Gamma(n'+l'_3+K'_3+3-k_2)\Gamma(n'-k_2+1)\Gamma(l'_3+k_2+2)} \times \\
 &\times (-1)^{n+n'-k_1-k_2} B\left(\frac{l_3+l'_3}{2}+2, n+n'-k_1-k_2+\frac{K_3+K'_3+5}{2}\right) \times \\
 &\times {}_2F_1\left(\frac{l_3+l'_3}{2}+2, -k_1-k_2, n+n'-k_1-k_2+\frac{K_3+K'_3+l_3+l'_3+7}{2}; -1\right), \quad (6)
 \end{aligned}$$

where $b^{-1/2}$ is related to the confinement region of electrons in quantum dot, ${}_2F_1$ is a generalized hypergeometric function, Γ is gamma function, B is beta function, $\langle (\tilde{l})\tilde{K}_3 | (l)K_3 \rangle_{KL}^J$ are unitary coefficients of Reynal-Revai [6].

Equation (5) describes the motion center of mass of the system. Equation (4) describes relative motion of four-electron confinement system.

In case there is no interaction between electrons the solution of equation (4) takes the form:

$$\begin{aligned}
 \psi(\rho) &= \frac{G^{(K+3)/4} \rho^{(2K+5)/2}}{(\Gamma(N+1))^{1/2}} \exp(-(G)^{1/2} \rho^2 / 2), \\
 &\frac{1}{\Gamma(N+K+3)} L_N^{K+2} \left((G)^{1/2} \rho^2 \right), \quad (7)
 \end{aligned}$$

where $G = \frac{m}{\hbar^2} \frac{b}{2^{1/3}}$; $L_N^\alpha(\rho)$ is Lager polynomial, E_0 is binding energy.

$$E_0 = -\frac{\hbar(4N + 2K + 7)}{2\mu} \sqrt{G} \quad (8)$$

We expand exact hyperradial function in terms of basic functions (7):

$$\chi_{KN}^{(l)K_3}(\rho) = \sum_N a_{KN}^{(l)K_3} \Psi_{KN}^{0(l)K_3}(\rho) \quad (9)$$

where $\mu = \frac{m}{\sqrt[3]{4}}$, $N = 0, 1, 2, \dots$ is global quantum number, the

coefficients $a_{KN}^{l_3 K_3}$ obey the normalization condition $\sum_{N=0}^{\infty} |a_{KN}^{l_3 K_3}|^2 = 1$.

Then the energy eigenvalues of the relative motion are obtained from the requirement of making the determinant of the infinite system of linear homogeneous algebraic equations vanish:

$$\det \left\| \left(E - E_0^{K'N'} \right) \delta_{KK'} \delta_{(l)(l')} \delta_{K_3 K_3'} \delta_{NN'} - I_{KK'; LL'; MM'}^{(l)(l'); K_3 K_3'} (1 - \delta_{KK'} \delta_{(l)(l')} \delta_{K_3 K_3'} \delta_{NN'}) \right\| = 0, \quad (10)$$

where $I_{KK'; LL'; MM'}^{(l)(l'); K_3 K_3'}$ is matrix element of total potential energy.

We have calculated the total energy of the system, which equals to the sum of motion energy of the system mass center and relative motion energy.

The dependence of the binding energy of the four-electron system upon the global quantum number (for the ground state $S = 0$) obtained in the result of solution of the expression (8) and equation (10) is given in the Table.

Dependence of the binding energy of the four-electron system in 2D space upon the global quantum number

Global quantum number N	Binding energy for confinement potential E_0^N (a.u.)	Binding energy with account of Coulomb interactions E (a.u.)
0	6.37	6.37
1	10.01	11.84
2	13.65	17.31
3	17.29	22.78
4	20.93	28.25
5	24.57	33.72

As it is seen from the Table the four-electron system binding energy is depended monotonically upon the global quantum number, besides due to taking into account the Coulomb interaction the disposition of energetic levels is changed.

REFERENCES

1. T.Chakraborty, Comments Condense Matter Phys. 16, 1992, 35.
2. Jia-Lin Zhu, Zhi-Qiang Li, et al. Phys. Rev. B.55, 1997, 15819.
3. Y. Alhassid Rev. Mod. Phys. 72, 2000, 895.
4. K. Varga, P. Navratil, J. Usukura, Y. Suzuki Cond. Matt. 0010 398.
5. L.M. Delves. Nucl. Phys. 9, 1959, 391; 20, 1960, 275; 29, 1962, 268.
6. I.A. Simonov. Sbornik dokladov na vtorom problemnom simpoziume po fizike iadra, Novosibirsk, 1970, M., 1971.
7. R.I. Jibuti, N.B. Krupennikova, V.I. Tomchinski. Sov. J. Nucl. Phys. 23, 1976, 539.
8. T.M. Macharadze, T.I. Mikhelashvili. Sov. J. Nucl. Phys., 5, 1971, 981.
9. R.I. Jibuti, V.I. Tomchinski, N.I. Shubitidze. Sov. J. Nucl. Phys.



- 18, 1973, 1164.
10. R.I. Jibuti, N.B. Krupennikova, N.I. Shubitidze. *Teor. Matem. Fizika*, **32**, 1977, 223.
 11. L.D. Fadeev. *J. Teoret. Fiziki*, **39**, 1960, 1459; *Trudy Matematicheskogo Instituta AN SSSR*, 1963, 69.
 12. S.P. Mercuriev, C. Gignoux, A. Laverne. *Ann. Phys.* **99**, 1976, 30.
 13. I.F. Simonov. *Sov. J. Nucl. Phys.*, **3**, 1966, 630. A.M. Badalian, I.F. Simonov. *Sov. J. Nucl. Phys.* **3**, 1966, 1032.
 14. R. Moshinski. *Garmonicheski oscilator v sovremennoi fizike ot atomov do kvarkov*. 1972 (Russian).
 15. A. Lomidze, Sh. Tsiklauri. *Proc. XXI -ICPEAC*, Senday, Japan, July, 22-27, **II**, 1999, 758.
 16. J. Reynal, J. Revai. *Nuovo Cimento A68*, 1970, 612.

Tbilisi State University

ა. ლომიძე, შ. წიკლაური

ოთხელექტრონიანი კვანტური ვერტიკლის თვისებები

დასკვნა

ნაშრომში თეორიულად შესწავლილია ოთხელექტრონიანი კვ 2D სივრცეში ჰიპერსფერული ფუნქციების მეთოდით, ნაწილაკებს შორის ურთიერთქმედების პოტენციალი კულონური. კონფაინმენტური პოტენციალი პარმონიული ოსცილატორის ტიპისაა.

გათვლებების შედეგად მივიღეთ, რომ ოთხელექტრონიანი სისტემის ბმის ენერგია მონოტონურად არის დამოკიდებული გლობალურ კვანტურ რიცხვზე, გარდა იმისა რომ კულონური ურთიერთქმედების გათვალისწინება მნიშვნელოვნად ცვლის ენერგეტიკული დონეების განლაგებას.

L.Kiknadze, Yu.Mamaladze

Accepted for publication July, 2001

ABSTRACT. The division of the flow energy into the energies of vortices and of a stream is preferable even if the flow is completely caused by vortices. Separation of the stream energy or, separation of the averaged flow at continual description of the many-vortex system is equivalent to the transformation of a reference frame. This allows to determine the effective radius of the vortex in a "reasonable" manner as equal or near to the size of the closed streamline vicinity of the vortex determined in the reference frame, where the stream is minimal. Then it becomes independent of the choice of a reference frame, which changes only the stream energy. The difference between the concepts of the effective radius and the vortex atmosphere is shown, and the possibility of great difference between those quantities as well as their casual equality is noted.

1. INTRODUCTION

The contribution of a vortex in the energy of flow usually is written as follows:

$$\varepsilon = \frac{1}{4\pi} \rho \Gamma^2 \ln \frac{b}{a}. \quad (1)$$

Here ε is the energy of the liquid rotation around a vortex line reduced to a unit length of this line, ρ is the density, Γ is the circulation, a is the radius of the vortex core (in this paper we mainly mean, the vortices in He II; in this case $\rho = \rho_s$ is the density of the superfluid component, Γ is the multiple of the quantum $2\pi\hbar/m$, m is a mass of an atom, and a is of order of the atom separation or the coherent length [1-4]), b is the effective radius of the vortex, which is determined as the minimal one between three characteristic lengths:

the size of the canal (the vessel), the distance from the vortex to the wall and the spacing between vortex lines. Sometimes it is determined as "the area which belongs to the vortex".

The meaning of these definitions is the effective separation of the area where the liquid effectively rotates around the given vortex. Such approach is justified to a certain degree. Because of the weak dependence of the logarithm on its large argument one can calculate the energy of a vortex with the sufficient accuracy using even rough estimations of the radiuses a and b if $b/a \gg 1$. But the situation is somewhat more complicated.

For instance Fig. 1a shows the streamlines of the flow caused by the vortex placed in homogeneous stream. It is clear that "the area belonging to the vortex" is inside the loop of the separatrix, and outside there is the area of the stream. Then the effective radius would be about $\Gamma/2\pi v_\infty$, where v_∞ is the velocity of the flow at infinity (because the junction of the separatrix is the critical point where the velocity is zero, i.e. $\Gamma/2\pi b - v_\infty \approx 0$). However the direct calculation, i.e. the integration of $\rho(v_x^2 + v_y^2)/2$, where

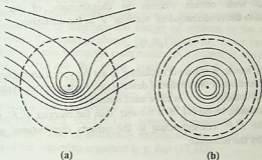
$$v_x = -\frac{\Gamma}{2\pi} \frac{y}{x^2 + y^2} + v_\infty \cdot v_y = \frac{\Gamma}{2\pi} \frac{x}{x^2 + y^2}, \quad (2)$$

shows that in any circular area with the center at the vortex point and with a radius R (one of such areas is encircled in Fig. 1a) the energy is:

$$E = \frac{1}{2} M v_\infty^2 + \frac{1}{4\pi} \rho \Gamma^2 \ln \frac{R}{a}. \quad (3)$$

Here the energy E and the mass $M = \pi R^2 \rho$ are reduced to the unit length perpendicular to the plane of a flow. Since the first term in the rhs of Eq.(3) is undoubtedly the energy of a stream, the second term is the contribution of a vortex which has the form of Eq.(1) with the effective radius $b = R$ and not $b \approx \Gamma/2\pi v_\infty$. Therefore, "the area

belonging to the vortex" may be much more than the loop of separatrix.



The reason will be clear if the same flow is considered in the reference frame of the vortex (Fig.1b) (if one recollects that the free vortex moves together with the stream and the fixed (forced) one can have any velocity then there also exists another interpretation of Figs. 1a,b for the case of a fixed vortex: Fig. 1b corresponds to $v_{\infty} = 0$, and Fig. 1a describes the same flow in the moving reference frame).

There exist situations, where the energy is successfully calculated by the estimation of an effective radius without any problems. But, more detailed consideration of the flow energy division into the energies of vortices and a stream, which is the subject of this paper, is useful because it not only confirms the expedience of this separation but also shows that it is possible to define the effective radius so that it would be independent from the choice of reference frame.

In this paper we use only the examples of plane flows and employ the methods of the complex potential [5]. The energy is determined by the area occupied by the considered flow on the plane of a complex potential and is used for comparison with Eq.(1) with the aim to improve the understanding of the effective radius concept and estimations of this quantity.

2. TRANSFORMATION OF ENERGY

The velocity of the liquid at infinity or some other velocity u justified with certain reasons as characteristic of the stream, determines the contribution of vortices v' as the difference

$$v' = v - u \quad (4)$$

(in other words, a stream is excluding to get the vortex contribution). E.g. in the case of the continual description of many-vortex system the averaged velocity $\langle v \rangle$ is to be used instead of u .

According to Eq.(4), if $u = \text{const}$ then the energies E, E' and the momenta P, P' corresponding to the velocity distributions v, v' are related by the formulae:

$$E = E' + uP' + \frac{1}{2}Mu^2, \quad (5)$$

$$P = P' + Mu. \quad (6)$$

If $u = \omega r$ and the angular velocity $\omega = \text{const}$ then we obtain the following expressions of the energy and the angular momentum:

$$E = E' + \omega L' + \frac{1}{2}I\omega^2, \quad (7)$$

$$L = L' + I\omega. \quad (8)$$

In Eqs.(5-8) M and I are the mass and the moment of inertia of the liquid (reduced to unit length as well as E, E', L, L'). The last terms of these equations represent the contribution of a stream, the first terms in rhs represent the contribution of vortices, and the existence of the interferential second terms in energies shows that in general case the energy cannot always be expressed as the simple sum of the stream and the vortex energies. In the case $u = \langle v \rangle$ we find $\langle v' \rangle = 0$ and

$P' = 0$ (P' is not the Kelvin's impulse but it is the momentum and exists only in finite volumes).

From the other point of view Eq.(4) is the transformation to the reference frame moving with the velocity u and Eqs.(5-8) are the corresponding transformations of energies and momenta. Hence, one can recommend to determine the energy of vortices in the reference frame where the stream is absent (as in Fig.1b) or, if it is impossible, in reference frame where the contribution of a stream in the energy is minimum. We use the prime symbols v', E', P', L' for values determined in such reference frame. One can see from Eqs.(5,7) that the behaviour of the terms differing E and E' is not logarithmic one, due to which their dependence on u and ω has no influence on the effective radius (e.g. Eqs.(10,12)), however sometimes, if these terms are small, they can be artificially introduced into ϵ as insignificant factors of the logarithm argument (e.g. Eqs.(17,18)).

3. ATMOSPHERE OF A VORTEX

The volume of the liquid moving with the vortex is its atmosphere (as it was called by Kelvin [6]). The size of the atmosphere is determined by the relative motion of the vortex and liquid. If the flow consists of the uniform stream and the single vortex then the finite atmosphere exists only in the case $v_\infty - v_L \neq 0$ (v_L is the velocity of the vortex line (point)). In the opposite case the atmosphere is infinite as it is shown in Fig.1b. The loop of separatrix shown in Fig.1a is an atmosphere only in the case where it is done in the vortex reference frame). One can see from the introduction that the size of atmosphere may be estimated as $\Gamma/2\pi|v_\infty - v_L|$ and the vortex energy can be concentrated outside the atmosphere.

4. CLOSED STREAMLINE VICINITY OF A VORTEX

The area of closed streamlines surrounded by the loop of separatrix, which accompanies each vortex, certainly may be considered as the area belonging to it. Generally speaking, the closed streamline vicinity of a vortex (let us call it "a vortex area") does not

coincide with an atmosphere. E.g. in Fig.1a the area surrounded by the separatrix is an atmosphere only in the vortex reference frame. The point is that flow patterns (consisting of streamlines) do not depend on the velocity of a vortex motion but they depend on a reference frame (i.e. on the velocity at infinity). As to the outline of an atmosphere, it is determined by the relative velocity $v_\infty - v_L$ and does not depend on the reference frame but depends on the vortex velocity. Thus, "a vortex area" coincides with an atmosphere only in the reference frame moving with a vortex.

5. SINGLE VORTEX IN A HOMOGENEOUS STREAM

Eq.1 with $b = R$ immediately follows from the velocity distribution $v = \Gamma / 2\pi r$ and Eq.(2) is a consequence of transformation (5) (transition from one reference frame to another is equivalent to the superposition of a stream).

6. PAIR OF VORTICES WITH THE OPPOSITE CIRCULATION

The stream is excluded in the reference frame where $v_\infty = 0$. In this reference frame the closed streamline vicinity of each vortex is a half-space but its energy is finite. It is given by Eq.1 with $b = d$ where d is the vortex spacing (such a small value of effective radius is due to the fact that the contribution of one vortex to velocity is partially canceled by the other one). Restricting the considered area by the square with a size $D \gg d$ (the center of the square is at the midpoint of the vortices) and using Eq.(5) with $P' = 0$ we receive

$$E = \frac{1}{2} M v_\infty^2 + \frac{1}{2\pi} \rho \Gamma^2 \ln \frac{d}{a}, \quad (9)$$

for any reference frame where $M = \rho D^2$. In the case $v_\infty = 0$ the pair of free vortices has "the own" velocity $v_L = \Gamma / 2\pi D$. In the reference

frame moving with the velocity $\Gamma/2\pi d$ ($v_\infty = -\Gamma/2\pi d$) the free vortex pair is motionless, and the closed streamline vicinities form the Kelvin's oval, which is the atmosphere of the pair in all cases where $v_\infty - v_L = -\Gamma/2\pi d$. Each of the semiovals has the energy expressed by Eq.(1) with $b = d/e^{1/2}$. The vortex energy and the outlines of the vortex area and atmosphere can be drastically changed by variation of v_∞ and v_L but these changes do not influence Eq.(9).

7. TWO VORTICES WITH POSITIVE CIRCULATION

Such vortices rotate around the center located in their midpoint. If the velocity at infinity is zero then

$$E' = \frac{1}{4\pi} \rho \Gamma^2 \left(4 \ln \frac{2R}{a} + 2 \ln \frac{d}{2a} \right), L' = \rho \Gamma \left(R^2 - \frac{1}{4} d^2 \right), \quad (10)$$

where $R \gg d$ is the arbitrary large radius of the circumference encircled around the same center to separate the considered area. The superposition of a circular stream with an angular velocity ω (or the transition to the reference frame rotating with the angular velocity $-\omega$) we can drastically change the flow pattern [7] (create and destroy "the eight", "the belt", "the umbrellas", change the outlines and sizes of a vortex area and an atmosphere) but the energy expression

$$E = \frac{1}{2} I \omega^2 + \frac{1}{4\pi} \rho \Gamma^2 \left(2 \ln \frac{d}{2a} + 4 \ln \frac{2R}{a} \right) + \rho \Gamma \left(R^2 - \frac{1}{4} d^2 \right) \omega \quad (11)$$

will not change ($I = \pi \rho R^4 / 2$).

Thus, in all the examples considered so far it turns out to be reasonable to determine the effective radius of the vortex by means of energy in the reference frame, where $v_\infty = 0$ (the latter can be called "the own reference frame of a liquid" or, in abbreviated form, "the

own frame"). Next example will show that what really matters is not $v_{\infty} = 0$ but the minimization of the stream.



8. CHAIN OF POSITIVE VORTICES

Though the contribution of each vortex in the velocity at infinity is zero in the own frame of the liquid, nevertheless at infinity the infinite chain of vortices causes the nonzero velocity $\pm u$ ($u = \Gamma/2l$, where l is the vortex spacing, the sign is opposite along different sides of the chain). If one restricts the area under consideration by a rectangle with sizes l and D ($D \gg l$) and with a vortex in the center then in the reference frame, which moves relatively to "own frame" with a velocity v_0 , the energy and the momentum on the different sides of the chain are:

$$E_{\pm} = \frac{1}{4}M(v_0 \pm u)^2 + \frac{1}{2}E', \quad E' = \frac{1}{4\pi}\rho\Gamma^2 \ln \frac{l}{2\pi a},$$

$$P_{\pm} = -\frac{1}{2}M(v_0 \pm u), \quad (12)$$

where $M = \rho l D$. The energy of the whole rectangle is

$$E = \frac{1}{2}M(u^2 + v_0^2) + E'. \quad (13)$$

The free vortices are motionless in the "own frame", and the area surrounded by the loop of the separatrix is the atmosphere in this case. Its energy is expressed by Eq.(1) with $b = l/\pi$ (not $l/2\pi l$), i.e. the part of the energy concentrated in the atmosphere belongs to contribution of the stream.

Although in this case we have only little difference between the energy of the atmosphere and the energy reduced to one vortex in the reference frame, where the stream is minimal, it should be noted that E' is not the former but the latter one.



To perform the transition to the reference frame, which minimizes the stream one has to exclude the velocity at infinity separately on both sides of the chain ($P' = 0$ on each of them). E' is mostly concentrated in "vortex area" but E' contains also the energy of the minimized stream (the situation is similar to that of Sec.10).

9. VORTEX STREET

The positive and the negative chains parallel to each other (the Karman's street) cause minimal stream in the own frame. Then the stream is concentrated near the chains, especially between them. It is not completely excluded but the velocity at infinite distance from the chains is zero. The energy reduced to one vortex is finite:

$$E' = \frac{1}{2}Mu^2 + \frac{1}{4\pi}\rho\Gamma^2 \ln\left(\frac{l}{2\pi a}\left(1 - \exp\left(-\frac{2\pi d}{l}\right)\right)\right) = \quad (14)$$

$$= \frac{1}{4\pi}\rho\Gamma^2 \ln\left(\frac{l}{\pi a} \sinh \frac{\pi d}{l}\right) \quad (15)$$

$$E' = \frac{1}{2}Mu^2 + \frac{1}{4\pi}\rho\Gamma^2 \ln\left(\frac{l}{2\pi a}\left(1 + \exp\left(-\frac{2\pi d}{l}\right)\right)\right) = \quad (16)$$

$$= \frac{1}{4\pi}\rho\Gamma^2 \ln\left(\cosh \frac{\pi d}{l}\right), \quad (17)$$

where $u = \Gamma/l, M = \rho d/2, d$ is the distance between the chains. Eqs.(14,15) are valid for symmetrical order of vortices, and Eqs.(16,17) are valid for chess board one. The energy of stream in Eqs.(14,16) exactly corresponds to continual description, and the dependance of the vortex energy on d/l in these equations is reasonable. Eqs.(15,17) are more compact but such expressions for the energy (withouth separation of the stream) are less corresponding to the spirit of continual description and to the aim of this paper.



The following example illustrates the advantage of the separation of a stream. To estimate the critical velocity of vortex formation Feynman [2] considered the immersed jet flowing out from a slit and being framed by symmetrical vortex street. He estimated the energy of each vortex by Eq.(1) with $b = d$. At the velocity $v = v_c$ estimated by Feynman [3] as critical one the values of d and $l(l = \Gamma / v_c)$ are of the same order of magnitude and each of them can be used as the effective radius of the vortex. But it would be more correct if the stream was separated as in Eq.(14) (because $\exp(-2\pi) \ll 1$), and the effective radius would be essentially larger if the stream was not separated as in Eq.(15) ($\sinh(\pi d / l) \approx 10$). But this quantitative difference is less important than the principal preference of stream separation which enables one to get clearer idea of considered phenomena (see Appendix for more details).

10. ROTATING HE II

The rotation of ideal liquid with characteristic two-dimensional lattice of vortices is so specific for the superfluid that in this section we concretize the considered liquid ($\Gamma = 2\pi\hbar / m$, m is the mass of a helium atom).

In the infinite rotating He II the quantized vortices rotate together with a normal component and form the stable triangular lattice [8-10]. The number of vortices in the unit surface is [3]:

$$N_1 = \frac{m\omega}{\pi\hbar} \tag{18}$$

The stream is minimal in the reference frame rotating together with the vortices and the normal component ($v_L = 0$) in which elementary cell of a vortex lattice includes a hexagonal "vortex area" (coinciding with the atmosphere of the vortex) and two triangular areas of opposite rotation (each of them has six times less area than the atmosphere) [10,11]. The energy and the angular momentum of this unit cell are [10]:

$$e' = \pi\rho_s \left(\frac{\hbar}{m}\right)^2 \ln\left(\frac{0.48}{a} \sqrt{\frac{\hbar}{m\omega}}\right), l' = \pi\rho_s \frac{\hbar}{m} \left(0.44 \frac{\hbar}{m\omega}\right) \quad (19)$$

Here the relatively small contribution of the minimized stream (i.e. the circular streams of opposite rotation in triangles mentioned above) is not separated.

In this case the own frame of the liquid coincides with the laboratory one (where each vortex gives the zero contribution into the velocity at infinity but the infinite array of the vortices causes the infinite velocity at infinity). In this reference frame the energy reduced to one vortex is:

$$\varepsilon = e' + \omega l' = \pi\rho_s \left(\frac{\hbar}{m}\right)^2 \ln\left(\frac{0.74}{a} \sqrt{\frac{\hbar}{m\omega}}\right), \quad (20)$$

and the energy concentrated in a circle with a large radius $R \gg N_1^{-1/2}$ is

$$E = \frac{1}{2} I \omega^2 + N \varepsilon, \quad (21)$$

where $I = \pi\rho_s R^4 / 2$, $N = m\omega R^2 / \hbar$, ε is expressed by Eq.(1) where according to Eq.(20) $b = 0.74(\hbar / m\omega)^{1/2}$.

If instead of fancied circumference one considers a real vessel then the existence of irrotational area adjacent to the wall of the vessel $R_1 < r < R$ must be taken into account. As to the image vortices they have a weak influence on the equilibrium state [12,13] and are absent in the continual description. The energy and the angular momentum of superfluid in the laboratory frame is:

$$E = \frac{1}{2} I_l \omega^2 + \pi\rho_s \left(\frac{\hbar}{m}\right)^2 \left(N_1 \ln \frac{b}{a} + N_l \ln \frac{R}{R_1} \right) \approx \frac{1}{2} I \omega^2, \quad (22)$$

$$L = \left(\frac{2R^2}{R_i^2} - 1 \right) I_i \omega,$$

where $I_i = \pi \rho_s R_i^4 / 2$, and $N_i = m \omega R_i^2 / \hbar$ is the number of vortices in a vessel. We would like to emphasize that in Eq.(22) the additional contribution of a vortex singularities is neutralized by the decrease of the velocity in the irrotational area (at any rate up to the second order in the expansion of the energy in series of $(R - R_i) / R$).

12. SUMMARY

Neither the atmosphere of the vortex nor "the vortex area" (which may be quite different) do concentrate all the energy caused by a vortex. But this energy, if one separates from it the energy of a stream, is exactly or approximately equal to the energy concentrated in "the vortex area". Thus, the characteristic size of "the vortex area" in the reference frame where a stream is minimal can be used as the estimation of the effective radius of the vortex. Then at transition to another reference frame only the energy of a stream will change but the effective radius will stay unchanged.

APPENDIX

THE CRITICAL VELOCITY OF VORTEX GENERATION BY AN IMMERSSED JET

Feynman [3] considered the energetical possibility of a vortex generation in a superfluid for the case where the immersed jet of the width d is flowing out from a plane slit into the semiinfinite liquid. He considered the jet as framed by symmetrical vortex street, and had not separated the energy of a stream from the vortex energies (expressed by Eq.(1) with $b = d$). It is quite sufficient for the rough estimation of the critical velocity but for better understanding of the sense of the considered processes it is preferable to separate the

contributions of a stream and vortices. Then in the energetical balance (written in the same continual approximation as Feynman's one) there appears a term describing the stream out of the slit

$$\frac{1}{2} \rho_s v_c^2 v_c d_0 = \frac{1}{2} \rho_s v^2 v d + \frac{v}{2l} 2\pi \rho_s \left(\frac{\hbar}{m} \right)^2 \ln \frac{b}{a}. \quad (\text{A1})$$

Here v_c is the critical value of the velocity in the slit, d_0 is its width, v and d are the velocity and the width of the jet, $1/l = mv/2\pi\hbar$ is the number of vortices per unit length (in each chain of the vortex street), $v/2l$ is the number of vortex pairs created per unit time (the velocity of vortex motion is $v/2$). The lhs of Eq.(A1) is the energy available per unit time, the rhs is the energy of a new section of the jet with corresponding number of new vortices (in Ref.3 the first term on the rhs is absent and $b = d$, moreover $v_c = v, d_0 = d$).

The similar equality describes conservation of the momentum

$$\rho_s v_c v_c d_0 = \rho_s v v d + \frac{v}{2l} 2\pi \rho_s \frac{\hbar}{m} d, \quad (\text{A2})$$

i.e. the momentum available per unit time is spent to provide the jet with the momentum of its new section and the momentum, which it has to spend to create new vortices (that is the Kelvin's impulse: $2\pi\rho_s \hbar d / m$ per unit length for each vortex pair).

We employ also the equation of continuity

$$v_c d_0 = v d, \quad \frac{v}{v_c} = \frac{d_0}{d} = \frac{2}{3}, \quad (\text{A3})$$

and obtain

$$v_c = \frac{4}{5} \frac{\hbar}{m d} \ln \frac{b}{a}. \quad (\text{A4})$$

REFERENCES

1. L. Onsager, *Nuovo Cim.* **6**, Supp I.2, 1949, 249.
2. R.P.Feynman, in *Prog. in Low Temp.Phys.*, N.-H. Publ. Co. Amsterdam, 1955, **I**, ch.2.
3. V.L.Ginzburg, L.P.Pitaevskii, *Zh.Exp.Teor.Fiz.* **35**, 1958, 408.
4. Yu.G.Mamaladze, *Zh.Exp.Teor.Fiz.* **52**, 1967, 729.
5. N.E. Kochin, I.A. Kibcl, N.V. Roze, *Teoreticheskaiia gidromekhanika* **1**, 1948.
6. W.Tomson, *Phil.Mag.*, ser.4, **34**, 1867, 15.
7. V.V.Meleshko, M.Yu.Konstantinov, *Dinamika vikhrevikh struktur*. 1993, Fig.6. (see also D.G.Dritschel, *J.Fluid Mech.* **157**, 1985, 95.
8. L.V.Kiknadze, Yu.G.Mamaladze, O.D.Cheishvili, *Zh. Exp. Teor. Fiz.* **48**, 1965, 1520.
9. V.K.Tkachenko, *Zh.Exp.Teor.Fiz.*, **49**, 1965, 1875.
10. V.K.Tkachenko, *Zh.Exp.Teor.Fiz.*, **50**, 1965, 1573.
11. E.L.Andronikashvili, Yu. G.Mamaladze, in *Prog. in Low Temp. Phys.* N.- H. Pub. Co. Amsterdam, 1967, **V**, ch.III.
12. L.V. Kiknadze, Yu.G.Mamaladze, *Fiz. Nizk.Temp.* **8**, 1982, 160..
13. L.J. Campbell, R.M.Ziff, *Phys.Rev.* **B20**, 1979, 1886.

Georgian Academy of Sciences
Institute of Physics
Tbilisi State University

ბრიტანის ენერჯია და ევმაქტური რადიუსი

დასკვნა

დინების ენერჯიის განცალკება გრიგალების და ნაკადის ენერჯიებად მიზანშეწონილია მაშინაც კი, როდესაც დინება განპირობებულია მხოლოდ გრიგალთა არსებობით. ნაკადის ენერჯიის გამოყოფა ან (გრიგალთა ერთობლიობის კონტინუალური აღწერისას) გასაშუალოებული დინების გამოყოფა ათვლის სისტემის გარდაქმნის ტოლფასია. ნაჩვენებია, რომ ევმაქტური რადიუსი შეიძლება ისე განისაზღვროს, რომ ის იყოს დამოუკიდებელი ათვლის სისტემის არჩევისაგან. ამ მიზნით ევმაქტურ რადიუსად უნდა გამოვიყენოთ გრიგალის გარშემო არსებული ჩაკეტილი დენის წირების არის ზომა ათვლის იმ სისტემაში, სადაც ნაკადი არ არის, ან მინიმალურია. მაშინ ათვლის სხვა სისტემაში გადასვლისას შეიცვლება მხოლოდ ნაკადის ენერჯია, ხოლო გრიგალის წვლილი ენერჯიაში და მასთან ერთად მისი ევმაქტური რადიუსი უცვლელი დარჩება.

ნაჩვენებია, რომ ევმაქტური რადიუსის ცნება მკვეთრად განირჩევა გრიგალის ატმოსფეროს ზომის ცნებისაგან. შესაძლებელია ამ სიდიდეთა დიდი განსხვავებაც და შემთხვევითი დამთხვევაც.

DEPLETION OF MASS CAUSED BY VORTEX AND VORTEX DYNAMICS



L.Kiknadze, Yu.Mamaladze

Accepted for publication July, 2001

ABSTRACT. It is shown that the own mass of a vortex in the classical polytropic liquid is negative, because the vortex decreases the density of the liquid rotating around it, and the contribution of the vortex motion into the momentum of a liquid is of opposite direction to this motion. The own mass of a vortex (the depletion of the liquid mass) is connected with the energy of the liquid rotation and with the velocity of the sound by "the Einstein's relation". The approximate expressions of mass depletion, of the energy of rotation, and the internal energy of a liquid are obtained, and the numerical calculations are performed to define more precisely the dependence of these quantities on the polytropic exponent.

1. INTRODUCTION

Recently the problem of vortex own mass is intensively discussed in the physics of quantum fluids (see e.g. [1]). Here it will be considered in the case of classical one.

2. VORTEX FILAMENT IN AN INCOMPRESSIBLE LIQUID

The concept of a mass is closely connected with the concept of a momentum. It is well known that the infinite liquid has no concept of a momentum, and the concept of the impulse in Kelvin's sense [2-4] is used instead of it. This impulse is unambiguous only in the case where the sum of circulations is equal to zero. But the momentum of the finite volume of the liquid is well determined as the production of its mass and the velocity of the center of inertia. Specifically, if the liquid is incompressible and if it fill up the volume with motionless boundaries then the momentum is zero independently of the kind of

flow. Thus, the momentum of a vortex filament (a vortex line) in incompressible liquid is zero (the momentum of liquid in the presence of a vortex does not differ from the momentum of the motionless liquid), and the mass of a vortex is zero (the momentum of the moving vortex is zero).

3. VORTEX WITH AN EMPTY CORE

If a vortex has an empty core, which is moving with the velocity \vec{v}_0 , then liquid acquires the momentum of opposite to this motion direction and the mass of the vortex is negative.

Really, the velocity of the center of the mass of the liquid \vec{v}_c in such case is equal to

$$\vec{v}_c = \frac{(M + \Delta M) \cdot 0 - \Delta M \cdot \vec{v}_0}{(M - \Delta M)} = -\frac{\Delta M}{M} \vec{v}_0$$

and the momentum of liquid is

$$\vec{p} = M \vec{v}_c = -\Delta M \cdot \vec{v}_0 \quad (1)$$

Thus, the mass of the vortex is ΔM . Here M is the mass of a liquid, and ΔM is the mass, which would have a liquid filling in the empty vortex core: $\Delta M = \pi a^2 \rho l$, a is the radius of a core, ρ is the density of a liquid.

We have meant that a vortex moves as a single whole. In more complicated cases the mass $-\delta M$ characterizes the small element of a vortex δl :

$$\delta M = \mu \delta l, \mu = \pi a^2 \rho, \quad (2)$$

where μ is the mass of the unit length of a vortex.

4. VORTEX IN THE COMPRESSIBLE LIQUID

In the case of a compressible liquid a vortex filament is the (generally speaking, curved) axis surrounded by the area of the variable density and rapid rotation (where $\rho \neq 0$). The expression of such a vortex mass may be similar to Eq.(2) but one must take into account that the density is not constant:

$$\mu = \int (\rho_0 - \rho) dS, \quad (3)$$

dS is an element of the cross section normal to the vortex line. The quantity μ is sensitive to a distribution of density, and therefore, depends on the neighborhood of the walls and other vortices. We shall return to this quantity in Sec. 6.

The force acting on the boundaries is

$$\vec{F} = -\frac{d\vec{p}}{dt} = \Delta M \frac{d\vec{v}_0}{dt}, \quad (4)$$

where \vec{v}_0 is the velocity of the center of inertia of the core. The strong definition of this quantity is

$$\vec{v}_0 = \frac{1}{\Delta M} \int (\rho_0 - \rho) \vec{v} dV \quad (5)$$

but in many cases (in "symmetrical" ones) it is equal or near to vortex point velocity or $d\vec{v}_0/dt$ is near to vortex point acceleration.

5. POLYTROPIC LIQUID

Let us consider the single rectilinear vortex displaced along the axis of a cylindrical vessel with the radius R . The rotation of a liquid is stationary and potential, the continuity equation is valid, and the Euler's equation of motion has the form:

$$\frac{1}{2} \overline{\nabla v}^2 = -\frac{1}{\rho} \overline{\nabla P} \quad (6)$$

We consider the ideal polytropic liquid with the relation between the pressure and the density:

$$\frac{P}{P_0} = \left(\frac{\rho}{\rho_0} \right)^n \quad (7)$$

where P_0, ρ_0 are the values at infinity.

Substituting the equations (7) and $v = \Gamma / 2\pi r$ (where Γ is a circulation) into Eq.(6) and integrating we obtain:

$$\rho = \rho_0 \left(1 + \frac{1-n}{n} \frac{a^2}{r^2} \right)^{-\frac{1}{1-n}} \quad (8)$$

where

$$a^2 = \frac{\Gamma^2}{8\pi^2 c_1^2}, \quad (9)$$

and c_1 is the sound velocity at the isothermal process (the sound velocity at polytropic process is expressed as $c_n^2 = n \cdot c_1^2$).

If $n < 1$ then the density smoothly decreases from ρ_0 at infinity to zero at $r = 0$. The situation is the same when $n = 1$ (the isothermal vortex):

$$\rho = \rho_0 \exp\left(-\frac{a^2}{r^2}\right). \quad (10)$$

Thus, in the case $n \leq 1$ the vortex is a line (a point) singularity ($v = \infty$) surrounded by the core with essentially decreased density. The characteristic size of the core is:

$$r_0 = \sqrt{\frac{n+1}{3n}} a \quad (11)$$

(at this distance from the axis $d^2\rho/dr^2 = 0$).

In the case $n > 1$ the core of the vortex is empty in the area $0 \leq r \leq r_h$,

$$r_h = \sqrt{\frac{n-1}{n}} a. \quad (12)$$

The distribution of the temperature is (according to Eq.(2) and the Clapeyron equation of a state):

$$T = T_0 \left(1 + \frac{1-n}{n} \frac{a^2}{r^2} \right), \quad (13)$$

T_0 is the temperature at infinity.

6. DEPLETION OF THE MASS, THE KINETIC AND INTERNAL ENERGIES

Using Eqs.(3), (8) one can determine the depletion of the mass

$$\mu = 2\pi\rho_0 a^2 \int_a^\beta \left[1 - \left(1 + \frac{1-n}{n} \frac{1}{\xi^2} \right)^{-1/(1-n)} \right] \xi a \xi_0 \quad (14)$$

and the kinetic energy ε of the unit length of a vortex:

$$\varepsilon = \frac{\rho_0 \Gamma^2}{4\pi} \int_{\alpha}^{\beta} \left(1 + \frac{1-n}{n} \frac{1}{\xi^2} \right)^{-1/(1-n)} \frac{d\xi}{\xi} \quad (15)$$

where β is R/a , $\alpha = 0$ if $n \leq 0$ and $\alpha = r_h/a$ if $n > 1$.

The main contribution to the integrals in Eqs.(14), (15) if $\beta \gg 1$ make the area $1 \ll \xi \leq \beta$. Therefore the first of them is approximately equal to $\ln(R/a)/n$, and the second is equal to $\ln(R/a)$. More exact results are obtained by numerical calculations and described in Sec. 7.

Taking into account the approximate values of integrals in Eqs.(14), (15) and Eq.(9) we obtain "the Einstein relation" between ε and μ :

$$\varepsilon \approx \mu c_n^2 \quad (16)$$

Here c_n is the sound velocity ($c_n^2 = n c_1^2$, $c_1^2 = (\partial P / \partial \rho)_T$). Let us note that the Duan's expression [1] of the vortex own mass in superfluid is similar to ours but it is positive.

We can determine also the internal energy of a vortex u , i.e. the difference between the energies of a liquid in the presence of a vortex and without it (the energy $\varepsilon + \mu$ has to be spent for the vortex formation from the initial state P_0, ρ_0, T_0):

$$u = 2\pi\rho_0 c_V T_0 \int_{\alpha}^{\beta} \left[\left(1 + \frac{1-n}{n} \frac{1}{\xi^2} \right)^{-n/(1-n)} - 1 \right] \xi d\xi, \quad (17)$$

where c_V is the specific heat at constant volume. The integral here is approximately equal to $\ln(R/a)$.

Thus, the mass of a vortex and its kinetic and internal energies are infinite if a liquid is infinite. But really, the dependence of a logarithm on its large argument is very weak, and that is why the use of the formulae of Secs. 7.8 is possible even in the case of noncylindrical

volumes and nonsingle vortices. The minimum d_n among the distances from the vortex to the nearest wall or the nearest vortex may be used then instead of R ($d_n \gg a$).

7. NUMERICAL CALCULATIONS

For the aim of numerical calculations we express the integrals in Eqs.(14),(15),(17) as

$$\int_{\alpha}^{\beta} \left[1 - \left(1 + \frac{1-n}{n} \frac{1}{\xi^2} \right)^{-1/(1-n)} \right] \xi d\xi = \frac{1}{n} \ln \frac{k_{\mu} R \sqrt{n}}{a}, \quad (18)$$

$$\int_{\alpha}^{\beta} \left(1 + \frac{1-n}{n} \frac{1}{\xi^2} \right)^{-1/(1-n)} \frac{d\xi}{\xi} = \ln \frac{k_e R}{a}, \quad (19)$$

$$\int_{\alpha}^{\beta} \left[\left(1 + \frac{1-n}{n} \frac{1}{\xi^2} \right)^{-n/(1-n)} - 1 \right] \xi d\xi = -\ln \frac{k_u R}{a}. \quad (20)$$

Here k_{μ}, k_e, k_u are of the order of 1, which are independent on R and weakly dependent on n . Namely, they stay in intervals $0.5 \leq k_{\mu} \leq 1.2$, $0.3 \leq k_e \leq 1$, $0.5 \leq k_u \leq 1.2$ when the range of n is $0.1 < n < 10$ (the empirically found factor \sqrt{n} in Eq.(18) improves the independence of k_{μ} on n).

This work is partly supported by the Grant INTAS Network Open-97-1643 and by the Grant 2.17.02 of the Georgian Academy of Sciences.

REFERENCES



1. J.-M. Duan, Phys. Rev. Lett. **75**, 974, 1995; Q. Niu, P. Ao, D.J. Thouless, Phys. Rev. Lett., **75**, 1995, 975..
2. W. Thomson, Transact. Roy. Soc. of Edinburg, **XXV**, 1869, 217.
3. Yu.G. Mamaladze. Low Temp. Phys. LT-9, ed. J.G. Daunt et al. Part A. Plenum Press, N. -Y, 1965.
4. E.R. Huggins, Phys. Rev. **1A**, 1970, 332.

Georgian Academy of Sciences,
Institute of Physics
Tbilisi State University

ლ. კიკნაძე, ი. მამალაძე

ბრიტანეთის ბანკორუბეზული მასის დანაკლისი და
ბრიტანეთის დინამიკა

დასკვნა

ნაჩვენებია, რომ კლასიკურ პოლიტროპულ სითხეში არსებული გრიგალის საკუთარი მასა უარყოფითია, რადგანაც გრიგალი ამცირებს მის გარშემო მბრუნავი სითხის სიმკვრივეს და მის მოძრაობას შეაქვს საწინააღმდეგო მიმართულების წვლილი სითხის მოძრაობის რადენობაში. გრიგალის საკუთარი მასის (სითხის მასის დანაკლისის) სიდიდე დაკავშირებულია გრიგალის ენერჯიასთან და ბგერის სიჩქარესთან "აინშტაინის თანაფარდობით" (16). მიღებულია მიახლოებითი ფორმულები მასის დანაკლისისათვის, გრიგალის გარშემო სითხის ბრუნვის ენერჯიისათვის და გრიგალის წვლილისათვის სითხის შინაგან ენერჯიაში. ამ სიდიდეთა პოლიტროპის მაჩვენებელზე დამოკიდებულების დასაზუსტებლად ჩატარდა რიცხვითი გამოთვლებიც.

POLARIZATION HOLOGRAPHIC CORRECTORS OF LASER RADIATION

Sh. Kahkhashvili V. Tarasashvili

Accepted for publication September, 2001

ABSTRACT. The possibility of using the photoinduced anisotropy in selenium-cadmium glass and alcoholic solution of kryptocyanine for the correction of polarization along the wave front has been proposed and experimentally tested. The installation of polarization holographic correctors in intra-resonator space of the laser enables us to achieve divergences near to the diffraction limit with a high-energy output.

The problem of the correction of laser beams - purposeful influence of their characteristics with the requirement for forming the new coherent beams with more acceptable properties in a practical way then with the initial input optical signal of the system - continues to remain the problem of today [1-3]. The characteristics of the laser beam the influence of which results in changing it's properties are: amplitude, phase and polarization state distribution of the electric field voltage. In the aspect of transforming space-angular characteristics of the laser beam the corrector must provide the decrease of beam divergence and the given distribution of the above-mentioned characteristics of the light field on the beam section.

At present two prospective methods of dynamic influence on the wave fronts of laser radiation are well known and studied rather in detail - these are the phenomenon of the wave front reversal discovered in 1972 [4-6] and the possibility of creating dynamic holographic gratings discovered by a number of authors [7-9].

The correction devices based on the methods of the wave front reversal, which are intended for reducing the divergence of the radiation of quantum amplifiers, have a number of advantages which consist in the possibility of watching dynamically the challenges of the initial field and correct the light field with a complex-mode structure [10].

The above said only refers to scalar characteristics of the laser radiation. Purposeful influence on the polarization state of the laser beam particularly in its homogeneous distribution on the front requires complete equipping of the elementary base of influencing of the beam, the devices which act on the principles of the vector polarization holography [11].

If a reconstructing wave in a polarization-holographic experiment is directed in the opposite direction with the initial reference wave, then we observe the polarization reversal of the wave front. This phenomenon can be used to correct radiation generated by the laser with a complex distribution of polarization on the front. Such a correction can be realized both by extra resonator and intra-resonator placement of the dynamic polarization sensitive medium [1].

Anisotropic bleaching of selenium-cadmium glass KC-19 and an alcoholic solution of Kryptocyanine under the influence of the linearly polarized radiation of a ruby laser of large density was discovered in the works [12, 13]. In the given work the possibility of using photo induced anisotropy in these media for correcting radiation generated by a ruby laser with a complex distribution of the polarization state on the wave front has been experimentally approved for the first time.

The scheme of the experimental device for polarization-holographic correction with intra-resonator placement of the dynamic polarization sensitive medium is given in Fig. 1.

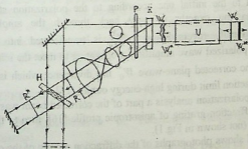


Fig. 1. Principal scheme of polarization holographic corrector

The principle of the simultaneous action on polarization and spatial-angular characteristics for the corrected beam is as follows. The weak linearly polarized plane wave W_0 , created by the given generator is transmitted from right to left through the inhomogeneous body of the amplifier U. Optical in-homogeneity of the amplifier results in the distribution of their wave and its transportation at the output into wave W_u of a complex form with inhomogeneous distribution of polarization on the front amplifier with respect to the original one. After passing through a polarizing prism K the laser beam is divided into two channels. The polarization states of the beams in these channels are orthogonal. A quarter-wave plate P standing in the way of both beams turns their polarization into right-hand circular and left-hand circular. The telescopic system at the expense of enlarging the section of the beam smoothes the unevenness of the wave front and forms a plane reference wave R.

As a result of the wave interference that came out of the amplifier and a plane reference wave R in a dynamic photo-anisotropic medium (K-19, alcoholic solution of kryptocyanine) three-dimensional polarization hologram H is formed. While reading such a hologram by a plane reference wave R^* , which propagates in the opposite direction with the initial one, in the place of the object is formed only the incident reversed front of the object wave W_u^* , which is fully intended to the initial one according to the polarization state [14]. After passing exactly its way back through the amplifier the polarizationally reversed wave W_u^* is transformed into a plane linearly polarized wave amplifier, propagating to meet the initial wave W_0 . The corrected plane-wave W_0^* has divergence which is close to the diffraction limit during high-energy output [15].

For polarization analysis a part of the corrected beam was directed to the diffraction grating of anisotropic profile [16], then to the linear analyzer (not shown in Fig. 1).

Fig. 2 shows photographs of the diffraction picture of the corrected laser beam W_0^* on the grating of anisotropic profile in two different positions of the linear analyzer.

In Fig.2a), in the center there is a non-diffracted linearly polarized zero order weakened by the orientation of the analyzer. To its left and right there are right-hand circularly polarized beams W_0^* , diffracted accordingly into +1 and -1 order. In Fig. b) there is no trace of zero or-

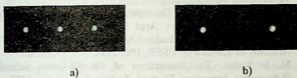


Fig. 2. A picture of diffraction of the corrected laser beam W_0^* on the grating of anisotropic profile.

der - the analyzer is oriented orthogonally to the direction of the oscillation of the electric vector of the corrected beam W_0^* .

In conclusion we may note that in order to study the possibilities of correcting laser beams by the polarization holographic method it is necessary to make measurements of space-angular characteristics of the corrected beams and also the efficiency of the wave front corrector, that in the general energy of the corrected beam irrespective of the effectiveness of the method of correction [2]. Such an analysis can also be of interest for using the method while recording dynamic polarized holograms and creating correctors with extra-resonator placement of polarization sensitive media.

REFERENCES

1. Sh. D. Kahkichashvili. In: Polarization Holography. 1989. (Russian).
2. A. V. Gnatovsky. Abstract of the thesis of the Doctor of Physical-mathematical sciences. 1988 (Russian).
3. A. M. Bikov, A. V. Gnatovsky. Materials of 5th All-Union Conference of Holography. Riga, 1985 (Russian).



4. V. Zeldovich, V. Popovichev, V. Ragulski, F. Faizulov. The Letters to journal of "Experimental and Technical Physics, 1972, 160 (Russian).
5. U. D. Nosach, V. I. Popovichev, V. V. Ragulski, F. S. Faizulov. The Letters to journal of "Experimental and Technical Physics, 16, 11, 1972, 617 (Russian).
6. U. A. Ananyev, Quantum Electronics. 1, 1974, 1669. (Russian).
7. D. F. Staebler, Y. Amocleyi. Appl. Phys., 43, 1972, 1042.
8. B. I. Stepanov, E. V. Ivakin, A. S. Rubanov. Papers of the Academy of Sciences of USSR, 196, 1971, 567. (Russian).
9. M. S. Soskin. The transactions of 4th All-Union School of Holography. Leningrad Physical Technical Institute, 1973, 231 (Russian).
10. P. Loginov. Abstract of the thesis of the candidate of physical - mathematical sciences. 1980, 16 (Russian).
11. Sh. D. Kahkichashvili. Abstract of the thesis of the Doctor of Physical-mathematical sciences. 1982 (Russian).
12. Sh. D. Kahkichashvili, V. I. Tarasashvili. Optics and Spektroskopy. 60, 5, 1986, 1071 (Russian).
13. Sh. D. Kahkichashvili. In: Photoanizotropic and Photogyrotropic phenomena in condensed media and polarization holography. 1987, 16 (Russian).
14. Sh. D. Kahkichashvili. In: Polarization Holography. 1989, 90 (Russian).
15. M. D. Bondarenko, A. I. Gnatovsky, M. S. Soskin. In: Quantum Electronics, 6, 1972, 71 (Russian).
16. Sh. D. Kahkichashvili, I. D. Shatalin, In the book: Photoanizotropic and Photogyrotropic phenomena in condensed media and polarization holography. 1987, 72 (Russian).

**Georgian Academy of Sciences
Institute of Cybernetics**

შ. ყაყინაშვილი, ვ. ტარასაშვილი

**ლაზერული ბამოსხივივის კოლარიზაციულ-
კოლობრაჟიული კორმქტორი**

დასკენა

შემოთავაზებულია და ექსპერიმენტულად აპრობირებულია სელენ-კადმიუმთან შინასა და კრიპტოციანინის სპირტხსნარში ფოტონინდუცირებული ანიზოტროპიის გამოყენების შესაძლებლობა ლაზერის მიერ გენერირებული გამოსხივების კორექციის მიზნით, ტალღის ფრონტზე პოლარიზაციის მდგომარეობის რთული, არაერთგვაროვანი განაწილების დროს. პოლარიზაციულ - პოლოგრაფიული კორექტორის განთავსებით ოპტიკური რეზონატორის სიერცეში მიიღწევა სინათლის კონის დიფრაქციულად ზღერული განშლადობა, მაღალი ენერგეტიკული გამოსავალის დროს.

THE INFLUENCE OF BOSON PEAK AND TWO-LEVEL SYSTEMS ON THE SHIFT OF ELECTRONIC MAGNETIC RESONANCE FREQUENCY



L.Zakharov*, L. Chotorlishvili

Accepted for publication September, 2001

ABSTRACT. The influence of tunnel two-level systems and "Boson peak" on the shift of the electronic magnetic resonance frequency have been studied. It is shown that in certain conditions the shift can be observed on experiments.

Lots of effort has been dedicated to the exploration of nuclear and electronic spin-lattice relaxation [1-6]. It has been established through these investigations that the relaxation rate in the amorphous solids is higher than in the corresponding crystal solids, besides the rate of relaxation in the amorphous solids is characterized by unusual dependence on temperature. In those investigations it has been supposed that the phenomenon is connected with the tunnel two level systems (TLS) [7-8]. By this means the anomalous low-temperature properties have been successfully explained. Various mechanisms of the nuclear spin-lattice relaxation, including TLS have been explored in [9-10]. In addition to the TLS there is an abundant density of oscillatory states (DOS) in the range of energy 3-15K in the amorphous solids [11-14].

Abundant DOS looks like the peak, maximum magnitude of which surpasses 2-6 times to the density of Debye's oscillatory states existing at the same temperature [12-13]. The abundant DOS is known in literature as "Boson peak". Presence of the "Boson peak" determines heat capacity and heat conductivity of amorphous solids near the temperature $T \sim 10$ K. The influence of "Boson peak" on the low-temperature spin-lattice relaxation has been investigated in Refs. [15-16].

The purpose of the present article is the investigation of the influence of TLS and "Boson peak" on the line shape of electronic paramagnetic resonance (EPR).

1. First of all, the influence of TLS on the line shape of EPR should be examined. Amorphous diamagnetic, including paramagnetic admixtures with $S = 1/2$ spins in the constant magnetic field directed along the Z axis should be examined. For the simplicity, suppose, paramagnetic admixtures form TLS. Tunneling of paramagnetic center from one balance state to another leads the modulation of g factor and consequent interaction of electronic spin with TLS. As is well known, for the $S = 1/2$ spins in the spin-phonon interaction and accordingly in the interaction of electronic spins with TLS Spin-Hamiltonian Zeeman's portion makes a basic contribution [17]:

$$H_Z = H_0 \sum_i \sum_{\alpha} g^{\alpha z}(\vec{r}_i) S_i^{\alpha} \quad (1)$$

After expanding (1) into series in terms of the small parameter $-\frac{\ell}{a}$ (where r is the interatomic distance and a - the average distance between the minimums of asymmetrical potential well) in the representation of TLS, interaction Hamiltonian of electronic spins with TLS can be obtained, as follows:

$$H_{DS} = \sum_i (D_i^- S_i^+ + D_i^+ S_i^-) + \sum_i D_i^z S_i^z, \\ D_i^z = H_0 G_i^{zz} \frac{\ell}{\alpha} (d_i^z \cos \theta_i - d_i^x \sin \theta_i), \\ D_i^{\pm} = H_0 G_i^{\pm z} \frac{l}{\alpha} (d_i^z \cos \theta_i - d_i^x \sin \theta_i), \quad (2)$$

$$G_i^{\pm z} = \sum_r n_r \left(\alpha \frac{\partial g^{\pm z}(\vec{r}_i)}{\partial \alpha_i^r} \right)_{\vec{r}_{i0}}, \quad G_i^{zz} = \sum_r n_r \left(\alpha \frac{\partial g^{zz}(\vec{r}_i)}{\partial \alpha_i^r} \right)_{\vec{r}_{i0}}$$

$$\sin \theta_i = \frac{\Delta_{0i}}{E_i}, \quad \cos \theta_i = \frac{\sqrt{E_i^2 - \Delta_{0i}^2}}{E_i}$$

where Δ_0 is the tunneling parameter, Δ the potential well asymmetry, $E = \sqrt{\Delta_0^2 + \Delta^2}$ is the TLS energy, d is the pseudo-spin with the properties of spin 1/2, \vec{r}_{0i} is the radius vector point lying between the minimums of asymmetrical potential and \vec{n}_i is the unit vector orientating along these minimums.

Let us calculate the first moment of absorption function, which, as is well known, determines the shift of resonance frequency and is defined by the following formula [17]:

$$M_1 = 2 \frac{\langle [S_x [H_{DS}, S_x]] \rangle}{\langle [S^-, S^+] \rangle}, \quad (3)$$

where $\langle \rangle$ denotes a statistical average. Considering the Hamiltonian (2), for the first moment in the approximation $T \ll \omega_s$, $\omega_s = H_0 \sum_i g^{zz} (\vec{r}_{i0}) S_i^z$ (Zeeman's frequency of electronic spin) we obtain:

$$M_1 \approx H_0 \frac{\ell}{\alpha} \left(\overline{G_i^{zz}} \right) \frac{\overline{p} E_{max}}{N_s}, \quad (4)$$

where p is the density of state of the TLS, E_{max} is the maximum energy of TLS, N_s is the concentration of paramagnetic centers (PC), \overline{G}^{zz} is the average magnitude of G^{zz} and in magnitude equal $\overline{G}^{zz} \sim \omega_s \frac{\ell}{\Lambda}$, here Λ is a characteristic range of change of g factor. If we take into account that $\overline{p} E_{max} = N_d$ is the concentration of TLS-s, for the first moment we obtain:

$$M_1 = c \omega_s \frac{\ell}{\Lambda}, \quad (5)$$

where c is the probability that PC forms TLS. Eq. (5) reveals that in certain conditions the shift of resonance frequency caused by

interaction (2) can be observed on experiments. In particular for the standard values of the parameters $\frac{l}{\Lambda} \approx 1$, $c \approx 0.01$, $\omega_s \approx 10^{11} \text{ Hz}$ [10]

we have $M_1 \approx 10^{-9} \text{ Hz}$.

2. The influence of "Boson peak" on the line shape of electronic magnetic resonance should be examined. By the analogy [18], the method of temperature functions of Green can be applied [19]. The total Hamiltonian in our case has a form:

$$H = \sum_{m,j} E_m a_{mj}^+ a_{mj} + \sum_q \hbar \omega_q b_q^+ b_q + i \sum_{j,m,n,q} C_{jmn}^q a_{mj}^+ a_{nj} (b_q e^{iqr_j} - b_q^+ e^{-iqr_j}),$$

where E_m is the electron energy, b_q^+ , b_q are the second-quantizing operators for phonons with wave vectors q , r_i is the reduce-vector for i -th spin, \hbar is the Planck constant, C_{jmn}^q is the interaction constant. The equation for Green function $\langle\langle A/B \rangle\rangle$ has a form [19]

$$i\hbar \frac{\partial}{\partial t} \langle\langle A/B \rangle\rangle = \hbar \delta(t) \langle[AB]\rangle - \langle\langle [H; A]B \rangle\rangle,$$

where $\langle\langle \rangle\rangle$ means statistical averaging, $\delta(t)$ is the Dirac function. We have to use some approximations to solve this equation, namely,

$$\langle\langle a_{m_1}^+ a_{n_1} a_{m_1'}^+ a_{n_1'} / a_{k_j}^+ a_{e_j} \rangle\rangle = \delta_{m_1 n_1'} \langle\langle a_{m_1}^+ a_{n_1} / a_{k_j}^+ a_{e_j} \rangle\rangle,$$

$$\langle\langle a_{m_1}^+ a_{n_1} (b_q e^{iqr_1} - b_q^+ e^{-iqr_1}) b_{q'} / a_{k_j}^+ a_{e_j} \rangle\rangle =$$

$$= -\delta_{qq'} e^{-iqr_1} \langle\langle a_{m_1}^+ a_{n_1} / a_{k_j}^+ a_{e_j} \rangle\rangle.$$

After all, for the shift frequency of electronic magnetic resonance caused by "Boson peak" we have:

$$\Delta\omega = \frac{4R^2(\gamma_S H)^2}{3\pi^2 \hbar^2 \rho v^5} \cdot f \cdot g(T), \quad (6)$$



where R is the distance from paramagnetic center to the proximate particle, ρ is the density of the material, v is the velocity of sound, $\gamma_S H$ is the frequency of electronic magnetic resonance (EPR), f is the characteristic magnitude of spine phonon interaction, and

$$g(T) = \frac{\omega_m^2 \mu}{\gamma_S H} V.P. \int \frac{\omega}{e^{\hbar\omega/KT} - 1} \cdot \frac{e^{-\frac{\omega_m}{2\sigma^2}}}{H\gamma_S - \omega} d\omega. \quad (7)$$

The results of numerical calculations for the parameters $\gamma_S H \sim 10^{11} \text{ Hz}$, $\omega_d \sim 10^{13} \text{ Hz}$, $\mu \sim 10$, $\sigma \sim 0.5$, $\omega_m \sim 8 \cdot 10^{11} \text{ Hz}$ are shown in Fig. 1,2.

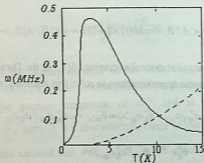


Fig.1. Dependence of the frequency change on temperature. The solid line corresponds to Boson peak. The dashed line corresponds to the Dedye model

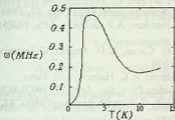


Fig.2. Full change of the frequency as a function of temperature

ω_m is the frequency that corresponds to maximum density state in "Boson peak".

Fig.2 shows the results of EPR frequency total shift caused by "Boson peak" as well as by acoustic phonons (the value of the latter is taken from 18)). It is obvious from the Fig.2 that at the temperature

$T < \frac{\hbar\omega_m}{K_B}$ the frequency shift of EPR is resulted by "Boson peak".

REFERENCES

1. T.L. Reinecke, K.L.Ngai. Phys.Rev. **B.12**, 1975, 3476.
2. M. Rubinstein, H.A. Reving. Phys.Rev. **B.13**, 1976, 959.
3. J. Szeftel, H.Alloul. J. Non-Crystal. Sol. **29**, 1978, 253.
4. S.R. Kurtz, J. Stapleton. Phys. Rev. **B.32**, 1980, 2195.
5. G. Balzer-Jollenbeck, O. Kanert, J. Steinert. Solid State Com. **65**, 1988, 303.
6. J. Dieckhousauffer, O. Kanert, R. Kuauchler. Phys. Rev. **B.55**, 1997, 14836. - S.Estalji, O.Kanert, J.Steinert, K.L.Ngai. Phys.Rev. **B43**, 1991, 7481.
7. P.W. Anderson, B.I. Halperin, C.M. Varma. Phil. Mag.**25**, 1972, 1.
8. W.A. Phillips. J. Low Temp. Phys.**7**, 1972, 351.
9. L.L.Buishvili, L.Zh.Zakharov, A.I.Tugushi, N.P.Fokina. Physica **B168**, 1991, 205.
10. T.L. Buishvili, N.P.Giorgadze, L. Zh. Zakharov. Phys. Stat. Solid.

209, 1998, 427.

11. V.K. Malinovsky, A.P. Sokolov. *Solid State Com.* **57**, 1986, 757.
12. V.K. Malinovsky, V.I. Novikov, A.P. Sokolov. *APS*, **163(5)**, 1993.
13. A. Fontana, F. Rossi, G. Carini, G.D. Angelo, G. Tripodo. *Phys. Rev. Lett.* **78**, 1997, 1078.
13. Martin P. Dove, M.J. Harris, A.C. Hannon, J.M. Parer, I.P. Swainson, M. Gamblir : *Phys. Rev. Lett.* **78** (1997) 1070
14. A. Lebanidze, T. Buishvili, G. Kobakhidze. *Biophysica.* **42**, 1997, 811.
16. N. Giorgadze, L. Zakharov, *Low. Temp. Phys.* **24**, 1998, 262.
17. S. Altshuler, B. Kozirev. *Electronic paramagnetic resonance (Russian)*, 1972.
18. L. Aminov, B. Kochalaev. *J. Solid State. Phys.* **4**, 1962, 6.
19. N.H. March, W.H. Young, S. Sampanthar. *The many-body problems in quantum mechanics.* Cambridge, 1967.
-Richard D. Mattuck. *A guide to Feynman diagrams in many-body problem.* London, 1967.

Georgian Academy of Sciences
Institute of Physics
Tbilisi State University

ლ. ზახაროვი , ლ. ჭოტორღიშვილი

“ბოზონური პიკის” და ორდონიანი სისტემების
გავლენა ელექტრონული მაგნიტური რეზონანსის
სიხშირის წანაცვლებაზე

დასკვნა

შესწავლილია ბოზონური პიკის და ორდონიანი სისტემების გავლენა ელექტრონული მაგნიტური რეზონანსის სიხშირის წანაცვლებაზე. ნაჩვენებია რომ გარკვეულ პირობებში ეს წანაცვლება დაკვირვებადია ექსპერიმენტზე.

DISTORTED PULSE SPIN ECHO IN TWO-LEVEL SYSTEMS INSIDE AMORPHOUS FERROMAGNETS



L. Chotorlishvili

(Accepted for publication September, 2001)

ABSTRACT. In the case of applied distorted pulse, the single pulse echo in amorphous magnets caused by the tunneling two-level systems (TLS) located inside 180° Bloch walls has been studied. It is shown that in case of TLS the single-pulse echo formation is characterized by some specificity due to the wide distribution of the TLS splitting energy.

This paper is devoted to the presentation of a theoretical model of the single-pulse spin echo stemming from two-level systems (TLS) inside 180° Bloch domain walls in an amorphous ferromagnetics.

Amorphous systems with tunneling two-level systems TLS are widely studied [1]. The TLS model was first developed for spin glasses and then - for hydrogenous metals [2,3] and solid solutions [4,5]. Amorphous ferromagnetic materials with TLS are considered in [6,7]. Excitations observed in experiments can be described by TLS [1]. According to the TLS model, it is assumed that TLS are formed by atoms or atom groups which can occupy two equivalent positions with almost equal probability in a double asymmetric well with splitting energy $E = \sqrt{\Delta_0^2 + \Delta^2}$ (Δ is the asymmetry parameter and Δ_0 is the TLS tunneling energy). The spin-echo method is very effective for TLS investigations. It allows establishing the relation between the experiment and the theory [8]. Polarized echo, caused by TLS in spin glasses, was investigated in [8] and in amorphous ferromagnetic in [9]. It is assumed that by "pulse methods" the two-pulse echo is meant. Recently, a single-pulse echo the mechanism of origination of which is not simple has provoked an interest [10]. This article deals with the investigation of single-pulse echo in amorphous ferromagnetics (caused by TLS located inside domain walls) within the frames of the distorted pulse model. As it was mentioned above, the model of amorphous ferromagnetics with TLS was first proposed

in [6-7]. Atoms, forming the TLS can be magnetic or non-magnetic. If atoms are magnetic they will be connected with the modulation of dipole-dipole, exchange and anisotropy energies. The dipole-dipole interaction between the magnetic moments of the atoms forming TLS and the electronic magnetic moments forming the ferromagnetic structure of the material (domains and 180° Bloch walls) provokes a significant interest. The fluctuations of dipole-dipole interaction constant, caused by the atom transition between TLS states, allow TLS pseudo-spin to experience the action of external magnetic field (static or variable) through the influence of this field on magnetic moments of electronic spins located in the domain walls. Briefly, to explain the above-mentioned mechanism we can apply the method used in [11]. Let us consider that $\vec{M}_i = \gamma_s \vec{S}_i$ is the magnetic moment of the atom located in the i -th TLS, where γ_s is the gyro-magnetic ratio for the electrons, \vec{S}_i is the electron spin operator. The dipole-

dipole interaction $H_{dd} = A \left(\frac{1}{r_{ij}^3} \right) \vec{M}_i \vec{M}_j$ between magnetic moment \vec{M}_i and electronic magnetic moments located in domain wall varies due to the fluctuation of the inter-atomic distance r_{ij} (as a result the tunneling of i -th atom from one state to another)

$$H_{dd} = \begin{pmatrix} A \left(\frac{1}{\left(r_{ij} + \frac{d}{2} \right)^3} \right) & 0 \\ 0 & A \left(\frac{1}{\left(r_{ij} - \frac{d}{2} \right)^3} \right) \end{pmatrix} \vec{M}_i \vec{M}_j$$

where d is the distance between the states of i -th TLS, A is the dipole-dipole interaction constant. Expression for H_{dd} can be expanded in a

series over $\frac{d}{r_{ij}} \approx 0,1$. Taking into account the linear term of this expansion we obtain the following expression for the frequency of i -th TLS

$$\omega_i = \frac{E_i'}{\hbar} = \left(E_i / \hbar + \frac{3d}{\bar{r}} \sum_j A_{ij} \vec{M}_i \vec{M}_j \right) d_i^z,$$

where d_i^z is the pseudo-spin operator of TLS, \hbar is the Planck constant and E is the TLS splitting energy. When the line width of TLS caused by Klauder-Anderson mechanism equals $\Delta\omega \sim 10^6 \text{ Hz}$ the magnitude of $\frac{3d}{\bar{r}} \bar{A} \gamma_s^2 \sim 0,3 \cdot 10^9 \text{ Hz}$ shows that the given mechanism is effective.

The influence of external magnetic field on the TLS frequency is not direct. The influence of the external magnetic field on the magnetic moment of i -th atom presented in the i -th TLS does not affect directly the frequency of this i -th TLS. This influence is displayed on other TLS, when the magnetic moment of the given i -th atom plays the role of external electronic moment. Let us consider the influence of external variable field on the frequency of two-level system in more detail. The insertion of variable field causes the change of δM electric magnetic moments orientation. These moments take the orientation of the effective field $H = H_0 + h(t)$, where H_0 is the static magnetic field and $h(t)$ is the variable magnetic field.

We can qualitatively estimate the change of the TLS frequency caused by this effect. Let us suppose that the variable field is in resonance with one of the packets of the magnetic moments with equal quasi-Zeeman frequencies, included in the sum $A_{ij} M_i M_j$. As M_i and M_j frequencies differ from each other the variable field cannot be in resonance with the both packets. Neglecting variable field influence on the nonresonant moments, we can see that above-mentioned effect must be linear to δM

$$\delta\omega' = \frac{3d}{\bar{r}} \bar{A} M \delta M,$$

where $\delta\omega'$ is the TLS frequency variation, \bar{A} is the average value of the dipole-dipole interaction constant, \bar{r} is the average value of the inter-atomic distance. Let us imagine that δM has the following form: $\delta M = \lambda h(t)$, where λ is the magnetic susceptibility of electric system (the tensor of magnetic susceptibility $\lambda^{\alpha\beta}$, as well as the tensor of enhancement $\eta^{\alpha\beta} \approx \lambda^{\alpha\beta}$, have only one component, which is not zero [12] in the 180° Bloch strip domain structure). We compare two kinds of changes when the radio-frequency field is applied on. The first change of TLS frequencies is caused by electrical spins existing in domain walls, and the second one is caused by spins in domains. As $\lambda_w > \lambda_\alpha$, where λ_w and λ_α are the magnetic susceptibilities for walls and domains [12], we can conclude that the interaction of TLS with domain walls prevails over the interaction with domains:

$$\frac{\delta\omega'_w}{\delta\omega'_\alpha} \sim \frac{\lambda_w}{\lambda_\alpha} \sim 10^3.$$

where $\delta\omega'_w$ is the change of TLS frequency caused by domain walls and $\delta\omega'_\alpha$ is the change caused by domains. To obtain the dependence of echo amplitude on time, we use the method described in [13] and the method used for studying the nuclear single-pulse echo within the frames of the distorted pulse model [14]. In contrast to single-pulse echo caused by nuclear spins the single-pulse echo caused by TLS must have some peculiarities caused by the wide distribution of TLS parameters and constancy of TLS state density. As it is known, the influence of pulse with the phase changed at the beginning and at the end of the pulse is equivalent to the influence of distorted pulse in the rotating system

$$h^+ = h \begin{cases} \exp(i\varphi_e) & 0 < t' < \tau_e \\ \exp(i\varphi) & \tau_e < t' < \tau_e + \tau \\ \exp(i\varphi_t) & \tau_e + \tau < t' < \tau_e + \tau + \tau_t \end{cases}$$

where $h^+ = h_x + ih_y$, τ_e and τ_t are the time intervals of distorted parts, τ is the interval of non-distorted part, φ is the phase of the part of non-distorted pulse, and h is the amplitude of radio frequency (RF) field.

Let us write Bloch's equations for pseudo-spins of TLS. Taking into account the interaction with domain walls and introducing the

notations $s = \frac{\mu_+}{\mu_0}$, $m = \frac{\mu_z}{\mu_0}$, $\delta = \frac{E}{h} - \omega$, $q = \gamma h^+$ we will obtain:

$$\begin{cases} s + i\delta s = iqm \\ \dot{s}^* - i\delta s = -iqm \\ m = 1/2iq(s - s^*) \end{cases}$$

where μ_0 is the equilibrium value of TLS state polarization [8], μ_+ and μ_z are the longitudinal and transverse components, ω is the frequency of RF. field, E is the TLS splitting energy, and $\gamma = \frac{3d}{r} \bar{A} \gamma_s \lambda_w$ is the constant describing the influence of variable field on TLS by means of electric magnetic moments. This constant is of the order of $\gamma \sim 10^3 \text{ Hz} \frac{M}{A}$.

Using the Laplace transform

$$\hat{s} = \hat{s}(p) = \int_0^{\infty} S(t) e^{-pt} dt$$

and also the transform for m , Bloch's differential equations take algebraic form:

$$\begin{cases} (p + i\delta)\hat{s} - iq\hat{m} = s_0 \\ (p - i\delta)\hat{s}^* + iq\hat{m} = s_0^* \\ p\hat{m} - \frac{i}{2}q(\hat{s} - \hat{s}^*) = m_0 \end{cases}$$

Taking into account the first equation, we can express \hat{s} , \hat{s}^* by means of \hat{m} , then introducing the obtained expression in the third equation we obtain:

$$\hat{m} = \frac{m_0(p^2 + \delta^2) + \frac{i}{2}q[s_0(p - i\delta) - s_0^*(p + i\delta)]}{p(p^2 + \delta^2 + q^2)}$$

Making the inverse Laplace transform

$$m(t) = \frac{1}{2i\pi} \int_{x-i\infty}^{x+i\infty} \hat{m}(p) e^{pt} dp$$

and taking into account that $\hat{s} = \frac{s_0 + iq\hat{m}}{p + i\delta}$, for the transverse component of the magnetization we obtain by solving the Bloch's equations the following:

$$\begin{aligned} \mu^+(t, E, \eta) = \mu_0 [& A_1^* (A_2 A_2' + A_3 A_1' + A_4^* A_4') + \\ & + A_1^{*o} (A_4 A_2^e + A_2^* A_4' + A_3^* A_1') + A_5^e (A_1 A_2' + A_3 A_1' + A_1^* A_4')] \exp(i\delta t) \end{aligned}$$

where

$$A_1 = \frac{\chi}{\phi} \left(-\frac{2\delta}{\phi} \sin^2 \frac{\phi\tau}{2} + i \sin \phi\tau \right) \exp(i\varphi) ,$$

$$A_2 = \cos \phi\tau + \left(\frac{\chi}{\phi} \right)^2 \sin^2 \frac{\phi\tau}{2} + i \frac{\delta}{\phi} \sin \phi\tau ,$$

$$A_3 = \frac{A_1}{2} \exp(-2i\phi) ,$$

$$A_4 = \left(\frac{\chi}{\phi} \right)^2 \sin \frac{\phi\tau}{2} \exp(2i\phi) ,$$

$$A_5 = 1 - 2 \left(\frac{\chi}{\phi} \right)^2 \sin^2 \frac{\phi\tau}{2} ,$$

$$\phi = (\delta^2 + \chi^2)^{1/2} , \quad \delta = \frac{E}{\hbar} - \omega , \quad \chi = \eta\gamma\hbar .$$

Here η is the enhancement factor for the domain walls, ω is the frequency of applied pulse, t and l indices correspond to $\tau_{i,l}$ and $\varphi_{i,l}$. $*$ means the complex conjugation. The effect of domain walls makes it necessary to take into account the effect of enhancement using the enhancement factor distribution function [15]

$$F_{\omega}(\eta) = \eta^{-1} \int_0^{\infty} \exp \left(\frac{[(\varepsilon^2 + \eta^2)^{1/2} - \bar{\eta}_0]^2}{\Delta\eta_0^2} \right) \eta d\eta , \quad (2)$$

where ε , $\bar{\eta}_0$, and $\Delta\eta_0$ are parameters described in [15]. After averaging of (1) by the TLS distribution function $p(\Delta_0 E) p$ [1], and using (2) we obtain:

$$M(t) = \left| \int_{E=0}^{E_{\max}} \int_{\Delta_0=0}^E \frac{\bar{\rho} E d E d \Delta_0}{\Delta_0 \sqrt{E^2 - \Delta_0^2}} \int_0^{\infty} F_{\omega}(\eta) \eta d \eta \mu^+(t, E, \eta) \right|, \quad (3)$$

where $\bar{\rho}$ is the TLS state density.

To analyze the obtained results we need the numerical methods. The result of numerical calculations for the parameters

$$\tau_1 = \tau_r = 1 \cdot 10^{-6} \text{ s}, \quad \gamma \hbar = 10^4 \text{ s}^{-1}, \quad \tau = 8 \cdot 10^{-6} \text{ s}, \quad \omega \sim 10^6 \text{ Hz}, \quad \varphi_1 = \frac{\pi}{6},$$

$$\varphi_r = \frac{\pi}{3}, \quad \varphi = 0, \quad \Delta \eta_0 = 100 \quad [12, 13],$$

is shown in Fig. 1.

Let us consider some peculiarities of single-pulse echo formation in case of TLS. Since in contrast to nuclear spins the pseudo-spins of the TLS are not directly affected by variable field, the mechanism of single-pulse echo formation, suggested in this paper, can be considered as original and different from that in [14]. There is another principal difference in the value of δ . For nuclear spins $\delta = \omega_0 - \omega_n$, where ω_0 is the frequency of nuclear magnetic relaxation (NMR) (the pulse frequency coincides with it), ω_n is the frequency of a specific nucleus (distribution of nuclear frequencies is considered to have the Gaussian form). In our case $\delta = \frac{E}{\hbar} - \omega$, where ω is the pulse

frequency, E is the TLS splitting energy. At the same time, the limits of E variation are sufficiently large $0,01\text{K} \leq E \leq 10\text{K}$, and we use the TLS distribution function $P(E, \Delta)$ to average the result obtained (exp. (3)). Thus, TLS, the pulse frequency of which is resonant and TLS the frequency of which differs from the pulse frequency take part in the echo formation. Since there is no other principal difference in author's opinion the fact that echo signal formed by TLS (Fig. 1) ceases more slowly in time than the signal formed by nuclear spins (ref. [14]) can be explained by the above-described peculiarities.

By this peculiarity in the low-temperature experiments, one can distinguish the subsystem of TLS from the nuclear subsystem.

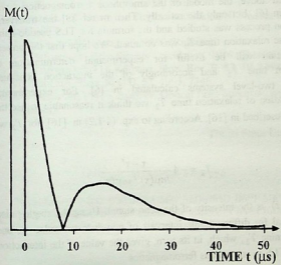


Fig.1. Curve of the free induction decay and echo amplitude as a function of time

Because of the lack of published experimental results on the single-pulse spin echo in amorphous magnets, we cannot present the experimental data in Fig. 1 to compare them with the theory. As it was mentioned above, the model of the amorphous ferromagnetics was studied in [6], but only theoretically. Then in ref. [9] the transverse relaxation process was studied and the formula for TLS pseudo-spins transverse relaxation time T_2 was obtained. We hope that the present investigation will be useful for experimental determination of relaxation time T_2 and accordingly of the interaction constants between two-level systems calculated in [6]. For experimental determination of relaxation time T_2 we think it reasonable to use the method described in [16]. According to exp. (4.1.2) in [16], for T_2 we have

$$T_2 = -4 \frac{\tau - \tau'}{\ln \mu(\tau) / \ln \mu(\tau')},$$

where $\mu(\tau)$ is the intensity of the echo signal. Using the single-pulse echo signal for different time intervals of non-distorted pulse τ , one can determine T_2 , which, in its turn, gives the value of the interaction between TLS in amorphous ferromagnetics.

REFERENCES

1. P.W. Anderson, B.I Halperin, C.Varma. *Phil. Mag.* **25**, 1972, 1.
- W. A. Phillips. *J. Low Temp. Phys.* **7**, 3/4, 1972, 351.
2. H. Wipf, K. Neumaiev. *Phys. Rev. Lett.* **52**, 15, 1984, 1308.
3. H. Wipf. *Phys. Rev. Lett.* **46**, 14, 1981, 947.
4. V. Narayanamurti, R. Pohl. *Rev. Mod. Phys.* **42**, 1970, 201.
5. S.K. Watson. *Phys. Rev. Lett.* **75**, 1995, 1965.
6. C.V. Maleev, I.N. Skriabin. *JETP.* **83**, 1, 1982, 380. (Russian).
7. Mucio A. J. Continentino. *J. Phys. C. Solid State Phys.* **14**, 1981, 3527.
8. S. Hunklinger. *Proc. of the 21st Int. Conf. on Low. Temp. Phys.*



Czech. J. of Phys. 46, S6, 1996, 3287.

9. L.L. Chotorlishvili, G.R. Kakabadze. J. Low. Temp. Phys. 26, 1, 2000, 62.

10. A.L. Bloom. Phys. Rev. 89, 1955, 1105.

11. Buishvili L., Zakharov L., Tugushi A., Fokina N. Physica B 168 1991, 205.

12. A Kurkin. NMR in magnets. 1990 (Russian).

13. V.I Tsifrinovich. Echo Signals Calculation, 1986. (Russian).

14. V.I. Tsifrinovich, I.G. Kiliptari. Phys. Rev. B. 57, 18, 1998, 11554

15. I.G. Kiliptari. Phys. Rev. B. 52, 1995, 7346.

16. E.A. Manykin, V.V. Samartsev. Optical Echo Spectroscopy. 1984 (Russian).

Tbilisi State University

დ. ჯორჯორელიშვილი

დამახინჯებულ იმპულსიან სპინური ექო ამორფულ ფერომაგნეტიკებში მყოფ ორდონიან სისტემებში

დასკვნა

დამახინჯებული იმპულსის ზემოქმედების შემთხვევაში შესწავლილია ბლოხის კედლებში მყოფი ტუნელური ორდონიანი სისტემებით განპირობებული ექო. ნაჩვენებია რომ ტუნელური ორდონიანი სისტემების შემთხვევაში ექოს ფორმირება ხასიათდება რიგი თავისებურებებით რომლებიც დაკავშირებულია ორდონიანი სისტემების გახლეჩის ენერჯის ფართო განაწილებასთან.

THE INFLUENCE OF LIGHT ON THE RATE OF THERMAL
EXPANSION OF MONOCRYSTALLIC SILICON AND ON DEBAY
TEMPERATURE



G. Chiradze

Accepted for publication October, 2001

ABSTRACT. Baseing on the example of monocrystalline and dislocation-free silicon, the paper experimentally presents that white lighting increases the thermal expansion rate and, subsequently, decreases Debay temperature as compared with their values at a given temperature in darkness, which is due to weakening of inter-atom chemical bonds by means of anti-bonding quasiparticles (free electrons and holes), produced by light.

According to [1,2], the probability, connected with the process of performance of an elementary act of motion of an atom from one spatial position into another in solid bodies, has been defined by the following expression:

$$W = A(n_i / N_A)^x \cdot W_\phi, \quad (1)$$

where A is a weakly changing numerical rate, the value of which is given in [1], n_i is a concentration of antibonding quasiparticles - AQP's (free electrons and holes, correspondingly, in anti-bonding and bonding zones (1)), N_A is a concentration of a substance's atoms, x is a necessary number of AQP's for performing an elementary act of the given process [1], and W_ϕ is a probability of approaching a given atom by phonons with maximum energy in the number achieved at the temperature of fusion having the following expression [3]:

$$W_\phi = [(n_\phi)^{n_\phi} / n_\phi!] \cdot \exp(-n_\phi), \quad (2)$$

where $n_\phi = 3T_{\text{melt}}/\theta$ is a number of phonons falling on an atom at the temperature of fusion (θ is Debay temperature), n_ϕ is a number of phonons falling on an atom at a given temperature.

As is seen in the expression (1), the more the probability of an atom's motion the more the concentration of AQP is at a given temperature. Besides, the processes, connected with an approach to a given atom of AQPs and phonons with maximum energy, have been considered mutually independent (as the probabilities of these processes have been multiplied by each other). Though, in some concrete cases, such an approach may not be quite correct. This is due to the fact that, if in a semiconductor, at unchanging temperature, a complementary concentration of AQPs is established (by the impact of illumination, electric field, ionization of mixtures), then these AQPs have a weakening impact on chemical bonds between atoms (which was experimentally proved in [4-6]). The mentioned weakening of chemical bonds should influence the value of W_{ϕ} , as far as, in this case, the phonon spectrum of the material will necessary change, the criterion of which is Debay temperature [7].

In [8] it was noticed that the introduction of electrically active mixtures into Ge causes the lowering of its Debay temperature. The present paper assesses the change of Si Debay temperature, caused by the influence of illumination and, based on the corresponding change, of the rate of thermal expansion (RTE).

There is a following expression for the RTE [9]:

$$\alpha \cong \gamma k / \beta^2 a_0 \quad (3)$$

where γ is a coefficient of anharmonicity, k is a Boltzmann constant, β is a coefficient of a quasi-resilient bond, a_0 is an equal value of interatomic distance. The coefficients β and γ are interdependent and approximately: $\gamma \sim \beta/a_0$ i.e. $\alpha \sim 1 / \beta a_0^2$.

The shift in interatomic distances towards the increase at the given temperature, owing to the weakening of chemical bonds by photoexcited AQPs, was presented in [10], by the way of illustration of Si. This phenomenon should be accompanied by the corresponding decrease of β , in comparison with its value in the dark. The change of β may be expressed by the way of the corresponding change of θ , if we use $\beta \sim \theta^2$. Then, the relative change of RTE may be expressed in the following way:

$$\Delta\alpha/\alpha_0 \cong 2\Delta\theta/\theta,$$



where $\Delta\theta = \theta_0 - \theta$, θ_0 is Debay temperature of a non-illuminated material, and θ is the same value in case of illumination.

Determination of the change of the RTE was conducted by the way of illustration of dislocation-free, monocrystalline Si, of the n-type of conductivity, with specific resistance 200 ohm-cm, and with the orientation of the surface (100). Deorienting did not exceed 0.3° .

The methods of preparing of surface samples, of measuring lattice dimensions (by x-ray diffractional method) in the dark and in case of illumination at different temperatures were described in [10]. The illumination was conducted by means of a glow-lamp with tungsten filament, of the type K21-150, while as the illumination of the surface of the investigated sample constituted $3 \cdot 10^5$ lucas. In this case $L_{\text{EXC}} \ll 1/\alpha$ (where L_{EXC} is the length of extinction, characteristic of the depth of penetration of X-rays in a crystal in ease of diffraction, and α is a rate of absorption in Si of the current light irradiation).

In accordance with the received experimental data, relative change of the dimension of the lattice, evoked by lighting, constituted $\Delta a/a_0 = 9.6 \cdot 10^{-5}$ and the addition of temperature equalled Si is given in Table 1. Conducted control measurements in the darkness at analogous temperatures, enabled the calculation of the RTE of the lighting - α_0 (which corresponds to the relative change of the RTE - $\Delta\alpha/\alpha_0$ has been also presented.

Table 1

Mode	Value RTE (degree ⁻¹)	$\Delta\alpha/\alpha_0$, %
Lighting	$\alpha = 3.3 \cdot 10^{-6}$	18
Darkness	$\alpha_0 = 2.8 \cdot 10^{-6}$	

Judging from the formula (4), the Debay temperature of the investigated Si in case of the above-described lighting should equal 575 K (as far as, for pure Si, the Debay temperature equals 625 K [11]).

It should be mentioned that the introduction of the correction on the Debay temperature in the expression W_d leads to the improvement of the agreement between W , defined from the formula (1), and the values of light microhardness of a material in the process of lighting) at different intensities of lighting.

I acknowledge the help of Prof. A.B. Gerasimov for the permanent interest to the work and discussion of the results.

REFERENCES

1. A.B. Gerasimov. Proc. of the Fourth Int. Conf. Materials of Science Forum, New York, 47, 1990, 66.
2. A.B. Gerasimov, G.D. Chiradze, Z. G. Bokhochadze. Bull. of the Kutaisi University, 1, 1994, 125.
3. I.G. Gverdsiteli, A.B. Gerasimov, Z.G. Gogua, Z.V. Jibuti, M.G. Pkhakadze. Bull. Georg. Acad. Sci., 127, 3, 1987, 517 (Russian).
4. A.B. Gerasimov, G.D. Chiradze, N.G. Kutivadze. Fiz. Tekh. Poluprovodn., 35, 2001, 70 (Russian).
5. A.B. Gerasimov, G.D. Chiradze, N.G. Kutivadze. Collection of Scientific Works "Intellecti", 3, 1998, 24 (Russian).
6. A.B. Gerasimov, G.D. Chiradze. Fiz. Tekh. Poluprovodn., 35, 2001, 384 (Russian).
7. G. Blakemore. Physics of Solid State. 1988, 606 (Russian).
8. Brianta and Keesom. Phys. Rev., 124, 1961, 698.
9. K.V. Shalimova. Physics of Semiconductors. 1985, 392 (Russian).
10. I.G. Gverdsiteli, A.B. Gerasimov, Z.V. Jibuti, G.D. Chiradze. Proc. of Tbilisi University, "Physics", 306, 32, 1991, 203 (Russian).
11. Physical Values Reference. Ed. J.S. Grigorieva and E.Z. Meilikhova. 1991, 457 (Russian).

Kutaisi State University



გ. ჩირაძე

სინათლის გავლენა მონოკრისტალური სილიციუმის
სითბური გაფართოების კოეფიციენტისა და დეპარტაციის
ტემპერატურაზე

დასკვნა

მონოკრისტალური და უდისლოკაციო სილიციუმის
მაგალითზე ნაშრომში ექსპერიმენტულად ნაჩვენებია, რომ
თეთრი სინათლით განათება იწვევს აღნიშნული ნივთიერე-
ბის სითბური გაფართოების კოეფიციენტის გაზრდას და
დეპარტაციის ტემპერატურის შემცირებას სიბნელეში მათ
მნიშვნელობებთან შედარებით.

DISTRIBUTION FUNCTION IN THE REGION OF INTERMEDIATE FIELDS IN p-Ge



Z.Kachlishvili, L.Kukutaria, G.Batzashvili

Accepted for publication October, 2001

ABSTRACT. The dependence of electron temperatures of heavy and light holes on the applied electric field under acoustic phonon scattering has been calculated in the electron temperature approximation. The regularities of mutual influence of heavy and light hole bands have been analyzed.

The increased interest in p-Ge is mostly connected with the strongly nonlinear phenomena observed at helium temperatures. Among these phenomena are stochastic current oscillations revealed in pure p-Ge samples [1], appearance of N[2,3]- and S [4]-type current-voltage characteristics, etc. Many works have been devoted to these phenomena (see e.g. [2-4]), however, so far there exists no fully consistent theory explaining the whole diversity of the observed phenomena. This might be due to the complex Ge valence band structure, which significantly complicates calculations. Even Monte-Carlo modeling [5] cannot clearly explain experimental results.

In [2] the authors, analyzing the experimental data of a low temperature breakdown, show that the light hole band and its influence on the heavy hole band is very important for formation of kinetic coefficients. It is also shown that a strongly nonlinear behavior of kinetic parameters is observed in the intermediate electric field region.

The problem of establishing the distribution function and the relevant kinetic coefficients in the region of intermediate electric fields (temperatures) was first analyzed in [6]. This problem was studied in [7,8] under single-band model conditions. In [9] general expressions for relaxation times and the dependence of the mobility on heavy and light hole electron temperature have been calculated.

In this paper the dependence of heavy and light hole electron temperature on the applied electric field under acoustic phonon

scattering has been calculated. The regularities of mutual influence of heavy and light hole bands have been analyzed.

General regularities of intra- and interband transitions in p-Ge are well-known. The hole density of states depends on the effective mass. In p-Ge the mass of heavy hole exceeds strongly that of light holes. Thus, under scattering in the heavy hole band there prevail the intraband transitions, while under scattering in the light hole band the transitions into the heavy hole band are predominant [10].

These statements do not fully hold under hole gas heating in p-Ge. The rate of escape from the heavy hole band is low. However, the number of heavy holes exceeds significantly that of light holes and the flow from the heavy hole band will be rather high. That is why we cannot ignore the processes of transition into the light hole band. Therefore, these processes should be allowed for in the energy balance equations. Proceeding from the above, the energy balance equation in the heavy and light hole bands under acoustic phonon scattering will take the form:

$$\left(\frac{\partial Q_1}{\partial t}\right)_E + \left(\frac{\partial Q_1}{\partial t}\right)_{12} + \left(\frac{\partial Q_1}{\partial t}\right)_{21} + \left(\frac{\partial Q_1}{\partial t}\right)_{acoust} = 0 \quad (1)$$

$$\left(\frac{\partial Q_2}{\partial t}\right)_E + \left(\frac{\partial Q_2}{\partial t}\right)_{12} + \left(\frac{\partial Q_2}{\partial t}\right)_{21} = 0 \quad (2)$$

where $\left(\frac{\partial Q_1}{\partial t}\right)_E$ and $\left(\frac{\partial Q_2}{\partial t}\right)_E$ are the energies imparted to heavy and

light holes by the external electric field in a unit time. $\left(\frac{\partial Q_1}{\partial t}\right)_{acoust}$ is

the rate of heavy hole energy losses under acoustic phonon scattering

and $\left(\frac{\partial Q}{\partial t}\right)_{12}$, $\left(\frac{\partial Q}{\partial t}\right)_{21}$ are interband energy flows, accordingly from

the heavy hole- to light hole band and vice versa.

The expressions for the power transmitted to heavy and light holes by the external electric field E have the form:

$$\left(\frac{\partial Q_y}{\partial t}\right)_E = ep_y \mu_y E^2, \quad y = 1, 2, \quad (3)$$

where e is the hole charge, p_1 and p_2 are the concentrations of heavy and light holes (here and hereinafter the subscript "1" is used for the heavy hole band and the subscript "2" – for the light hole band), and μ_1 and μ_2 are the mobilities in the relevant bands.

We can easily calculate expressions (3) in the electron temperature approximation using the approximated expressions for the mobility dependence in the heavy and light hole bands on relevant electron temperatures T_1 and T_2 , given in [9].

In energy balance equations (1) and (2) energy losses during acoustic transitions of light holes are not taken into account. The quasi-elasticity condition for acoustic phonon scattering is fulfilled far better for light holes. Therefore, energy losses in the light hole band will be comparatively small. The rate of heavy hole energy losses can be calculated using the approximated expression for the intraband transition time [9]. As a result, we have:

$$\left(\frac{\partial Q_1}{\partial t}\right)_{acoust} = -p_1 W_{01} \zeta_1^2 \left(1 - \frac{1}{z_{e1}}\right) \left(1 + D_1 F_2[C_{2,1} \zeta_1]\right) \quad (4)$$

where $W_{01} = \frac{15}{4} \frac{A_{2,1} (k_0 T)^2}{\tau_{01} 2m_1 s^2}$, $D_1 = \frac{8}{15\pi^{1/5}} \frac{B_{2,1} C_{2,1}}{A_{2,1}}$, and

$$F_2(z) = \int_0^\infty \tau^2 e^{-\tau - z\tau^{1/2}} d\tau = \frac{2}{z} + \frac{9z}{8} + \frac{z^3}{16} - \pi^{1/2} \left(\frac{15}{8} + \frac{5z^2}{8} + \frac{z^4}{32}\right) e^{\frac{z^2}{4}} \operatorname{erfc}\left(\frac{z}{2}\right) \quad (5)$$

where $\psi_{1,y} = 1 + C_{1,y} \zeta_y^2$, $\zeta_y^2 = \frac{2m_1 s^2}{k_0 T} z_{ey}$, $z_{ey} = \frac{T_{ey}}{T}$, $\text{erf}(z)$ is the complementary error function, and A, B and C are the approximated coefficients (see Table in [9]).

We calculate the heavy hole- to light hole band energy flow using the approximated expression for the relevant transition time τ_{21} obtained in [9], and to calculate the energy flow of the inverse transitions we will use the well-known relation between the interband transition times [10]:

$$\tau_{21} = \left(\frac{m_2}{m_1}\right)^{3/2} \tau_{12}. \quad (6)$$

Thus, for power expressions during transition to and escape from the heavy hole zone we get, respectively:

$$\left(\frac{\partial Q_1}{\partial t}\right)_{21} = p_2 W_{02} \zeta_2^4 (1 + D_2 F_2 [C_{2,2} \zeta_2]) \quad (7)$$

$$\left(\frac{\partial Q_1}{\partial t}\right)_{12} = -p_1 \left(\frac{m_2}{m_1}\right)^{3/2} W_{02} \zeta_1^4 (1 + D_2 F_2 [C_{2,2} \zeta_1])$$

where
$$W_{02} = \frac{15}{4} \frac{A_{2,2}}{\tau_{01}} \frac{(k_0 T)^2}{2m_1 s^2}, \quad D_2 = \frac{8}{15\pi^{1/5}} \frac{B_{2,2} C_{2,2}}{A_{2,2}}.$$

Expressions (7) in the light hole band have the same form but the opposite sign. This can be easily demonstrated from the stationarity condition for interband energy flows:

$$\left(\frac{\partial Q_1}{\partial t}\right)_{12} + \left(\frac{\partial Q_2}{\partial t}\right)_{12} = \left(\frac{\partial Q_1}{\partial t}\right)_{21} + \left(\frac{\partial Q_2}{\partial t}\right)_{21} = 0 \quad (8)$$

Similar equations also hold for interband hole flows. In the light hole band only interband transitions are predominant. Therefore, the

stationarity conditions for the hole flow in the heavy and light hole bands coincide. They have the following form:

$$\left(\frac{\partial p_y}{\partial t}\right)_{12} + \left(\frac{\partial p_y}{\partial t}\right)_{21} = 0, \quad y=1,2 \quad (9)$$

where, respectively,

$$\begin{aligned} \left(\frac{\partial p_1}{\partial t}\right)_{21} = & p_2 p_0 \zeta_2^2 \left(1 + \frac{3}{2} D_2 \left[\frac{1}{C_{2,2} \zeta_2} + \right. \right. \\ & \left. \left. + \frac{C_{2,2} \zeta_2}{4} - \pi^{1/2} \left(\frac{3}{4} + \frac{(C_{2,2} \zeta_2)^2}{8} \right) e^{-\frac{(C_{2,2} \zeta_2)^2}{4}} \operatorname{erfc} \left(\frac{C_{2,2} \zeta_2}{2} \right) \right] \right) \end{aligned} \quad (10)$$

is the concentration of light holes transported into the heavy hole zone in a unit time, and

$$\begin{aligned} \left(\frac{\partial p_1}{\partial t}\right)_{12} = & -p_1 \left(\frac{m_2}{m_1}\right)^{3/2} p_0 \zeta_1^2 \left(1 + \frac{3}{2} D_1 \left[\frac{1}{C_{2,2} \zeta_1} + \right. \right. \\ & \left. \left. + \frac{C_{2,2} \zeta_1}{4} - \pi^{1/2} \left(\frac{3}{4} + \frac{(C_{2,2} \zeta_1)^2}{8} \right) e^{-\frac{(C_{2,2} \zeta_1)^2}{4}} \operatorname{erfc} \left(\frac{C_{2,2} \zeta_1}{2} \right) \right] \right) \end{aligned} \quad (11)$$

is the concentration of holes escaped from this band in a unit time. In expressions (10) and (11): $p_0 = \frac{3 A_{2,1}}{2 \tau_{01}}$.

Adding the normalization condition over the total number of holes p to equations (1), (2) and (10):

$$p_1 + p_2 = p, \quad (12)$$

we obtain a full set of equations to establish the field dependence of electron temperatures and concentrations in the heavy and light hole bands.

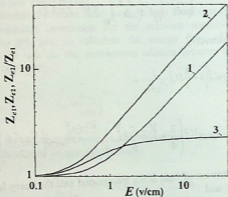


Fig.1. Dependence of dimensionless electron temperatures of heavy (z_{e1}) and light (z_{e2}) holes and of their ratios (z_{e1}/z_{e2}) on the applied electric field;
 curve 1 - electron temperature in the heavy hole band;
 curve 2 - electron temperature in the light hole band;
 curve 3 - the electron temperature ratio for heavy and light holes

In Fig.1 the curves for electron temperatures of heavy and light holes (curves 1 and 2) and their dependence (curve 3) on the applied electric field are presented. It is clear from the figure that starting from the electric field strength 0,1-0,2v/cm the electron temperatures in the bands begin to increase. Here the light holes are heated more rapidly than the heavy holes; and the electron temperature ratio also increases gradually and at the electric field higher than 10v/cm it becomes saturated reaching the value 2,3. In fields of the order of ~ 10 v/cm the light hole energy reaches 80-100K, which is sufficient for intensive optical phonon emission [11].

In Fig.2 the curves of a field dependence of hole concentrations normalized to equilibrium values are given. It is clear from the figure that the light hole concentration decreases with the increasing electric field. In 10v/cm fields the concentration is twice as low compared to its equilibrium value. At the same time the number of heavy holes increases, but this increase is so slight that it cannot exert any influence on the kinetic properties of p-Ge.

The decrease in the light hole concentration can easily be understood. With an increase in its mean energy the flow to the heavy hole band becomes very intensive. The heavy hole band itself is less sensitive to the electric field increase. Accordingly, the increase of the inverse flow to the light hole band is small and, as a result, under stationary conditions the accumulation of heavy holes compared to the equilibrium value takes place.

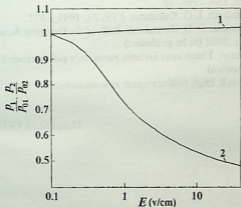


Fig.2. Dependences of concentrations of heavy (p_1) and light (p_2) holes normalized over relevant equilibrium values (p_{01} , p_{02}) on the applied electric field;
 curve 1 - the heavy hole concentration;
 curve 2 - the light hole concentration

REFERENCES



1. S.W. Teitsworth, R.M. Westervelt, E.E. Haller. Phys. Rev. Lett. **51**, 1983, 825.
2. V.F. Bannaia, L.I. Veselova, E.M. Gershenson, V.A. Chuenkov. FTP. **10**, 1976, 338.
3. V.F. Bannaia, L.I. Veselova, E.M. Gershenson, I.A. Gurvich. FTP. **10**, 1976, 452.
4. J. Peinke, A. Mühlbach, R.P. Huebener, J. Parisi. Phys. Lett. **108A**, 1985, 407.
5. W. Quade, G. Hüpper, E. Schöll, T. Kuhn. Phys. Rev. B, **49**, 1994, 13408.
6. Z.S. Kachlishvili. F TP. **2**, 1968, 580.
7. Z.S. Kachlishvili, L.G. Kukutaria. Bull. of the Georgian Academy of Sciences. **140**, 1990, 49.
8. Z.S. Kachlishvili, L.G. Kukutaria. FTP. **31**, 1997, 1071.
9. L. G. Kukutaria, G. B. Batsashvili. Bull. of the Georgian Academy of Sciences. 2002 (to be published).
10. B.M. Askerov. Electronnie iavlenia perenosa v poluprovodnikakh. 1985, (Russian).
11. E.M. Conwell. High field transport in semiconductors. 1967.

Tbilisi State University

ბანაწილების უნეცია p-Ge-ში შუალედური
ველებების არეში

დასკენა

გამოთვლილია p-Ge-ში მძიმე და მსუბუქი ხერელების ელექტრონული ტემპერატურების დამოკიდებულება მოდებული ელექტრული ველის მნიშვნელობებზე აკუსტიკურ ფონონებზე გაბნევის პირობებში. გაანალიზებულია მძიმე და მსუბუქი ხერელების ქვეზონებს შორის ურთიერთგაველების კანონზომიერებები.

MODELLING AND FORECASTING OF DIURNAL VARIATION OF CRITICAL FREQUENCY OF THE IONOSPHERE LAYER F2 CONSIDERING SOLAR ACTIVITY



K. Tukhashvili, V. Kandashvili, M. Devnozashvili,
J. Mdinardze

Accepted for publication October, 2001

ABSTRACT. The foF2 dependence on the solar activity (F10.7) has been studied. The sort of foF2(F10.7) function is established. The method allowing to make a model of diurnal variation of foF2 for each month is worked out at any point of the Earth (where foF2 is measured). The model depending only on F10.7 allows to predict foF2.

INTRODUCTION

Solar-terrestrial physics as a scientific discipline appeared recently and actually is still in the process of development. It is a direction of science researching the Sun and its radiation action on the natural phenomena of the Earth. This action spreads partially via the ultraviolet and X-ray radiation, and partially via corpuscular solar radiation. The interest in solar-terrestrial relation in a wide sense such as the effect of the Sun on meteorological, biological and other processes arose long ago.

In solar-terrestrial physics mainly the influence of the solar activity on geophysical processes is considered. The main problem is to explain the mechanism of this relation on the ground of physical and chemical processes. One of the primary problems is to consider the effect of direct influence of different types of solar radiation (especially such as short-wave, ultra-violet and X-rays) and interplanetary space (solar wind action on its magnetic field) on the upper atmosphere and magnetosphere of the Earth [1].

It is necessary to apply the aeronomial theory of the upper atmosphere to describe and interpret the variations observed in the ionosphere at 100-200 km. Aeronomy is a part of science studying the

upper atmosphere, its properties, spatial distribution, variation in time and the properties of natural phenomena.

One of the main tasks of aeronomy is to determine the elementary processes happening in different heights and to define the structure of the upper atmosphere.

The more we know about a phenomenon, the easier to predict it. But, unfortunately, there are some difficulties with respect to the Sun. Astrophysical and radio-astronomical observations permit to study only the surface and atmosphere of the Sun. As to the internal structure there are only hypotheses. Not knowing the internal structure of the Sun and the processes happening in its depth we can not solve the problem of the sun activity mechanism.

Although recently certain steps have been taken in this way there is not a complete theory. All the theories are based on various hypotheses. Thus, the study of the Sun is still based on empirical-statistical predictions, which require long-term observations on the sun.

The longest observational series are the Zurich/Wolf number i.e. latireve number of spots (since 1749) and the area of sunspots' group by Greenwich (since 1874) [2].

Nevertheless the regional Wolf formula is prime, $R = k(10G+N)$, where G and N are the number of spot groups and total number of spots in every group of the visual surface of the solar disk, respectively, and k is the coefficient deduced from practical consideration. Many problems arise at using the given coefficient. For example, there are three systems of relative numbers of the sunspots [3] differing by the method of calculation of G and N (in particular, by mass multiplier). At the same time the longest observation periods: Zurich (1749-1980), on the one hand, and Pulkow, on the other (since 1933), and American (since 1945) belong to different systems. Besides, Zurich series was made in 1749-1848 time interval; Wolf's average monthly number was re-calculated by other European institutes.

The question of Wolf's number was viewed several times [3]. Statistical analysis of R-number leads us to the result that Wolf's long series are mutual-heterogeneous, so in the process of statistical researches of the sunspots' origin we must use one of the methods from [3]. As to the Zurich series, there exists a proved guess on its

internal heterogeneity until 1849 [3]. Wolf number determination was offered to "Royal astronomical observatory" in Ucla and these data are currently published as international Wolf number R.

Registration of R has been aborted near the 21st maximal cycle, and for description of the full course of the cycle we must use new R-index or use new index as some authors consider new R-index to be less stabilized [3].

The radiation of 10.7 cm wavelength (2800 MHz) – F10.7 is also the solar activity parameter.

This radio flux, which originates from atmospheric layers high in the Sun's chromosphere and low in its corona, changes gradually from day-to-day, in response to the number of spot groups on the disk. Radio intensity levels consist of emission from three sources: from the undisturbed solar surface, from developing active regions, and from short-lived enhancements above the daily level. Solar flux density at 2800 MHz has been recorded routinely by radio telescope near Ottawa since February 14, 1947. Each day, levels are determined at local noon (17.00 GMT) and then corrected to within a few percent for factors such as antenna gain, atmospheric absorption, bursts in progress, and background sky temperature.

There is a correlation between R and F10.7, the coefficient of which equals 0.95 [3].

Wolf showed that the number of sunspots is characterized by cycle periodicity. Average length of the cycle is approximately 11.1 years but it is considerably changeable and varies within 7.3 – 17.1 years. The part of the cycle with maximal quantity of spots is called "Maximum epoch" and the part of the cycle with minimal quantity of spots - "Minimum epoch"[2].

It is important to solve some practical problems of the sun and earth relation, namely, to determine the functional dependence between the ionosphere parameters and individual indices of the solar activity for reliability of radio-communication and forecasting.

The F-layer is at 250-400 km above the of the Earth's surface. Maximal concentration of electrons is in this layer of ionosphere. Diurnal and annual variation of ionization in this layer is much more difficult than in the E-layer. The F-layer is the main layer reflecting the short waves and is very important for radio-communication [4].

For establishing the radio-connection in SW band it is very important to choose working frequency. The latter is limited by the maximum usable frequency (MUF), which in its turn is limited by critical frequency of the layer F2. The MUF forecasting is necessary for creation and development of new radio-lines and equipments, etc [5].

Critical frequency of the F2 layer is main option to determine MUF. The parameters of F2 layer of the ionosphere are characterized by rather complex distribution in time and space. Main goal of studying the upper atmosphere is to determine the changes of atmosphere parameters in height and time. The description of the upper atmosphere with the help of the model is necessary for better study of the reasons of changes. Therefore, to make the model of the upper atmosphere is one of the main directions of the researches carried out by means of spaceships and satellites [6]. Nowadays, the best models of ionosphere show only 20-30% deviation from the experimental data [7,8].

The authors [8] using the data of 1954-1968 years assert that the relation between the ultraviolet radiation of the sun, foF2 and F10.7 is of hysteretic character, and the use of F10.7 in ionosphere modeling for characterization of the long-term ultraviolet changes can cause 20-30% error in the measured and evaluated foF2 layer.

In our opinion, if the authors have used the data of a longer period of observations they would be convinced that the above-stated relation is not hysteretic but usual linking (scattering) of the dots. The present work shows that F10.7 can be successfully used to develop the models of diurnal changes of foF2.

EXPERIMENTAL RESULTS

Critical frequency of F2 layer - foF2 in fixed point for current month depends on the solar activity as well as on the Sun's zenith angle i.e. on local time T: foF2 (F10.7; T). To study the foF2 dependence on F10.7 it is necessary to fix T in current month. For this we need to arrange all the data as given in Table 1. The terminal column of the Table represents the relevant value of F10.7. Each line of the Table shows diurnal variation of median values of foF2 in January of the given year. The sun's zenith angle for each column of

the Table is constant permitting to study mutual relation between foF2 and solar activity. This relation we will show in 2 linear function:

$$\left. \begin{aligned} \text{foF2} &= A1 * \text{F10.7} + B1 & \text{F10.7} < 160 \\ \text{foF2} &= A2 * \text{F10.7} + B2 & \text{F10.7} > 160 \end{aligned} \right\} \quad (1)$$

Table 1

Station: Juliusruh $\varphi = 54^{\circ}38'$ foF2 -monthly medians and
F10.7
January

Time Year	0	1	2	3...	...21	22	23	F10.7
1958	45	44	42	40	58	49	47	2434
1959	41	38	35	32	51	45	44	2657
1960	35	33	32	30	38	38	37	1961
1961	28	28	28	26	30	27	27	1181
1962	27	30	30	26	26	27	28	919
...								
...								
...								
1986	26	27	26	24	22	24	25	709

In Fig.1 this relation is shown graphically- for 0^h a), and 12^h b). Dots in the inferior part of the diagram with connected pieces show the deviation of experimental values from the line in percent. The coefficients A and B are calculated for each hour. By means of formulas (1) foF2 depends on F10.7. Knowing these coefficients it is possible to make the models of diurnal variation of foF2 for any values of F10.7.

How much right the model shows the real picture can be seen in Fig.2.

Fig.2a represents 1987 year (quiet year F10.7=70), and Fig.2b shows 1990 year (active year F10.7 = 203). The curve is the model



foF2-10 [MHz]

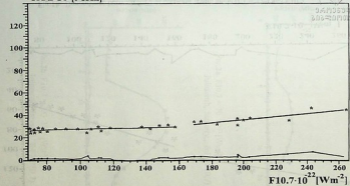


Fig.1a. Dependence between foF2 at constant zenith angle (LT = 0°) and F10.7. Juliusrah, January A1 = 0.03; B1 = 24.56; A2 = 0.12; B2 = 9.65

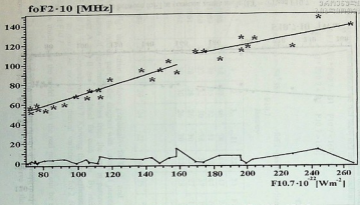


Fig.1b. Dependence between $foF2$ at constant zenith angle ($LT = 12^\circ$) and $F10.7$.
Juliusruh, January $A1 = 0.30$; $B1 = 42$; $A2 = 0.23$; $B2 = 80$.

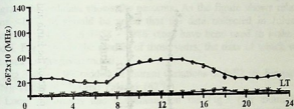


FIG.2a. $F_{10,7} = 70 \cdot 10^{-22} [Wm^{-2}]$
 Juliusruh, January,, foF2(F10,7) 1987

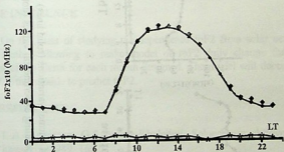


FIG.2b. $F_{10,7} = 203 \cdot 10^{-22} [Wm^{-2}]$
 Juliusruh, January, foF2(F10,7) 1990

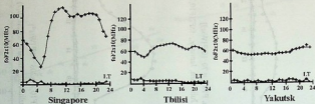


Fig.3. Models of diurnal variations (solid lines) of foF2 for different points of the Earth and corresponding experimental values (dots) for June 1971

and the dots are real values of foF2. In the inferior part of the diagram the dots connected with the broken lines show the relative deviation (%) from the foF2 model of experimental value. In this part of diagram the ordinate shows the percents. As the figure shows relative error <10%. It should be noted that the data collected in Julusruh (Germany, 54° N) in 1958 - 1986 years have been used to make the model. Fig.2 shows the models of those years, the data of which were not used for the given model.

Fig.3 shows the models of diurnal variations of foF2 for Singapore (1°N), Tbilisi (42°N) and Yakutsk (62°N).

Local minimums and maximums on the Fig.3 (for example a minimum of sunrise, a sunset and noon maximums) are not deduced because of an error of evaluation coefficients A and B [9]. Analogously it is possible to make models on a relative number of solar spots. In [10] the method of indexation of reference forecasting of the performance of solar activity is shown. If we know R or F10,7 then we may receive foF2 model of daily change.

THE INFERENCE

On the basis of studying the dependence foF2 from solar activity the method allowing to make model of foF2 daily change for any point of the Earth for each month designed. The model will depend on F10,7, that enable to predict foF2.

REFERENCES

1. L.A. Antonova, G.S Ivanov-Kholodnii. Solnechnaia aktivnost i ionosfera. 1989, 168.
2. Iu.I. Vitinskii. Prognozi Solnechnoi Aktivnosti. 1963, 150.
3. A.G. Ivanov-Kholodnii, V.E. Chertoprud. Itogi Nauki i Tekhniki. Seria Issledovanie Kosmicheskogo Prostranstva. 33, 1990.
4. G.P. Grudinskaia. Rasprostranenie radiovoln. 1967, 244.
5. O.V. Chernishev, T.N. Vasileva. Prognoz maksimalnikh primenimikh chastot. 1975, 340.
6. A. G. Ivanov-Kholodnii, G.M. Nikolskii. Solntse i ionosfera. 1969, 456.

7. A.G. Ivanov-Kholodnii, A.V. Mikhailov. Prognozirovanie sostoiania ionosferi. 1980, 190.
8. A.G. Kolesnik, V.I. Chernishev. Geomagnetizm i aeronomia **30**, 6, 1990, 1030.
9. K. Tukhashvili, V. Kandashvili. Bull. Georg. Acad. Sci., **146**, 3, 1992, 541.
10. A. G. McNish, J. V. Lincoln. Trans. AGU. **30**, 1949, 408.

Tbilisi State University

ქ. ტუხაშვილი, ვ. ყანდაშვილი, მ. დევნოზაშვილი,
 ჯ. მდინარაძე

იონოსფეროს F2 შენის კრიტიკული სიხშირის
 დღეღამური ცვლილების მოდელირება და
 პროგნოზირება მზის აქტივობის ბათვალისწინებით

დასკვნა

foF2-ის მზის აქტივობაზე დამოკიდებულების შესწავლის საფუძველზე შემუშავებულია მეთოდიკა, რომლის საშუალებითაც შესაძლებელია დედამიწის ნებისმიერი პუნქტისთვის (სადაც იზომება foF2) შედგეს დღეღამური ცვლილების მოდელი ყოველი თვისათვის. მოდელი ცალსახად იქნება დამოკიდებული F10,7-ზე, რაც საშუალებას იძლევა გაკეთდეს foF2-ის პროგნოზი.

INTERACTION OF IMPURITY ATOMS WITH THE VACANCY AND THE INTERSTITIAL ATOM IN MONATOMIC SEMICONDUCTORS



Z. Bokhochadze, A. Gerasimov, I. Lomidze,
Z. Samadashvili

Accepted for publication October, 2001

ABSTRACT. A new mechanism of interaction of different types of impurity atoms with the vacancy and the interstitial atom in monatomic semiconductors is suggested, which completely explains earlier inexplicable experimental facts. It is shown that the weaker the interstitial atom is bound to the lattice, the easier it is ejected to the interstitial space by the proper interstitial atom of the lattice and the more difficult it is to decompose the complex "impurity atom of the node + vacancy."

The technology of building up the semiconductor devices is based on the purposeful formation of defective areas in the crystal [1]. Nevertheless there are several mechanisms describing the interaction of point defects in semiconductor crystal [2-4], none of them can explain all the experimental facts.

Present work considers a mechanism of interaction of different types of impurity atoms with the vacancy and proper interstitial atom in monatomic semiconductors. This interaction, as shown below, is defined by the energy of binding of the impurity atom with the lattice. To compute the binding energy of the impurity atom has been an insoluble problem up to now [5].

General judgment shows that the more the characteristics determining the chemical binding of the impurity atom with the lattice atoms differ from the characteristics of binding of the lattice atoms with each other, the weaker their binding in the lattice [6]. Such characteristics are the number of valence electrons, their quantum state, ionization potential, hybridization energy, electronegativeness, influence of the inner electron cloud on the valent one, but not the atomic and ionic radii, which are frequently appealed by numerous authors [2,3,5]. As shown in [7-9] the atomic, ionic, and covalent radii

of the impurities do not play any role in defining the energy of binding of these atoms to the lattice, and there might be cases where the atom with the lesser radius than the main atom "expands" the lattice and the atom with the bigger radius, conversely, "compresses" it. For power comparison (which of the impurity atoms have more binding energy in the given crystal) in the first approximation the number of electrons and their quantum state might be taken into account. For example, in monatomic semiconductors every atom carries out four bindings to sp^3 hybrid orbital, therefore the atoms of III, IV and V basic groups of Mendelyev's periodic classification, which have s and p -electrons, will be bound stronger than the others. The atoms of II nonbasic group, which have two electrons in state s , will be bound comparatively weakly and the atoms of I nonbasic group, which have only one electron in state s will be bound far weaker.

Disposition of the local energy levels of the impurity atoms in the forbidden zone could be assumed as the characteristic value for comparison of the binding energies of the atoms of different elements within one periodic group. In the forbidden zone the acceptor energy levels of the impurity atoms correspond to the bonding orbitals (Fig.1), and the donor ones to the antibonding orbitals. The nearer the atom energy level to the valence zone, the bigger its energy of binding to the lattice.

Let us consider the interaction of impurity atoms with the point defects of other type – the proper interstitial atom and vacancy.

It should be noted that interstitial state of the proper atom is not experimentally registered. There are only theoretical viewpoints and ideas about it [10]. According to one of them the proper atom in interstitial state (PAIS), or the extra atom of the elemental cell shifts the nearest atom from the node and forms the so-called dumbbell configuration with it (Fig.2a). Both atoms are in equal distance from the center. Calculations show that such a configuration has lesser energy than the other configurations [10]. Motion of PAIS is carried out by means of formation and decomposition of the dumbbell [11]. After breaking the dumbbell one of the atoms occur in the node in an equal possibility, and the other one forms another dumbbell with any of the neighboring atoms, i.e. the dumbbell configuration is displaced.

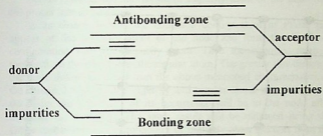


Fig.1. Energy spot levels of bonding and antibonding defects of molecular orbit



Fig.2. Formation of dumbbell configuration in lattice

a) For proper atom;

b,c) For impurity atoms of different groups

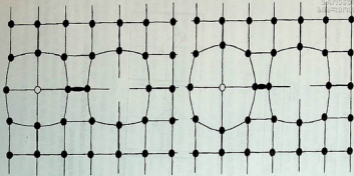


Fig.3. Formation of defect areas by different groups of impurity atoms of the node

Let us consider the interaction of impurity atom of the node with the proper interstitial atom.

In its chaotic motion the dumbbell configuration of PAIS may appear at the impurity atom of the node and form the dumbbell configuration with the impurity atom. Then the impurity atom is farther from the center than the regular atom. The greater this distance, the more difference is between the above-mentioned characteristics of the chemical bonds of the impurity and regular atoms (Fig.2b, g), and the lesser the possibility of its occurrence will be in the node after breaking the dumbbell. The same result will be obtained using the Gibbs distribution. The probability of impurity atom ejection from the node can be written as follows:

$$W = \frac{1}{1 + \exp\left[\frac{(|E_{imp}| - |E_0|)}{kT}\right]}$$

where E_0 and E_{imp} are the energies of binding the regular and impurity atoms to the lattice. If $\left[\frac{(|E_{imp}| - |E_0|)}{kT}\right] \rightarrow -\infty$ and $W \rightarrow 1$ then the impurity atom will be ejected from the node in great probability. if $|E_0| \ll |E_{imp}|$, then $W \rightarrow 0$ and the impurity atom will not be ejected from the node, and if $|E_0| = |E_{imp}| = 1/2$, then the impurity and regular atoms will be ejected from the node in equal probability. Thus, the weaker the interstitial atom binds to the lattice, the easier it is ejected to the interstitial space by the PAIS. It is proved by the experimental data, by the dependence of the ejection rate of the impurity atoms of I, III and V periodic groups from the energy of their binding to the lattice in Ge and Si [12+15].

The greater the difference between the chemical and regular bonds of the atom the lesser the interaction of the impurity atom of the node (IAN). Indeed, the greater this difference the lesser electrons of the nearest neighbors take part in binding, and the more negative charges shift to the bonds of the neighbor atoms and intensify them. Thus, around the impurity zone the defective zone is formed, where the regular atoms have stronger bonds than in the normal state (Fig.3). In its chaotic motion the vacancy can approach the impurity atom in the node so that its electrons weaken the bonds of the defective zone of

the IAN [16]. The stronger the bonds of this zone the lesser the probability of transfer the atoms of defective zone to the vacancy compared to the other atoms, and the more difficult for the vacancy to approach IAN. Thus, the weaker the IAN binds to the lattice the lesser it attracts the vacancy and vice versa (Fig.3).

When vacancy approaches to IAN there is formed a complex IAN+ vacancy, which is experimentally proved [2]. In certain conditions (exposition or the higher temperature) this complex decomposes. The vacancy leaves the IAN, which is called "the complex burning" and is experimentally registered [2]. This process has different probabilities for different impurity atoms [2,13]. The weaker the impurity atom binds to the lattice, the more it is shifted to the interstitial space in comparison with the vacancy surrounding regular atoms, and the more probable its transfer to the vacancy and the reverse transfer, in the result of which the impurity atom and the free node periodically change places, but the complex will exist longer. The fact that the proper atom transfer to the vacancy is complicated can be explained by the existence of the complex vacancy + IAN.

Temperature growth reduces the effect of the vacancy "repulsion" and "restraint" and increases the probability of vacancy approach to IAN and the vacancy leaving. These viewpoints are completely proved on the example of Ge and Si alloyed with the atoms of I, III and V periodic groups [13-15], where the vacancies were formed by 1.5÷3 meV exposition at a low $T < 100K$ temperature. The initial temperatures of formation and decomposition of the complex IAN+ vacancy correlate with the energies of binding the impurity atoms to the lattice, which we explain by the number of the valency electrons and deep-laid disposition of local energetic levels of impurity atoms. .

Thus, the weaker the impurity atom binds to the lattice, the more it shifts the mobile vacancy i.e. the weaker the probability of formation and decomposition of the complex IAN+ vacancy is. Actually, at the distance greater than the one atom interval such an impurity atom shifts the vacancy, and at one atom interval attracts it.

REFERENCES

1. S.M. Sze. Physics of semiconductor devices. 1, 1986.
2. V.V. Emtsev, T.V. Mashovec. Impurities and dotted defects in semiconductors. 1981, 248.
3. V.S.Vavilov, A.E.Kiyv, D.R.Niyazova. Mechanism of generation and migration of imperfection defects in semiconductors. 1981, 368.
4. V.S. Vavilov. Atom migration in semiconductors and changing of number and structure of defects initiated by stimulation of electronic subsystem. Phys. Sci. Succeses., 167, 4, 1997, 407.
5. B.I. Boltaks. Diffusion and dotted defects in semiconductors, 1972, 384.
6. A.B. Gerasimov, Z.G. Bokhochadze, N.D. Gochaleishvili, Z.D. Samadashvili, G.D. Chiradze, Res. In: "Intelkti". 3, Tbilisi, 1998, 17.
7. B.A.Gerasimov, A.B.Gerasimov, A.A.Cercvadze. Influence of charging state of impurities on their diffusion in semiconductors. Reports of Academy of Sciences GSSR, 1975, 77, 1, 53.
8. U. Lindfeld. Forces around defects. Proceeding of the fourth "Lund" International conference of deep level impurities in semiconductors. May 20 - June 3, 1983, Eger, Hungary, 6.
9. M. Scheffer, C.B. Bachlet, J.P. Vigheron. Electronic structure and Lattice Distractions around simple defects in Si and Ge. Proceeding of the fourth "Lund" International conference of deep level impurities in semiconductors. May 20 - June 3, 1983, Eger, Hungary, 7.
10. S. Khu. Diffusion in silitium and germanium" - In: Atomic diffusion in semiconductors. 1975, 253.
11. I.G.Gverciteli, A.B.Gerasimov, Z.G.Gogua, Z.V.Djibuty, M.G.Pkhakadze. About mechanizm of diffusion in covalent crystalls. Reports of Academy of Sciences GSSR, 128, 1987, 2, 293.
12. N.M.Alanyia, A.B.Gerasimov, M.S.Djandieri, K.I.Kasparyan, A.A.Cercvadze. About the mechanizm of interaction of radiation defects with impurities during radiation selfdiffusion process.

13. A.R.Bassman, A.B.Gerasimov, M.K.Gogotishvili, N.D.Dolidze, K.I.Kasparyan, N.G.Kakhadze, B.M.Konovalenko. Influence of donor impurities on cinetics of annealing of radiation defects in Ge. PTS, 7, 1973, 1377.
14. A.B.Gerasimov, M.K.Gogotishvili, B.M.Konovalenko. Influence of atom binding energy with lattice on cinetics of radiation defects annealing in p-type Ge. PTS, 20, 1986, 5, 794.
15. A.B.Gerasimov, N.D.Dolidze, K.I.Kasparyan, N.G.Kakhadze, B.M.Konovalenko, M.G.Mckhvetadze. Influence of copper on cinetics radiation defects annealing in Ge.PTS, 6, 1972, 8, 1587.
16. A.B.Gerasimov, A.P.Bibilashvili, Z.G.Bokhochadze, R.E. Kazarov, I.J. Lomidze. Creation mechanism of divacancy. Bull. Georg. Acad. Sci. (in the given collection).

Tbilisi State University

ზ. ბოხოჩაძე, ა. გერასიმოვი, ი. ლომიძე,
ზ. სამადაშვილი

**მინარეული ატომების ურთიერთქმედება ვაკანსიასთან
და კვანძთაშორისო ატომთან მონოატომურ
ნახევარგამტარებში**

დასკვნა

ნაშრომში შემოთავაზებულია სხვადასხვა ტიპის მინარეული ატომის ურთიერთქმედების ახალი მექანიზმი ვაკანსიასთან და კვანძთაშორისო საკუთარ ატომთან მონოატომურ ნახევარგამტარებში, რომელიც სრულად ხსნის აქამდე აუხსნელ ექსპერიმენტალურ ფაქტებს. ნაჩვენებია, რომ რაც უფრო სუსტადაა ბმული მინარეული ატომი მესერთან, მით უფრო ადვილად გამოიღვენება იგი კვანძთაშორის მდგომარეობაში მესერის საკუთარი კვანძთაშორისო ატომის მიერ და მით ძნელად იშლება კომპლექსი "მინარეული ატომი კვანძში + ვაკანსია".

DEPENDENCE OF THE ISOTHERMAL COEFFICIENT OF
ZINC DIFFUSION ON THE INITIAL CONCENTRATION OF
Zn IN GaAs



A.B. Gerasimov, N.G. Gochaleishvili, I. J. Lomidze,
Z. D. Samadashvili, E.N.Maziashvili, T.K.Ratiani

Accepted for publication October, 2001

ABSTRACT. The present work proposes a new mechanism of dependence of the coefficient of isothermal diffusion of Zn in GaAs on the initial concentration of Zn. It is assumed that Zn is diffused by dumbbell mechanism and the dumbbells have donor properties. Taking into account that these donors carry out compensation at first and ionization of the initial atoms of Zn in the sample, the weakening action of the AQP is changed, which explains the change of D_T due to concentration of the initial atoms of Zn in the sample.

It is known that isothermal coefficient of zinc diffusion D_T in GaAs greatly depends on the initial concentration of Zn in the sample (N_i) (Fig.1) [1,2]. To explain the dependence $D_T = \varphi(N_i)$ it has been proposed [1-5] that Zn, which is the shallow acceptor in GaAs and is found mostly in the nodes of Ga, is diffused mainly by vacancy and interstitial state, where it shows to be a positively charged donor. That is proved by the experiments of electric diffusion of Zn [6,7]. As the authors suppose, nevertheless the concentration of interstitial state of Zn is far less than that of the nodal state due to the significantly great coefficient of diffusion of the interstitial state they influence the isothermal coefficient of diffusion. Calculations for dissociative mechanism of Zn in [8,9] show that by increasing N_i the effective coefficient of diffusion D_T increases. These suppositions to some extent explain the growth of D_T by the increase of N_i , but they can not explain the decrease and further increase of D_T depending on the increase of N_i , as well as the shift of the maximum and minimum of $D_T = \varphi(N_i)$ to the greater values of N_i by increasing the diffusion temperature.

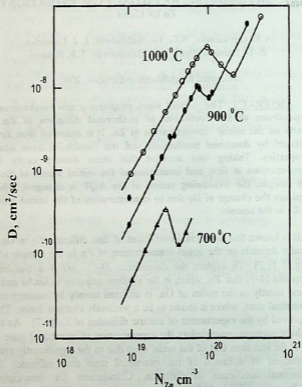


Fig.1. Dependence of the isothermal effective coefficient of Zn diffusion in GaAs on the initial concentration of Zn in the crystal at different temperatures (experimental [1])



These regularities can easily be explained by means of the double diffusion mechanism proposed in [10]. As shown in [11], potential binding energy of the atoms changes due to anti-bonding quasi-particles (AQP) – free electrons and holes, formed by all means (temperature, light, injection, impurities, defects, etc). AQP decrease the energy of binding among the atoms in the crystal and facilitate their movement increasing the coefficient of diffusion D_T . However, the value of binding energy decrease at this concentration of AQP might be different depending on the character and concentration of impurities and defects [10,12,13]. As shown in [12,13], AQP formed by ionization of the defects or impurities decrease the binding energy among the atoms far less than AQP formed by zone-by-zone transition. This is related with the fact that the charge of the ionized impurity attracts free carriers and increases the density of the surrounding free charges, i.e. effects non-uniform distribution of free charges, that does not permit AQP to move chaotically and outrun as many atoms as it can outrun when it is not attracted by the impurity center.

In the first approach this change of the specific binding energy might be evaluated [10,12]. If assumed that every charged atom of the impurity effectively contains only one electron, the weakening action of which is less than that of the electrons conditionally not interacting with the impurity, then the concentration of the electrons with less weakening action at the diffusion temperature will be equal to the impurity concentration N_d . The specific binding energy decrease in proper semiconductors is

$$\Delta U_e = (n_i + p_i) Eg(T)/2 \quad (1)$$

and in the n-type impurity semiconductors

$$\Delta U_{imp} = n_i Eg(T)/2 + pEg(T)/2 + n_{imp}E_{imp}$$

or

$$n_i Eg(T)/2 + [n_i^2 / (n_i + N_d - N_a)] n_i Eg(T)/2 + (N_a - N_d) E_{imp}, \quad (2)$$

where n_i is the proper concentration of the electrons, n_{imp} concentration of the electrons received by ionization of the donor centers N_d , E_{imp} the weakening energy of the electron effectively impeded by the charged impurity atom,

$$p = n_i^2 / (n_i + N_d - N_a). \quad (3)$$

Comparison of (1) and (2) shows that the presence of charged impurities in semiconductors influence the binding energy in two ways: increases the AQP concentration, which must decrease the binding energy, and decreases the AQP mobility, which at the given concentration increases the binding energy of the AQP in comparison with the proper semiconductors of the same concentration as AQP in the sphere, where $[PE_g(T)/2 + n_{imp} E_{imp}] < p_i E_g / 2$ in n -type [10,13]. During compensation the charges of dissimilar impurities neutralize their "binding" action on AQP and their weakening action increases, since $p = n_i^2 / (n_i + n)$, and $n = (N_d - N_a)$ in n -type or $n = n_i^2 / (p_i + p)$, and $p = (N_a - N_d)$ in p -type. After overcompensation due to the increase of the concentration of the other type the special binding energy U_{imp} increases again, since p or n decreases, and D_T decreases correspondingly. After the AQP concentration is as much as

$$(nE_g(T)/2 + p_{imp}E_{imp}) > p_i E_g(T)/2,$$

or

$$(N_d - N_a)E_g(T)/2 + N_a E_{imp} > p_i E_g(T)/2 \quad (4)$$

weakening of the binding energy increases again [10,13].

Proceeding from the above said the mechanism of the thermal diffusion of Zn in GaAs with the presence of Zn in the sample can be presented as follows. The atoms of Zn penetrate into volume of GaAs through the surface covered with Zn in the form of the dumbbell Zn-Ga near the node of Ga and Zn-As near the node of As (Fig.2,a). Both of these dumbbell configurations must have donor properties since the presence of Zn near every node increases the number of electrons

more than they are necessary in this sphere of the perfect crystal. These donors are compensated by Zn atoms presenting in the nodes of Ga having acceptor properties. At the diffusion temperature a part of these atoms appear in the interstitial space and form the dumbbell (Fig.2b), which requires more activating energy than penetration of the dumbbell configuration through the surface, where they are formed in the process of laying Zn on the surface of GaAs and they need only to orient for dumbbell penetration through the surface (Fig.2,c). Therefore, the dumbbell concentration formed in the volume is less than the dumbbells penetrated through the surface. Naturally, temperature increase arises the probability of the formation and penetration of the dumbbells in the volume. Motion of the dumbbells in the crystal is carried out in alternate stages of dumbbell formation, reorientation, decomposition and formation of a new dumbbell again [10,14]

Attraction of the AQP by Zn to the dumbbell state of a donor type is partially neutralized by the acceptor property of Zn in the nodes and ionized at the diffusion temperature, increasing D_T . After overcompensation, when the concentration of Zn acceptor is more attraction increases, AQP weakening action decreases and consequently, D_T decreases. On further increase of N_1 inequality (4) is fulfilled and U and consequently D_T are increased. Fig. 3 shows the change of the binding energy at a definite temperature depending on the initial concentration of Zn in the sample. During calculation it was taken into account that along with the increase of the temperature the concentration of dumbbells and the weakening action of AQP are decreased [12,13]. The Figure shows, that this dependence correlate well enough with the dependence of D_T on the initial concentration of Zn in the sample N_1 .

The shift of maximums and minimums to great concentrations of N_1 with the increase of the temperature of conducting the diffusion processes is related with the increase of the concentration of donor-type dumbbells, penetrating through the surface as well as formed in the volume, for compensation of which more initial acceptors were necessary.

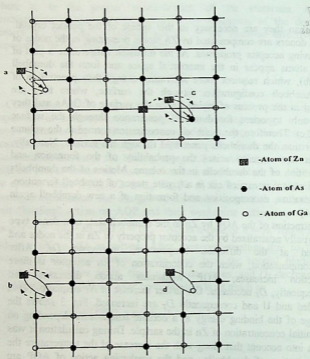


Fig.2. Schematic representation of thermal diffusion of Zn in GaAs:

- a) Zn atoms form the dumbbells Zn-Ga or Zn-As on the surface of GaAs near the node of Ga or As;
- b) At the diffusion temperature a part of Zn atoms initially present in the Ga nodes of the GaAs volume penetrate through the interstitial space and form the dumbbells Zn-Ga or Zn-As;
- c) Reorientation of the dumbbells Zn-Ga or Zn-As on the surface of GaAs;
- d) Reorientation of the dumbbells Zn-Ga or Zn-As in the volume of GaAs

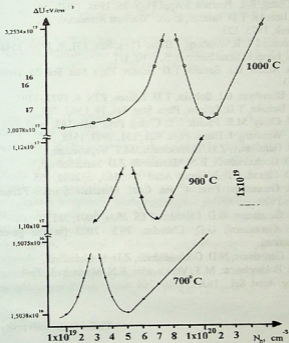


Fig.3. Dependence of the change of specific binding energy at Zn diffusion in GaAs on the initial concentration of Zn in the crystal at $T = 700^{\circ}\text{C}$, concentration of the dumbbell of donor type $N_d = 310^{19}\text{cm}^{-3}$, $E_{imp} = 10^{-6}\text{eV}$, $T = 900^{\circ}\text{C}$, $N_d = 510^{19}\text{cm}^{-3}$, $E_{imp} = 710^{-3}\text{eV}$, $T = 1000^{\circ}\text{C}$, $N_d = 910^{19}\text{cm}^{-3}$, $E_{imp} = 510^{-4}\text{eV}$, (Theory (2))

REFERENCES



1. L. Chang, R.L. Pearson, J. Appl. Phys. **35**, 1964, 1960.
2. B.I. Boltaks, T.D. Jafarov, in col. "Gallium Arsenicum". **6**, Tomsk, 1975, 123.
3. R. Leonard, L.R. Weisberg, J. Blanc. Phys. Rev. **131**, 4, 1963, 1548.
4. R.L. Longini. State Electron, **5**, 1962, 127.
5. K.A. Arseni, B.I. Boltaks, T.D. Jafarov. Phys. Stat. Sol. **35**, 1969, 1053.
6. A.I. Blanshyiu, B.I. Boltaks, T.D. Jafarov, PTS. **6**, 1972, 1791.
7. B.I. Boltaks, T.D. Jafarov, Phys. Stat. Sol. **19**, I 1967, 705.
8. H.C. Casey, M.B. Panish. L.L. Chang. Phys. Rev. **162**, 1967, 660.
9. L.R. Weisberg, J. Blanc. Phys. Rev. **131**, 1963, 1548.
10. A.B. Gerasimov, Z.G. Bokhochadze, M.T. Vepkhvadze, N.D. Gochaleishvili, E.N. Maziashvili Z.D. Samadashvili, G.D. Chiradze. Bull. Georg. Acad. Sci., **163**, 3, 2001, 455.
11. A.B. Gerasimov. Proc. 4th Int. Conf. Materials Science Forum N.Y. 1990.
12. A.B. Gerasimov, G.D. Chiradze. PTS. **35**, 4, 2001, 385.
13. A.B. Gerasimov, G.D. Chiradze. PTS. 2002 (in the given collection).
14. A.B. Gerasimov, N.D. Gochaleishvili, Z.D. Samadashvili, Z.G. Bokhochadze, M.T. Vepkhvadze, E.N. Maziashvili, Bull. Georg. Acad. Sci., **163**, 2, 2001, 266.

Tbilisi State University

ა. გერასიმოვი, ნ. გონაღვიშვილი, ი. ლომიძე,
ზ. სამადაშვილი, ე. მაზიაშვილი, თ. რატიანი

თუთიის დიფუზიის იზოთერმული კოეფიციენტის
დამოკიდებულება GaAs-ში საწყისად მყოფ Zn-ის
კონცენტრაციაზე

დასკვნა

მოცემულ ნაშრომში შემოთავაზებულია ახალი მექანიზმი GaAs-ში თუთიის იზოთერმული დიფუზიის კოეფიციენტის დამოკიდებულებისა, ნიმუშში საწყისად მყოფ Zn-ის კონცენტრაციაზე. დაშვებულია, რომ Zn დიფუნდირებს პანტელური მექანიზმით და პანტელებს გააჩნიათ დონორული თვისებები. იმის გათვალისწინებით, რომ ამ დონორებით თავიდან ხორციელდება კომპენსაცია, ხოლო შემდეგ პერეკომპენსაცია ხვრელებისა, რომლებიც წარმოიქმნებიან ნიმუშში საწყისად არსებული Zn-ის ატომების იონიზაციით, იცვლება ანტიდამაკავშირებელი კვაზინაწილაკების შემასუსტებელი მოქმედება, რაც ხსნის D-ს ცვლილების დამოკიდებულებას GaAs-ის ნიმუშში საწყისად არსებულ Zn-ის ატომების კონცენტრაციაზე.

CONTENTS



N. Toloraya - On the optimal configuration of the geomagnetic tail	3
T. Gegechkori, G. Mamniashvili - On formation mechanisms of single-pulse and secondary echoes in systems with a large inhomogeneous broadening of nmr lines	12
T. Jalagania, G. Kuratashvili, Yu. Tevzadze, G. Vanishvili - Modified kno-scaling for the multiplicity distribution of charged secondary π^- -mesons created in the collisions of relativistic nuclei	19
P. Defrance, T. Kereselidze, I. Noselidze, M. Tsulukidze - Double ionization of helium-like ions in the metastable states by fast electron ..	34
Sh. Kekutia, N. Chkhaidze - Hydrodynamics equations for three component system "helium II - porous media" and including coefficients	49
R. Kokhreidze, S. Odenov, J. Sanikidze - The percolation and Josephson effect in high-temperature superconductors	68
A. Lomidze, Sh. Tsiklauri - The properties of four-electron quantum dot ..	74
L. Kiknadze, Yu. Mamaladze - Energy and effective radius of a vortex ..	81
L. Kiknadze, Yu. Mamaladze - Depletion of a mass caused by a vortex and the vortex dynamics	96
Sh. Kakhichashvili, V. Tarasashvili - Polarization holographic correctors of laser radiation	104
L. Zakharov, L. Chotorlishvili - The influence of boson peak and two-level systems on the shift of electronic magnetic resonance frequency	110
L. Chotorlishvili - Distorted pulse spin echo in two-level systems inside amorphous ferromagnets	117
G. Chiradze - The influence of light on the rate of thermal expansion of monocrystalline silicon and on debay temperature	128
Z. Kachlishvili, L. Kukutaria, G. Batsashvili - Distribution function in the region of intermediate fields in p-Ge	133
K. Tukhashvili, V. Kandashvili, M. Devnozashvili, G. Mdinaradze - Modelling and forecasting of diurnal variations in critical frequency of the ionosphere layer f2 considering the sun activity	142
Z. G. Bokhochadze, A.B. Gerasimov, I. J. Lomidze, Z. D. Samadashvili - Interaction of impurity atoms with the vacancy and interstitial atom in monatomic semiconductors	153
A.B. Gerasimov, N.G. Gochaleishvili, I. J. Lomidze, Z. D. Samadashvili, E.N. Maziashvili, T.K. Ratiani - Dependence of the isothermal coefficient of zinc diffusion on the initial concentration of Zn in GaAs	161

6. თელთრია - გეომანიტური კუდის კონფიგურაციის ლატიმალურობა	3
ტ. ვეგეტიკორი, გ. მაშნიაშვილი - ერთიმუდსიანი ექოს და მუორადი ექობის ფორმირების შექანიშები ბმრ ხასების არაერთგვარობანი ვაგანიტურების მქონე სისტემებში	12
თ. ჯალაღანია, გ. კურატაშვილი, ი. თევზაძე, გ. ვანიშვილი - რელატიური ბირთვების ურთიერთქმედებებში დაბადებული დამუხტული მუორადი π - მუონების მრავლობითობის განა- წილების ანალიზი მოდიფიცირებული კნოსკეილინგის ფარ- გლებში	19
პ. დეფრანსი, თ. კერესელიძე, ი. ნოსელიძე, შ. წულუკიძე - მეტასტაბილურ 2^1S და 2^3S მდგომარეობაში მყოფი პელიუმის მაგარი იონების სწრაფი ელექტრონებით ორჯერადი იონი- ზაცია	34
შ. კეკუტია, ნ. სხაიძე - სამკომპონენტანი სისტემის "პელიუმ II - ფოროვანი ვარემო" პიდროდინამიკის განტოლებები და მათში შემავალი კოეფიციენტები	49
რ. კობრიძე, ს. ოდენოვი, ჯ. სანიკიძე - პერკოლაცია და ჯოზეფსონის ეფექტი მაღალტემპერატურულ ზეგამ - ტარებში	68
ა. ლომიძე, შ. წიკლაური - ოთხელექტრონიანი კვანტური წერტილის თვისებები	74
ლ. კიკნაძე, ი. მამალაძე - გრიგალის ენერგია და ეფექტური რადიუსი	81
ლ. კიკნაძე, ი. მამალაძე - გრიგალით განპირობებული მასის დანაკლისი და გრიგალთა დინამიკა	96
წ. ყაყინაშვილი, ვ. ტარასაშვილი - ლაზერული გამოსხივების პოლარიზაციულ-პოლოგრაფიული კორექტორი	104
ლ. სახაროვი, ლ. ჭოტორლიშვილი - "ბოზონური პიკის და ორდონიანი სისტემების გავლენა ელექტრონული მაგნიტური რესონანსის სისშირის წანაცვლებაზე	110
ლ. ჭოტორლიშვილი - დამახინჯებულ იმპულსიანი სპინური ექო ამორფულ ფერომაგნეტიკებში მყოფ ორდონიან სისტემებში	117
გ. ჩირაძე - სინათლის გავლენა მონოკრისტალური სილიციუმის სითბური გაფართოების კოეფიციენტსა და დეზაის ტემპე - რატურაზე	128

- ზ. ქაჩიშვილი, ლ. კუკუტარია, გ. ბაწაშვილი - განაწილების ფუნქცია p-Ge-ში შუალედური ველების არეში 133
- ქ. ტუხაშვილი, ვ. ყანდაშვილი, მ. დვენოზაშვილი, ჯ. მდინარაძე - იონოსფეროს F2 ფენის კრიტიკული სიხშირის დღევამური ცვლილების მოდელირება და პროგნოზირება მზის აქტივობის გათვალისწინებით 142
- ზ. ბოხონაძე, ა. გერასიმოვი, ი. ღომიძე, ზ. სამადაშვილი - მინარეული ატომების ურთიერთქმედება ვაკანსიასთან და კვანძთაშორისო ატომთან მონოატომურ ნახევარგამტარებში 153
- ა. გერასიმოვი, ნ. გოჩალეიშვილი, ი. ღომიძე, ზ. სამადაშვილი, ე. მაზიაშვილი, თ. რატიანი - თუთიის დიფუზიის იზოთერმული კოეფიციენტის დამოკიდებულება GaAs-ში საწყისად მყოფ Zn-ის კონცენტრაციაზე 161

გამომცემლობის რედაქტორები: შ. ინასარიძე,
ნ. სოლოდი

კორექტორები: რ. კვაჭანტირაძე, ნ. ჩახაია
კომპიუტერული უზრუნველყოფა ს. ჩხაიძე

3-

gp 24/2

